TAPER-SECTIONING TECHNIQUES IN SURFACE ANALYSIS

by

IAN KENNETH BROWN

A Master's Thesis submitted in partial fulfilment for the award of M.Phil. of the Loughborough University of Technology.

ABSTRACT

The provision of accurate composition-depth profiles is important in the investigation and characterization of thin and thick films, surface coatings, surface treatments and many other technological applications. Such profiles are normally obtained using a combination of sputter ion etching and surface analytical techniques. However, there are problems with this approach, particularly at depths greater than 1μm, since surfaces are generally eroded in a non-uniform way. Profiles to these depths are best achieved by using Auger electron spectroscopy in combination with a technique for mechanically tapering the specimen surface. Ball-cratering, which employs a rotating steel ball coated in fine diamond paste to abrade a well-defined spherical crater in the surface, is shown to be a convenient and accurate method.

The depth resolution of composition-depth profiles obtained by ball-cratering depends on the crater geometry, the diameter of the probing electron beam and the degree of surface roughness produced by the wear process. A model system, consisting of an electrodeposited hard chrome coating on a polished mild steel substrate, is used for a series of experiments aimed at defining the depth resolution as a function of the operating parameters.

The wear mechanisms in ball-cratering are examined in detail for a series of metals with a range of hardness, under a variety of conditions. Useful information concerning the nature of the wear mechanisms is given by the value of the wear coefficient , obtained from measurements of the wear rate. The surface topography produced is characterised by means of scanning electron microscopy and stylus measuring techniques.

Finally, composition-depth profiles through some commercially important protective coatings and nitrocarburised surface treatments are presented to illustrate the usefulness of the techniques.

CONTENTS

Chapter 1 INTRODUCTION

The top few atomic layers of a material may determine its characteristics with regard to processes which occur at the surface. Such processes may be of great scientific and technological interest, for example adhesion, corrosion, wear, catalysis and other chemical reactions. The study of surfaces, especially of metals, can help to reduce corrosion and improve their mechanical and chemical properties. Since a monolayer of contamination can condense onto a clean surface in less than an hour, even at a pressure of 10^{-12} atmospheres, the current use of surface analytical techniques is due in part to the development of ultra high vacuum technology.

1. Surface analysis techniques

A number of techniques are available, principally Auger electron spectroscopy, X-ray photoelectron spectroscopy and secondary ion mass spectrometry which enable the chemical composition of the outermost atomic layers to be determined. These techniques employ a beam of electrons, photons or ions which give rise to the emission of secondary particles characteristic of the surface composition. Each method of surface analysis is described in Chapter 2, with emphasis on Auger electron spectroscopy. The capabilities and limitations of the methods are discussed and a comparison is made of their relative merits. A more detailed description of AES is then presented, since it is the most suitable method for use with taper sectioning techniques. Particular reference is made to quantitative analysis, and some electron beam artefacts are discussed.

2. Composition-depth profiling

It is often desirable to compare the chemical composition of the

surface layers with that of the bulk. Such composition-depth profiles can be obtained by one of several methods, discussed in Chapter 3, according to the ultimate depth required. For shallow profiles use can be made of non-destructive methods which depend on variations in the escape depth for the emitted electrons. The electron escape depth is a function of energy, and the angle at which they emerge from the surface.

Profiles to greater depths are required for the investigation and characterization of thin and thick films, surface coatings and surface treatments. The combination of ion beam etching and Auger electron spectroscopy is normally used to obtain these profiles. Although ion etching is a good means for composition-depth profiling, there are several artefacts of the sputtering process. Surfaces are generally eroded in a non-uniform way, particularly in the case of industrial samples, causing a roughening of the surface. This leads to a corresponding deterioration of the depth resolution with sputtered depth.

There is an increasing requirement for profiles to depths greater than 1μm for the examination of industrially important protective coatings such as those produced by electrodeposition, and nitrocarburised surface treatments. In addition to the artefacts mentioned above, sputtering to these depths is relatively slow, making it inefficient and wasteful of instrument time. This has lead to the adoption of external mechanical tapering techniques, including ball-cratering which is described in Chapter 3. The ball-cratering instrument employs a rotating steel ball, coated with fine diamond paste, to abrade a well-defined spherical crater in the specimen, the depth and width of which can be accurately controlled. Composition-depth profiles can be obtained from point to point Auger analysis down the walls of the crater or by means of elemental linescans.

3. Depth resolution

The definition of depth resolution used in ball-cratering follows from that which has been applied to sputter depth profiles. The factors affecting the depth resolution in profiles obtained by ion etching are discussed in Chapter 4. The main contributions are atomic mixing effects, ion-induced microtopography, and factors due to the statistical nature of the sputtering process itself. Consideration of the statistical sputtering contribution predicts that the profile of an initially sharp interface will have the shape of a Gaussian error function. The broadening of the interface is defined as twice the standard deviation of the Gaussian, which is equivalent to the depth over which the intensity of the output signal decreases from 84% to 16% of its maximum value. This definition is generally used as a measure of the depth resolution in all depth profiling techniques.

Taper-sectioning has an important advantage over ion etching in that the depth resolution is independent of depth. The main factors affecting the depth resolution are the surface roughness produced by the wear process, and a geometrical term due to the finite diameter of the probing electron beam. A series of experiments is described in Chapter 4 in which an electroplated hard chrome coating is used as a model system, in order to investigate the relative importance of these contributions.

4. Wear mechanisms

The depth resolution of composition depth profiles obtained with ball-cratering is a function of the surface roughness produced by the wear process. The ultimate surface finish is dependant upon the nature of the wear mechanism itself. A survey of the principal wear mechanisms is presented in Chapter 5, with emphasis on abrasive and adhesive wear. A

detailed study of the wear processes involved in ball-cratering is made under a variety of conditions for a series of metals with a range of hardness Useful information concerning the nature of the wear mechanism in each case is obtained from measurements of the wear rate, and the corresponding value of the wear coefficient. The surface finish obtained is characterised using scanning electron microscopy and stylus measuring teachniques. Finally, the effect of the cratering process on the surface topography of the ball is discussed.

5. Applications

In order to illustrate the usefulness of ball-cratering for the provision of composition-depth profiles, the technique is applied to a range of industrially important protective surface coatings and treatments. Electroplating is an important process for the protection of steel surfaces, and an example is given of a profile through a commercially available zinc coating. The usefulness of the technique is further illustrated in the case of ion plated coatings and nitrocarburised surface treatments.

Chapter 2 SURFACE ANALYSIS TECHNIQUES

1. Introduction

There are now a considerable number of techniques available which provide valuable information on the chemical composition of surfaces (Kane and Larrabee 1974 Czanderna 1975Park 1975, Treitz 1977, Werner 1980) The characteristics of the most common methods of surface analysis are discussed and a comparison is made of their capabilities and limitations. Auger electron spectroscopy is described in more detail since this is the most appropriate technique for composition-depth profiling, particularly when used in combination with taper-sectioning techniques. The major constituents of the spectrometer are described, and the means for obtaining quantitative analysis are outlined.

2. Classification of techniques

Surface analysis techniques may be classified according to the incident probe and the type of emitted particles or radiation (Lichtman 1975) The most widely used incident probes are electrons, photons and ions. The electron probe commonly gives rise to secondary electrons (Auger electron spectroscopy (AES)) and X-ray photons (electron probe microanalysis (EPMA)). Incident X-ray photons generate electrons in X-ray photoelectron spectroscopy (XPS), while ions are the incident particles in secondary ion mass spectrometry (SIMS), ion scattering spectrometry (ISS) and Rutherford backscattering (RBS).

Table 2.1 summarises the incident probe and type of emitted radiation for the main surface analysis techniques (AES, XPS, SIMS, ISS and RBS). The electron microprobe (EPMA) is also included although it is not strictly a surface sensitive technique since it provides information from depths of up to one micron.

INCIDENT PROBE	EMITTED PARTICLES OR RADIATION		
	Electrons	Photons	Ions
Electrons	AES	EPMA	
Photons	XPS (ESCA)		
Ions			SIMS ISS RBS

Table 2.1 The type of emitted particles or radiation and the usual means of excitation for the major surface analytical techniques

2.1 Incident Electrons

An incident electron with sufficient energy can remove an inner shell electron from an atom. An electron from an outer shell will then drop into the vacant site, with the emission of energy equal to the difference between the initial and final atomic states. This energy may be released in the form of an X ray photon characteristic of the emitting atom. This process forms the basis of electron probe microanalysis (EPMA) (Hutchins 1974). Alternatively the energy can be given to another electron, causing it to leave the atom and the material. The energy of this emitted electron is also related to the energy level differences in the atom and it is known as an Auger electron. The kinetic energy of both the Auger electrons and emitted X ray photons is not dependent on the primary beam energy but only on the energies of the initial and final states of the atom.

Auger emission and X ray fluorescence do not occur with equal probability in all elements (Hercules and Hercules 1974), and the dependence on atomic number is shown in figure 2.1. The probability of X-ray emission is very small for the lighter atoms, but above atomic number 11 for sodium Auger emission decreases as the probability for X ray emission becomes greater.

An X ray spectrum consists of characteristic X ray lines of the elements present in the bombarded volume. This spectrum is then dispersed using either an energy or wavelength spectrometer. Elements are identified according to the wavelength of the characteristic lines, and quantitative information can be obtained by measurement of the appropriate line intensities. The mean free path of X rays is much greater than the penetration depth of the incident electron beam. The degree of surface sensitivity is therefore dependent on the accelerating voltage of the electrons, typically 10-30kv, and is generally about one micron.

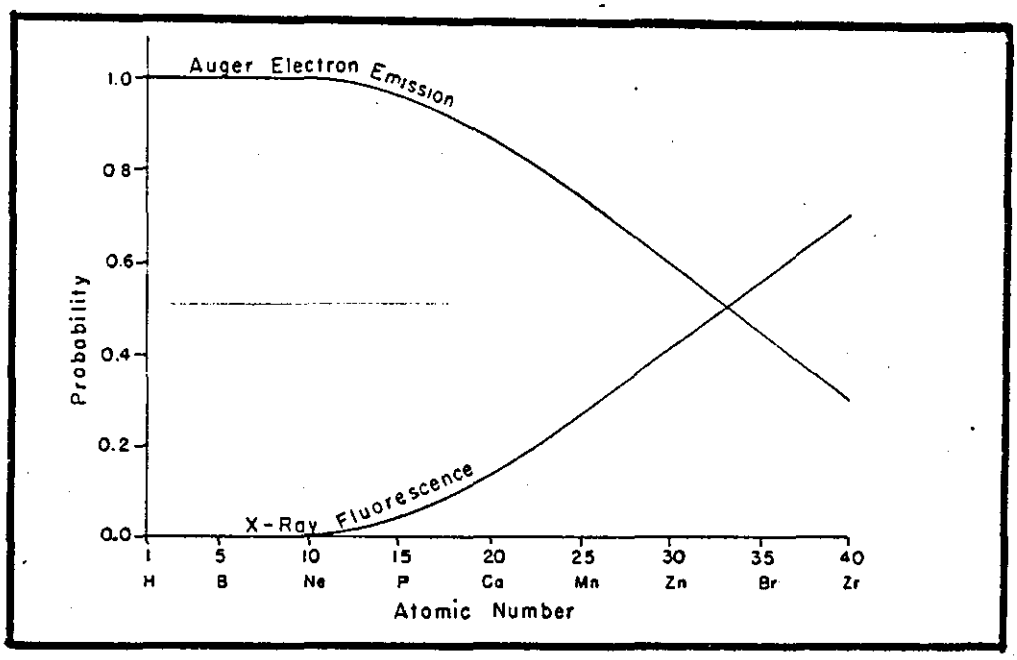

Figure 2.1 Probability of Auger electron emission and X-ray emission as a function of atomic number (Hercules and Hercules 1974)

However Auger electrons can in practice only be detected from a maximum of ten atomic layers. This is limited by the mean free path of the electrons which have a high probability of undergoing inelastic collisions in leaving the material. Composition depth profiles can be obtained in Auger electron spectroscopy, either using ion etching for material removal or by mechanically tapering the specimen surface.

2.2 Incident photons

The well known photoelectric effect whereby incoming photons give rise to the emission of electrons forms the basis of X ray photoelectron spectroscopy (Siegbahn et al 1967, Carlson 1975, Briggs 1977) . Photons are well suited to the study of surfaces since they have negligible momentum, causing minimum disturbance, and being neutral the problem of charging of the specimen is greatly reduced.

Electrons from all orbitals with a binding energy E_B less than the X ray energy are excited, but not all with equal probability. If the kinetic energy E_K of the ejected electron is measured, and the X ray energy is known then by the law of conservation of energy

$$E_B = h\nu - E_K + \phi_s \qquad (2.1)$$

where ϕ_s is a correction for the spectrometer work function.

Although the X rays penetrate deep into the sample, the ejected electrons come from only the top few atomic or molecular layers. This is determined by the mean free path of the electrons, and therefore the technique has a similar surface sensitivity to that of Auger electron spectroscopy.

The binding energy E_B of the emitted electrons is affected by the

chemical environment and varies for a series of compounds containing that atom. A core electron experiences a strong attractive force proportional to the atomic number, and a repulsive force from the outer, valence electrons. If an electron is removed from the outer shell the core electrons experience an increased force of attraction from the nucleus, effectively increasing the binding energy. The gain of an outer electron has the opposite effect. These "chemical shifts" were observed in the early work of Siegbahn and his co-workers (Nordling et al 1958), which led him to coin the name "Electron spectroscopy for chemical analysis". The term ESCA is now widely used and is synonymous with X ray photoelectron spectroscopy.

A disadvantage of XPS is the poor spatial resolution due to the difficulty in focussing X rays, which means that large diameter, greater than 1cm, ion beams are required for depth profiling.

2.3 Incident ions

A probing ion beam can give rise to reflected primary ions as well as secondary ions from the target materials. The number of emitted ions may be determined as a function of energy as in ion scattering spectroscopy (ISS) or of mass in secondary ion mass spectrometry (SIMS).

In ISS (Buck 1975) a monoenergetic beam of inert gas ions with an energy of several KeV strikes the specimen surface and the energy distribution of ions scattered at some particular angle, usually 90 degrees, is measured. It is assumed that the bombarding ion undergoes a simple binary collision with a surface atom and loses energy according to a simple kinetic exchange. The relative energy loss of the ion is governed by the conservation laws of energy and momentum, and in the special case when the angle is 90 degrees the relation may be written

$$\frac{E\ final}{E\ initial} = \frac{(Matom - Mion)}{(Matom + Mion)} \qquad (2.2)$$

Information is obtained essentially from the uppermost atomic layer, making ion scattering spectrometry a specifically surface technique.

In contrast to ISS, Rutherford backscattering (RBS) employs a beam of high energy (1-3 MeV) ions in order to provide depth information on the distribution of atomic species (Reuter and Baglin 1981) . The method is non destructive since low atomic number primary particles (H^+ or He^+) are used for which the sputtering yield is negligible. Elements can be detected to a depth of a few microns, the upper limit being determined by the mass of the constituent atoms. Quantitative analysis can be obtained using values of the stopping power and the scattering cross-section for the target atoms which are known and tabulated. The best mass resolution is achieved when the incident ion has a mass close to that of the target atom, but low mass ions are used to avoid inelastic scattering.

Rutherford backscattering is generally restricted to species which contain only a few elements, and is best suited to the study of implanted heavy dopants in a matrix of lighter atoms, or to a system where the surface elements have a higher mass than those of the bulk. It is not suitable for the measurement of light constituents in a matrix of heavier atoms due to the low scattering cross-section of light elements, and the presence of the large background from the matrix.

Ion bombardment also causes sputtering which is the ejection of surface atoms either in the form of neutrals, or of positive or negative ions. In secondary ion mass spectrometry (SIMS) (McHugh 1975) the sputtered ions are analysed by a mass spectrometer. SIMS is extremely sensitive, 10^{-6} monolayer or 10^{-13} gram being possible, and has an important advantage over AES and XPS in that all elements, including hydrogen, can be detected while isotopes can be separated. It is also possible to obtain images showing the distribution of the various elements and isotopes over the specimen surface using the secondary ions emitted (Castaing 1980).

Since the surface layer is removed by sputtering during an intense ion bombardment, SIMS was initially regarded as unsuitable for the analysis of individual monomolecular layers. The introduction of a "static" method (Benninghoven 1972) reduced sputtering to a negligible level by the use of extremely low primary ion current densities, making it into a non-destructive technique.

In view of the inherent sputtering process occurring in SIMS, it appears to be a straightforward technique for composition-depth profiling (Liebl 1975 However there are difficulties in quantification since the sensitivity factors for the various elements can cover several orders of magnitude. When the technique is used for depth profiling it is generally referred to as "dynamic" SIMS or the ion microprobe.

2.4 A comparison

The major characteristics of each of the surface analytical techniques which have been discussed are compiled in Table 2.2 The capabilities and limitations of the most important techniques are evaluated for surface and thin film analysis in a review by Hofmann (1979). Chang (1981) has considered the relative merits of XPS and AES both in view of their current performance and of that which is theoretically possible.

Each method of surface analysis has its particular advantages and shortcomings. However the information they provide is often complementary and more than one technique may be used in the analysis of a specific specimen.

The surface sensitivity and high spatial resolution of AES make it the ideal technique for composition-depth profiling. Good spatial resolution is essential, both in sputter depth profiling, where the diameter of the incident electron beam should be small compared to that of the ion beam, and

	AES	XPS	SIMS	ISS	RBS	EPMA
Incident probe	electrons	X rays	ions	ions	ions	electrons
Emission of	electrons	electrons	ions	ions	ions	X rays
Element range	$Z \geqslant 3$	$Z \geqslant 2$	$Z \geqslant 1$	$Z \geqslant 3$	$Z \geqslant 6$	$Z \geqslant 12$
Sensitivity (ppm)	1000	1000	0.1	1000	100	1000
(at %)	0.1%	0.1%	10^{-5}%	0.1%	10^{-2}%	0.1%
Information depth (Angstroms)	5-30	10-30	3-10	3-10	30-10^4	10^4
Lateral resolution	$\geqslant$ 0.5μm	$\geqslant$ 1 mm	$\geqslant$ 0.5μm	100μm	$\geqslant$ 1μm	$\geqslant$ 1μm

Table 2.2 The characteristic properties of the major surface analytical techniques

in combination with taper sectioning techniques. In view of this a more detailed description of Auger electron spectroscopy will be presented.

3. Auger electron spectrosopy

The Auger effect was discovered by Pierre Auger (1925) who observed their tracks in a Wilson cloud chamber. James Lander (1953) identified Auger electrons in the secondary electron energy distribution of electron bombarded surfaces and pointed out that they could be used to determine surface chemical composition. The Auger electrons appear as small peaks in the total energy distribution, and it was not until Harris (1968) used electronic differentiation to suppress the large background that the high sensitivity of the technique was realised. AES became popular when it was demonstrated (Weber and Peria 1967) that readily available LEED instruments could be used as retarding potential analysers to record secondary electron emission spectra. Most modern instruments employ the cylindrical mirror analyser, introduced by Palmberg (1969), which greatly increases the speed and sensitivity of Auger electron spectrometers. Comprehensive reviews of Auger electron spectroscopy, with emphasis on the experimental aspects (Grant 1982) and applications (Holloway 1980) have recently been published.

3.1 The Auger effect

The production of Auger electrons can be understood by considering the electron re-arrangement which takes places when an atom is ionised under electron bombardment (figure 2.2). If an electron with primary energy E_p ionises an atom by removing an electron from a core level K then the vacancy is immediately filled by an electron from an outer shell, L_1 for example. The energy released as a result of this transition $E_k - E_{L_1}$ may be emitted in the form of an X ray photon, as in X ray fluorescence or EPMA, or it may be transferred to another electron, in the L_2 level for example, causing it to leave the atom. Such an electron would be a KL_1L_2 Auger electron with an

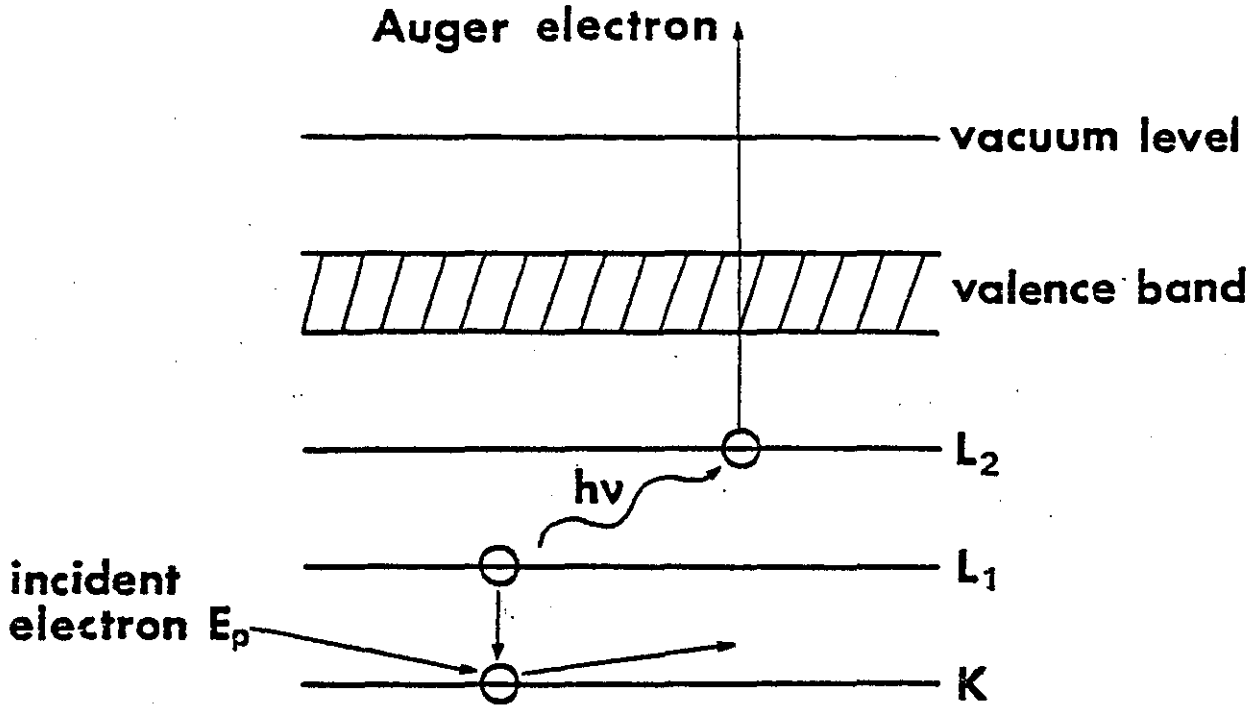

Figure 2.2 Energy level diagram showing the production of an Auger electron

energy given by the relation

$$E_{KL_1L_2} = E_K - E_{L_1} - E_{L_2} - \phi_s \qquad (2.3)$$

where ϕ_s is the work function of the spectrometer. The Auger electron energy is dependent only on the specimen material and is independent of the primary electron energy. Since at least two energy states and three electrons are required for Auger electron emission, Hydrogen and Helium atoms cannot give rise to Auger electrons. The electron energies of the principal Auger transitions are shown in figure 2.3, taken from the 'Handbook of Auger electron spectroscopy' (Davis et al 1976).

3.2 The secondary electron energy distribution

The electron energy distribution N(E) is shown in figure 2.4(a) where the Auger electrons appear as small peaks. The large peak at Ep is due to the elastically scattered primary electrons and is useful for calibrating the energy scale and aligning the electron analyser. The small peaks near Ep are characteristic energy loss peaks, due to plasmon and ionization losses, and are studied in electron energy loss spectroscopy (EELS). The large peak near E=0 is due to collisions between the primary electrons and surface atoms leading to the production of secondary electrons. These secondaries in turn create more secondaries which give rise to a cascade of electrons with ever decreasing energy. The peak does not occur quite at E=0, but at a value limited by the work function of the emitting surface. The Auger electron peaks themselves occur between these features on a slowly changing background and are considerably enhanced by differentiation (figure 2.4 (b)).

Compilations of standard Auger spectra for most elements have been published in this differential form (Davis et al 1976, McGuire 1979). The size of the peaks is dependent on the primary electron energy and this dependence is shown in figure 2.5 (McGuire 1979) for the 356 eV silver peak.

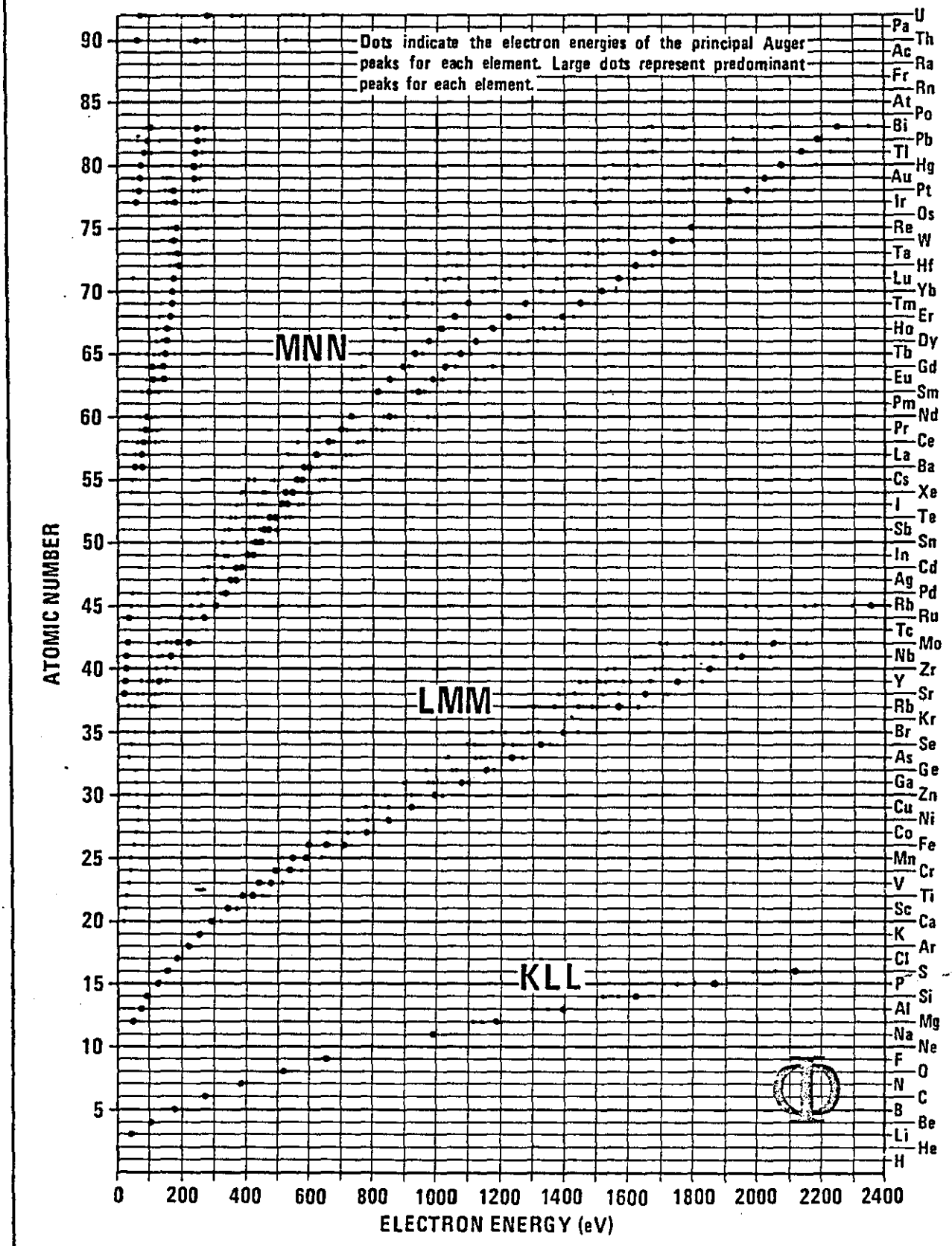

Figure 2.3 The electron energies of the principal Auger transitions (Davis et al 1976)

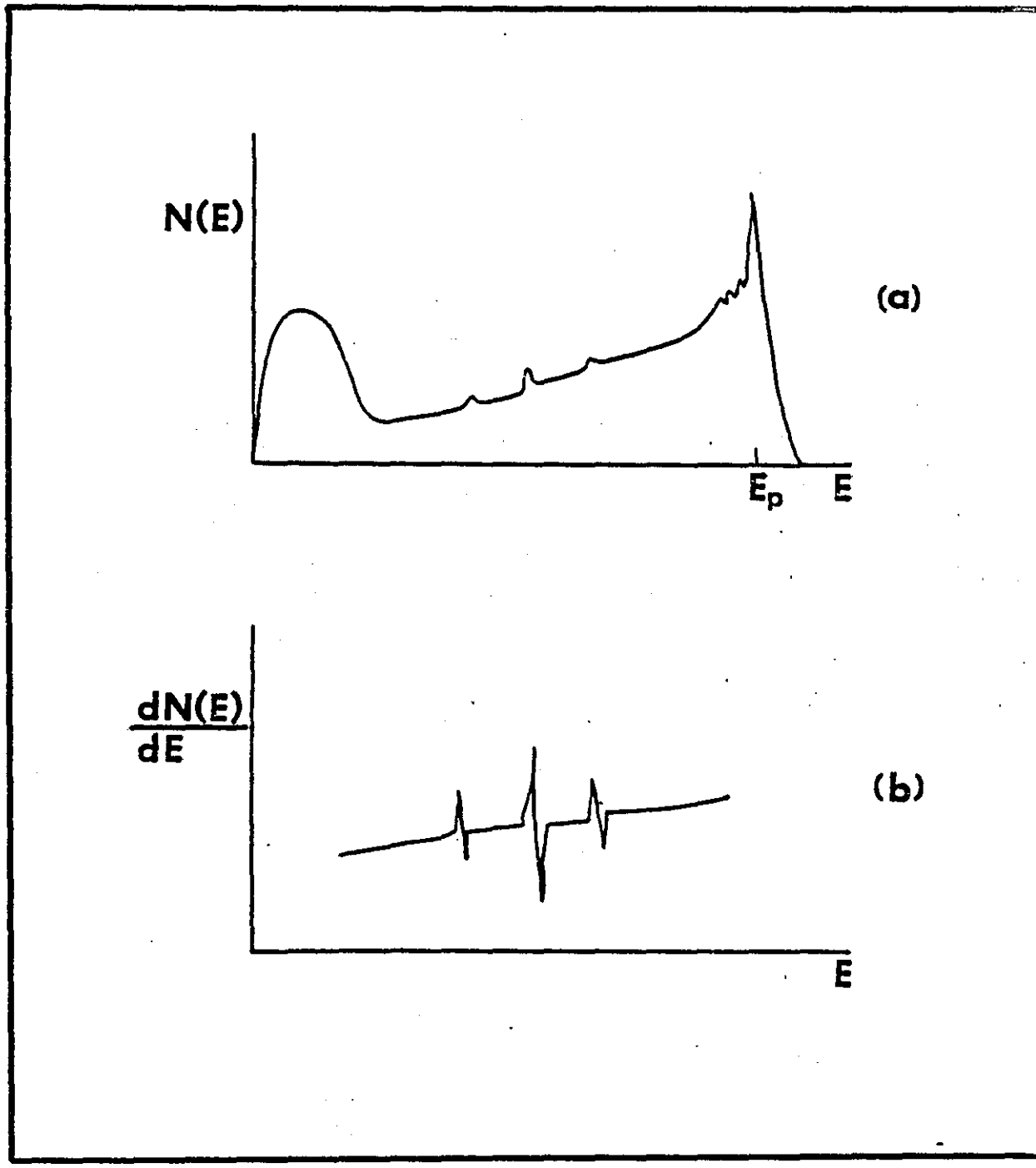

Figure 2.4 Schematic diagram showing (a) the number of detected electrons N and (b) the differentiated function $\frac{dN}{dE}$ as a function of the electron energy

In practice certain fixed energies are used for ease of comparison with standard spectra, an example of which is shown in figure 2.6 (Davis et al 1976) for silver obtained with 3keV primary electrons.

3.3 Experimental Methods

An Auger electron spectrometer consists of an ultra high vacuum system, capable of pressures of less than 10^{-9} Torr, an electron gun to provide the primary excitation and an energy analyser for the emitted secondary electrons. Since uhv conditions may take many hours to attain many Auger systems are equipped with a carousel, which enables a number of specimens to be housed in the system at any one time. Alternatively a fast entry lock is employed so that specimens may be admitted one at a time without taking the whole system up to atmospheric pressure.

3.3.1 Vacuum requirements

When studying the composition of surfaces it is important that they should be clean and free from contamination. The current use of surface analytical techniques is due in part to the development of ultra high vacuum technology. The vacuum requirements can be estimated from a consideration of the kinetic theory of gases. The rate at which gas molecules impinge on unit area of a surface is given by the relation (Yarwood 1967)

$$N = \frac{pN_A}{(2\pi MRT)^{\frac{1}{2}}} \qquad (2.4)$$

where p is the pressure, T the temperature and M is the molecular weight of the gas. N_A is Avogadros number = 6.025×10^{23} and R is the universal gas constant = 8.317 Joule deg $^{-1}$ mol.$^{-1}$

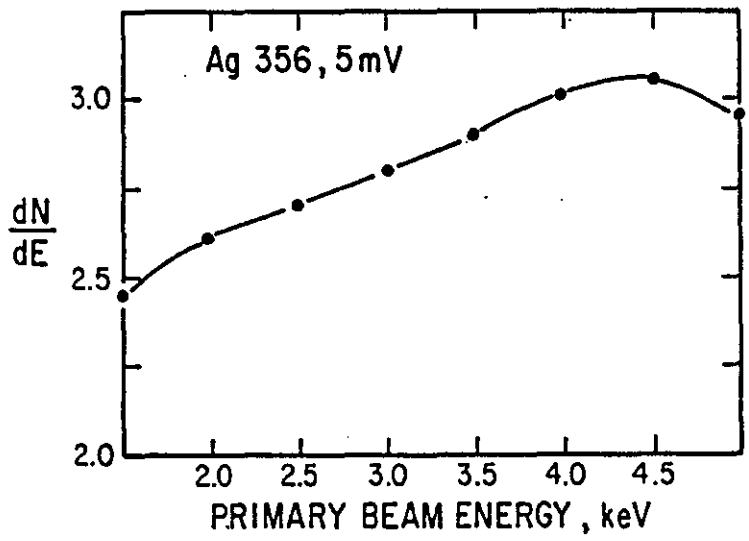

Figure 2.5 The peak to peak height of the differentiated function $\frac{dN}{dE}$ as a function of the primary beam energy for the 356 eV silver peak (McGuire 1979)

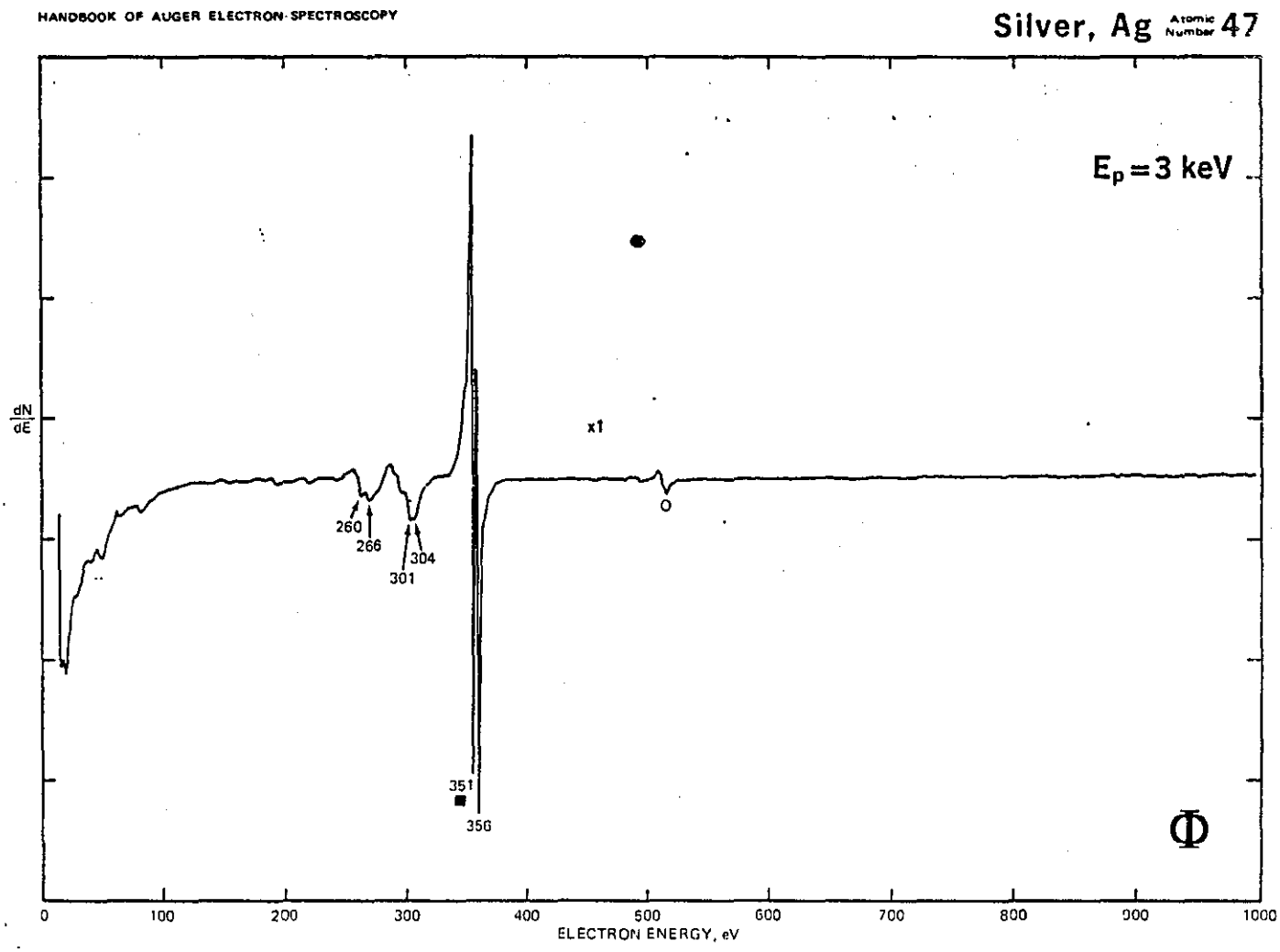

Figure 2.6 Typical Auger spectrum for a silver specimen obtained with a primary beam energy of 3Kev (Davis et al 1976)

For nitrogen at room temperature

$$N = \frac{6.025 \times 10^{23} p}{(27 \times 28 \times 10^{-3} \times 8.317 \times 293)^{\frac{1}{2}}} = 2.9 \times 10^{22}\ p\ m^{-2}$$

At a pressure of 10^{-9} Torr, equivalent to 1.33×10^{-7} Nm^{-2}, the number of molecular collisions per second with a boundary of area $1m^2$ is therefore

$$N = 2.9 \times 10^{22} \times 1.33 \times 10^{-7} = 3.86 \times 10^{15}$$

and in one hour the number is 1.39×10^{19}

An atomic monolayer contains about 10^{19} atoms m^{-2} so that if every molecule impinging on the surface sticks to it, then it will become completely covered in about an hour, which is normally sufficient time for an experiment to be undertaken.

The vacuum requirements in practice, however, are less stringent, particularly when the surface is continually eroded by an ion beam in sputter depth profiling.

3.3.2 The energy analyser

Several types of energy analyser have been employed in the development of Auger electron spectroscopy. Harris (1968) used a 127 degree cylindrical analyser for his early work, while the retarding field analyser of the LEED-Auger apparatus (Weber and Peria 1967) has been widely used. However, because of its speed and excellent signal to noise ratio, the cylindrical mirror analyser (CMA) (Palmberg et al 1969) is the one most commonly employed in modern AES apparatus. A schematic diagram illustrating the essential features of an Auger electron spectrometer incorporating a

CMA is shown in figure 2.7, taken from the Handbook of Auger electron spectroscopy (Davis et al 1976) .

The CMA incorporates an internal electron gun, providing a beam of electrons which is focussed on to the surface of the specimen. Secondary electrons ejected from this point, located at the source of the CMA, pass through an aperture on the inner cylinder. Electrons with a specific energy, determined by the negative potential applied to the outer cylinder, are able to pass through a second aperture on the inner cylinder and reach the small exit aperture. The electrons enter an electron multiplier and the amplified signal is recorded as a function of the potential applied to the outer cylinder. If a small a.c. voltage is superimposed on this potential and the in phase signal from the electron multiplier is synchronously detected with a lock-in amplifier, then the differential function $\frac{dN(E)}{dE}$ may be obtained.

The resolution $\frac{\Delta E}{E}$ of the CMA is determined by the precise geometry but is typically 0.5%. This provides optimum signal to noise since the Auger peaks of interest usually occur between 20 and 2000eV and are typically 2 to 10 eV wide. Some increase in signal to noise can be achieved by increasing the modulation voltage but only at the expense of energy resolution. The influence of modulation voltage on the amplitude and resolution for the example of the silver MNN peak is shown in figure 2.8.

The hemispherical sector analyser (HSA) is also widely used for Auger analysis, particularly in combined XPS and AES spectrometers. It consists (figure 2.9) of two concentric hemispheres with a potential difference applied between them so that only electrons with a particular energy can reach the exit aperture and enter the electron multiplier. The analyser can be operated in two modes, fixed retard ratio (FRR) or fixed analyser transmission (FAT). In the FRR mode the voltage between the hemispheres is swept over a range of

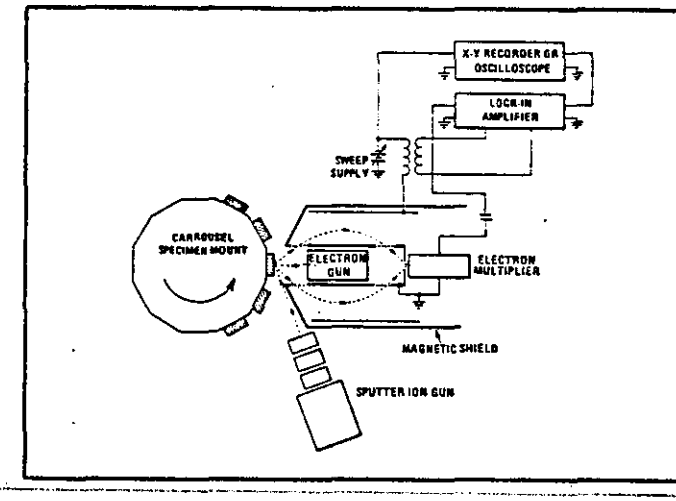

Figure 2.7 A schematic diagram showing the experimental arrangement employed for obtaining an Auger spectrum using a cylindrical mirror analyser (Davis et al 1976)

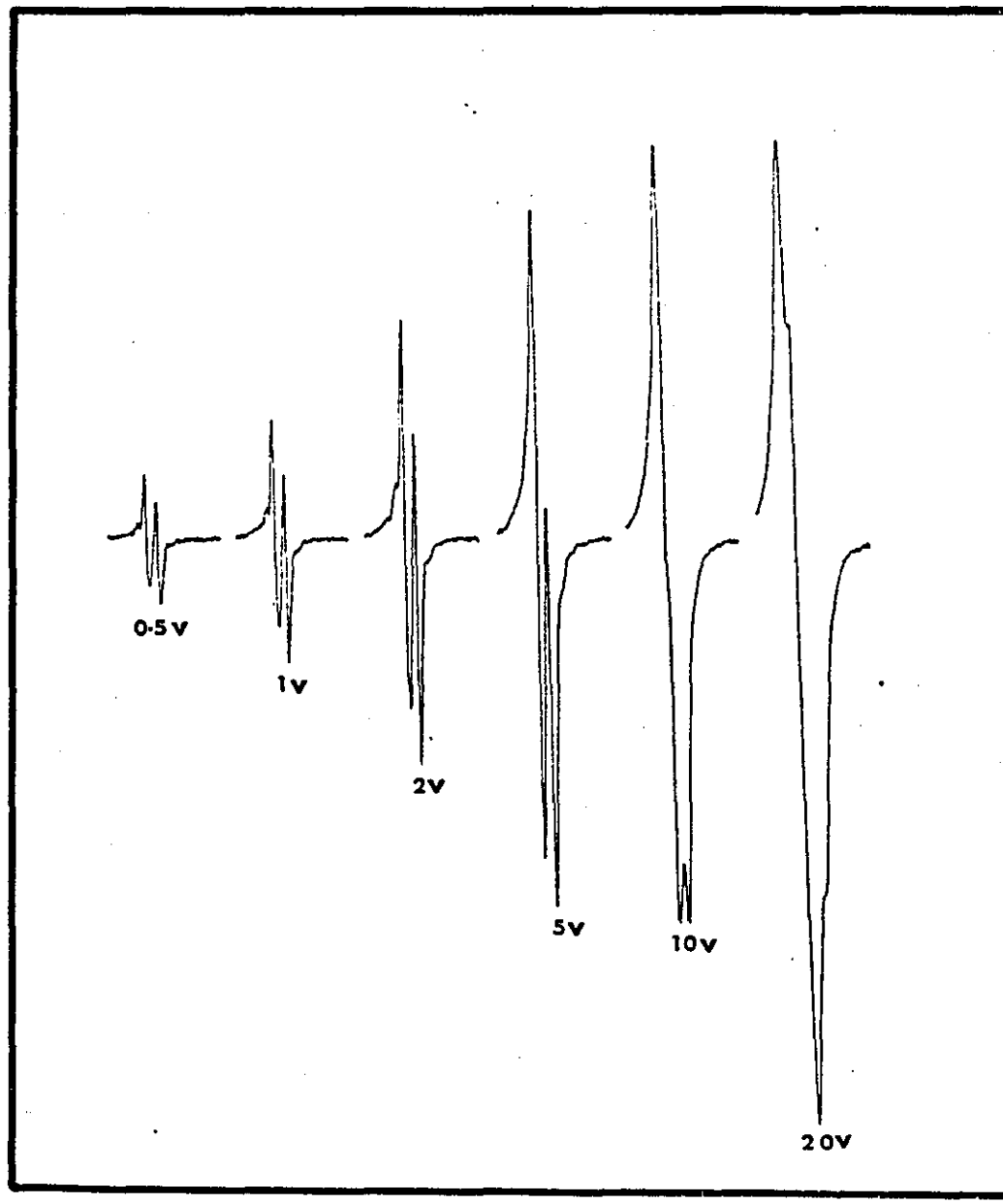

Figure 2.8 Variation of the silver MNN peak with modulation voltage obtained using a cylindrical mirror analyser

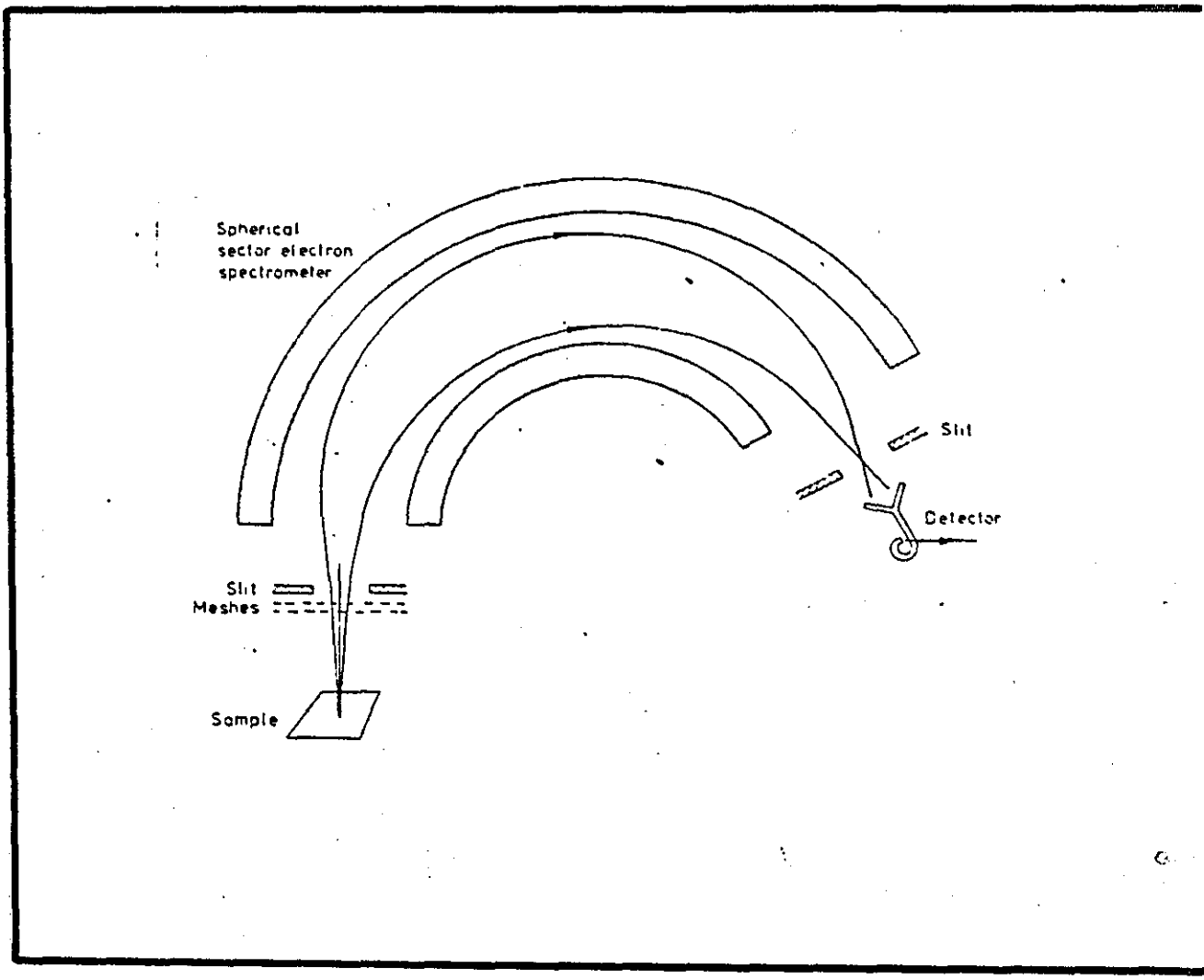

Figure 2.9 A schematic diagram showing the essential features of a hemispherical mirror analyser

values to select the energy of the transmitted electrons. In this mode, which is used for AES, the analyser operates in the same way as the CMA, and gives a resolution which is proportional to energy. The resolution is superior to that of the CMA but this advantage is offset by a decrease in transmission.

Alternatively the potential difference between the hemispheres may be held constant and the electrons are pre-retarded by a potential applied to a mesh in front of the entrance slit. In this FAT mode, generally used for XPS, the retarding potential is swept through the required energy range, and the analyser resolution remains constant throughout the spectrum.

3.3.3 The electron gun

The electron gun employs electrostatic lenses enabling the beam to be finely focussed and rastered over the specimen surface. Monitoring the secondary electron current enables an SEM image of the surface to be obtained which is useful for identifying areas of specific interest.

The spectrometer can be set up to monitor a particular Auger peak and the electron beam slowly scanned over the surface to give an elemental linescan. This facility may be extended to produce an elemental map by rastering the beam and using the output of the spectrometer to modulate the intensity of an oscilloscope spot (MacDonald and Waldrop 1971). Modern scanning Auger systems are equipped with sub-micron electron beam diameters for optimum spatial resolution, although this is not required for most applications of AES.

3.3.4 The ion gun

The ion gun has a dual role in an Auger electron spectrometer where it is used for sample cleaning and the provision of composition-depth

profiles. It produces a beam of monoenergetic ions, usually of a noble gas such as argon, which may be focussed or scanned over the specimen surface to remove atoms by sputtering. The ion beam and electron beam are arranged to be coincident at the specimen surface, and it is desirable for the ion beam diameter to be much greater than that of the electron beam.

3.4 Quantitative Analysis

The current I_i from an Auger transition i, collected by an analyser is given by (Chang 1974)

$$I_i = AI_p X_i \rho DB\phi\psi RT \qquad (2.5)$$

where

A is the area irradiated by the primary electron beam

I_p is the primary electron beam intensity

ρ is the atomic density of element i

X_i is the concentration of element i $(0 \leqslant X_i \leqslant 1)$

D is the escape depth of electrons

B is the backscattering factor

ϕ is the ionization cross-section

ψ is the Auger transition probability

R is the surface roughness factor

T is the instrument transmission.

However each symbol represents a complicated function of several variables and so the product notation is only symbolic. The escape depth D specifies the region from which Auger electrons are emitted and is perhaps the most important factor for quantitative analysis. The value of D is governed by the mean free path of electrons which depends on their energy and the material, but is independent of the primary energy. Values of the mean free path, expressed in monolayers, are shown in figure 2.10 (Seah and Dench 1979)

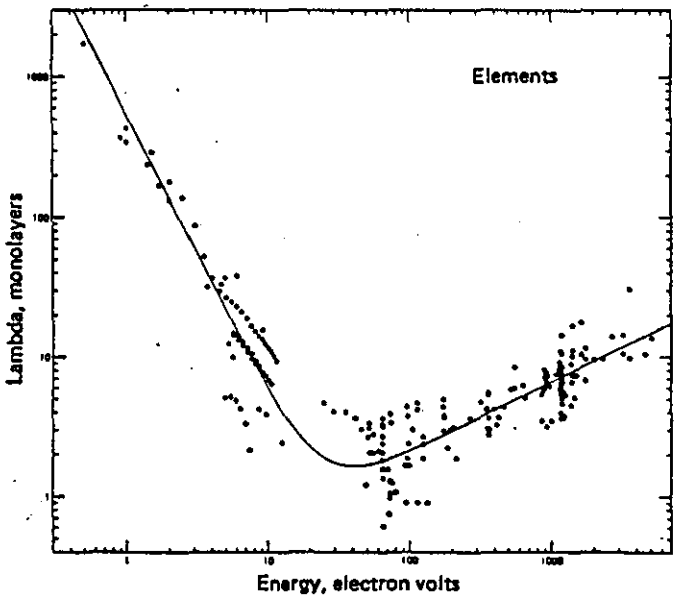

Figure 2.10 Experimental measurements of the inelastic mean free paths for elements, expressed in monolayers (Seah and Dench 1979)

for various elements as a function of energy. The mean free path is very high at low energies, falling to a minimum between 30 and 100 eV and then rising again approximately as $E^{\frac{1}{2}}$. At low energies the electrons have insufficient energy with which to excite any of the transitions by which they may lose energy, while at high energies the cross-sections for such transitio become small. In the energy range corresponding to the principal Auger transitions, 20 to 2000 eV, the mean free path lies between 1 and 10 monolayers. This is the depth from which Auger electrons can be detected and gives AES its high degree of surface sensitivity.

3.4.1 Elemental sensitivity factors

Quantitative analysis from first principles is not practical at the present time. However the atomic concentration of element i can be expressed as

$$X_i = \frac{S_i I_i}{\sum_j S_j I_j} \qquad (2.6)$$

where S_i and S_j are the inverse Auger sensitivity factors of elements i and j. This is the most useful equation for quantitative analysis, but it cannot be expected to provide answers with a high degree of accuracy since variations in the backscattering factor and escape depth with material are neglected. Sensitivity factors, relative to the standard element silver are shown for all the elements in figure 2.11 (Davis et al 1976) as a function of atomic number. Values for three types of Auger transition are given, obtained with a primary beam energy of 3KeV.

3.5 Chemical information

Changes in the electron binding energies of atoms occur when elements

Relative Auger Sensitivities of the Elements

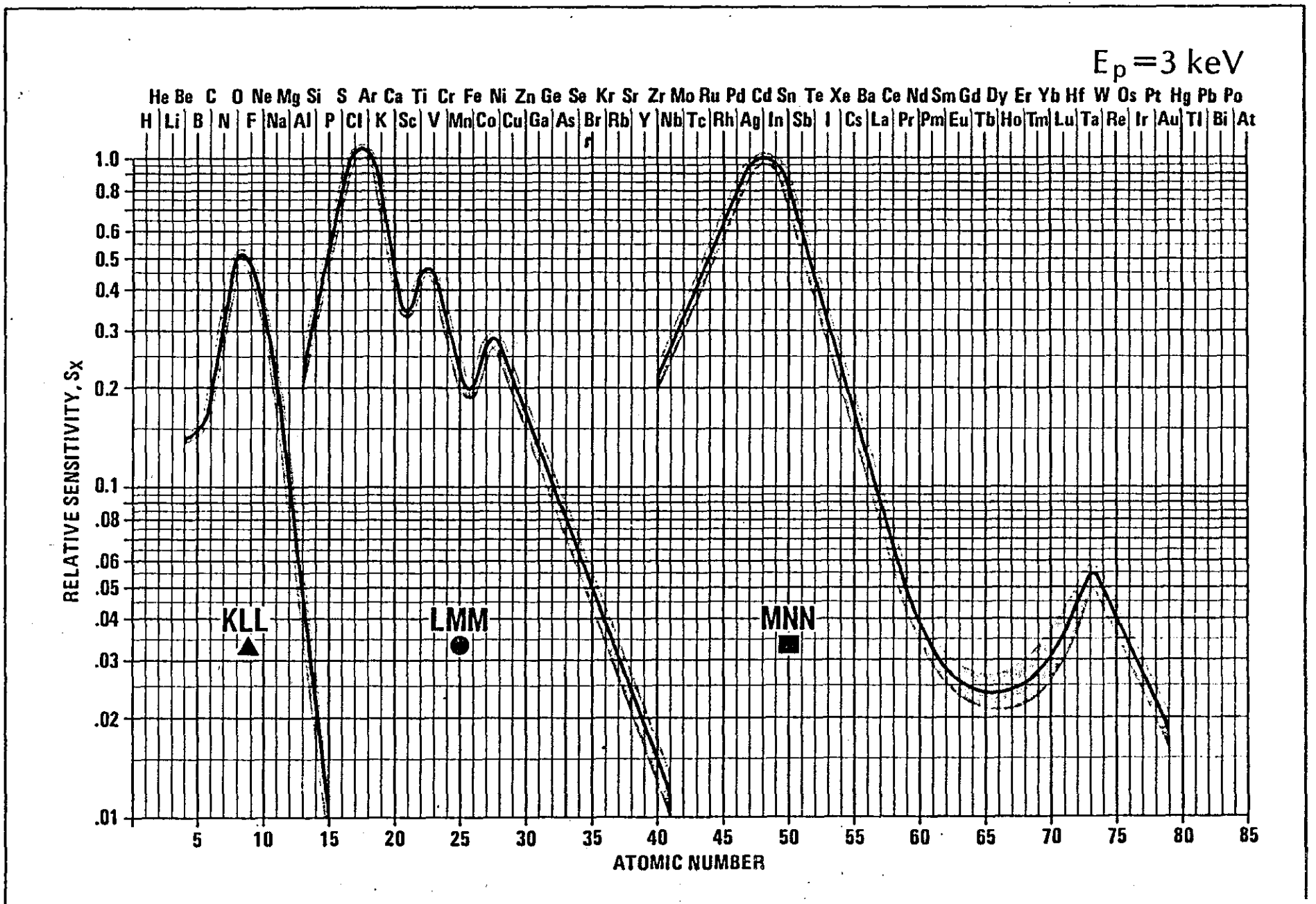

Figure 2.11 Relative sensitivity factors for the principal Auger transitions of the elements, obtained with a primary electron beam energy of 3 keV (Davis et al 1976)

combine together to form a compound. This leads to changes in both the energy and the shape of the Auger peak (Rye et al 1978). These effects are collectively term "chemical shifts" and have been used for some years to provide empirical information on the chemical state (Haas and Grant 1970).

Although attempts have been made to predict and explain such shifts (Coad and Riviere 1972, Jennison 1980) it is more usual to use a "fingerprint" technique to identify compounds from Auger spectra. Bauer (1972) has observed changes in the peak position and shape for a range of carbides, while Allen and Wild (1974) give examples of shifts occuring in metal oxides. There have also been recent studies of the changes in the shape of the sulphur peak in various compounds (Turner et al 1980). The nature of the chemical information which can be obtained from Auger electron spectroscopy has been reviewed by Madden (1981). He presents a survey of the known energy shifts with emphasis on those which result from the oxidation of solid materials.

However, chemical shifts may lead to problems in quantification since changes in the peak width are combined with changes in the peak to peak height (Hall et al 1977). Nevertheless such effects may be corrected by using the area of the Auger peak which is proportioned to the current. Grant et al (1977) have described a technique whereby the Auger peak area values can be obtained directly from the phase sensitive detector and plotted using conventional multiplexing equipment.

3.6 Electron beam artefacts

The incident electron beam can cause several effects which may adversely affect the quality of Auger spectra and lead to difficulties in their interpretation. These effects include electrostatic charging, specimen heating and certain composition changes.

3.6.1 Electrostatic charging

This is a particular problem in the case of insulators (Carriere and Lang 1977) when the specimen becomes negatively charged if the secondary electron yield is below unity. The Auger peaks are shifted along the energy axis, but this is not a major problem if the whole spectrum is shifted by a fixed determinable amount of energy. The secondary electron yield is dependent on the primary beam voltage and the angle of incidence, and so the effects of charging may be minimised by careful selection of these parameters.

3.6.2 Specimen heating

The temperature rise for a homogenous material of thermal conductivity K is given by (Pittaway 1964)

$$T = \frac{2EI}{\pi Kd} \qquad (2.7)$$

where E, I and d are respectively the energy, current and diameter of the primary electron beam. Specimen heating is not a problem for metals but can become important in the case of semiconductors and insulators. High temperature rises may occur in the case of metallic films deposited on insulating substrates such as glass (Hofmann and Zalar 1979a), and can also be predicted (Roll 1980).

Specimen heating may cause inter-diffusion and its effect on composition-depth profiles has been studied by Roll et al (1979) in the case of multilayer films of copper and nickel. Localised heating is likely to be a particular problem in Auger microanalysis where high beam energies and extremely small spot sizes are used.

3.6.3 Composition changes

Electron stimulated desorption (ESD) (Madey and Yates 1971) causes compositional changes which can have serious consequences in Auger electron spectroscopy, and has been the subject of thorough studies (Pantano and Madey 1981). Hooker and Grant (1976) have obtained direct evidence for the desorption of oxygen ions in studies of CO monolayers on nickel. Van Oostrom (1979) has examined the case of the decomposition of Al_2O_3 under electron bombardment. He observed a decrease in the Auger peak at 54eV, corresponding to Aluminium in the oxidised state, together with an increase in the metallic Aluminium peak at 68eV. The loss of oxygen leads to a reduction of the surface oxide, though changes in bulk composition can occur provided there is diffusion of oxygen atoms to the surface. ESD has been shown to adversely affect the depth resolution of composition-depth profiles since it may lead to enhanced sputtering in the electron irradiated area (Ahn et al 1975).

The presence of background gases in the vacuum chamber can also lead to composition changes as a result of electron stimulated adsorption (ESA). Although adsorption of residual gases may be expected on any clean surface, enhanced adsorption of oxygen has been shown to occur on silicon in the presence of carbon monoxide under electron bombardment (Coad et al 1970). Tompkins (1977) observed electron beam induced adsorption of oxygen on clean nickel surfaces, the rate of which was dependent on the partial pressure of H_2O. Decomposition of water vapour in the electron beam is particularly important for semiconductor materials and Van Oostrom (1979) shows the adsorption of oxygen on a GaAs surface. The most common example of ESA is the build up of carbon contamination at the surface due to the cracking of hydrocarbons, and has been shown to occur by Joyce and Neave (1973) in the case of silicon.

4. Discussion

The principles and major characteristics of the most widely used surface analytical techniques have been described, and a comparison has been made of their relative merits. Auger electron spectroscopy is the most suitable technique for depth profiling due to its surface sensitivity and high spatial resolution. A more detailed description of AES was then given, with emphasis on the experimental aspects, and the means for obtaining quantitative information were discussed.

Chapter 3 COMPOSITION-DEPTH PROFILING

1. Introduction

Composition-depth profiles enable the chemical composition of the surface to be compared with that of deeper layers. There are a number of techniques for obtaining such information, depending on the ultimate depth required. Methods which depend on the variation of the electron escape depth with energy are non-destructive but are only applicable to depths of a few atomic layers. Profiles to greater depths are generally obtained by a combination of ion beam etching and Auger electron spectroscopy. However surfaces may be eroded in a non-uniform way, particularly in the case of industrial specimens, causing a deterioration in the depth resolution. An alternative approach, which is suitable for profiles to depths greater than 1μm, is to use techniques for mechanically tapering the specimen surface in combination with Auger electron spectroscopy. The principles of each of these methods are described in this chapter, and their capabilities and limitations are discussed.

2. Non-destructive methods

2.1 Angular dependence of Auger electron emission

Some information concerning the depth distribution of elements can be found by changing the angle of incidence of the primary electron beam (Harris 1969) . Reducing the angle towards glancing incidence causes the surface atoms to be preferentially excited compared to normal incidence. Meyer and Vrakking (1974) calculated the ratio of the peak to peak heights measured in the case of low and high energy primary electrons at glancing incidence. This ratio decreased as a function of depth which can be explained by the greater degree of scattering for the lower energy electrons, making them less effective in exciting Auger transitions.

2.2 Escape depth variations

The dependence of the electron escape depth with energy provides a means of obtaining information on depth distribution since many elements have both high and low energy Auger transitions (figure 2.3). For electrons emerging along the surface normal the escape depth is equal to the mean free path (figure 2.8) which varies between 0.4 and 4 nm (Seah and Dench 1979) over the energy range of interest, 20-2000eV.

The use of this technique has been demonstrated (P.H. Holloway 1975) for determining the thickness and uniformity of ultra thin films of chromium oxide on gold substrates. The Auger signal from the substrate material decays exponentially on the thickness of the uniform overlayer according to the equation

$$I_s = I_o \exp(-x/\lambda_s) \qquad (3.1)$$

where I_o is the Auger signal from a clean infinitely thick sample of the substrate material and x is the overlayer thickness. λ_s is the mean free path of the Auger electrons from the substrate in the overlayer material, but includes an analyser geometry term.

The effective escape depth λ of Auger electrons emerging from an angle θ to the surface normal is given by

$$\lambda = \lambda_o \cos\theta \qquad (3.2)$$

where λ_o is the inelastic mean free path.

According to this relation, depth information can be obtained by tilting the specimen with respect to the analyser. However, in practice it is usually limited to systems employing the concentric hemispherical analyser (CHA), commonly used in X-ray photoelectron spectroscopy, since this has a small acceptance angle. The technique is rarely used with the CMA, which

has a more complicated geometry and shows a deviation from the cosine law (Hofmann 1981) .

Escape depth variations provide a means for depth profiling which is non-destructive, but the method cannot be used beyond about 5 nm. It is however useful for studies of adsorption, oxidation, contamination and surface segregation.

3. Ion etching

Ion etching was first introduced in surface science as a means of cleaning solid surfaces in situ prior to examination (Farnsworth 1958). It is necessary to remove grease and other contaminants which are acquired from the environment during handling as well as the remnants of cleaning acids and solvents. Ions of noble gases such as Ar^+ are generally used as they do not react with the specimen surface or with hot filaments in the vacuum system.

Noble gas ions behave closely like hard spheres and physical sputtering is the result of independent binary collisions in billiard ball fashion (Carter and Colligan 1968, McCracken 1975). The basic assumptions of conventional sputtering theory have been reviewed by Oechsner (1975) and Sigmund (1980).

3.1 Sputter depth profiling

Combining sputter-etching with a surface analytical technique such as Auger electron spectroscopy provides a means for obtaining composition-depth profiles (Palmberg 1972) . The erosion rate is determined by the value of the sputtering yield which is the number of atoms removed from the surface per incident ion. This depends on the mass, energy, electronic

configuration and angle of incidence of the incident ion, and on the atomic mass, electronic structure, crystal structure, orientation, binding energy and surface topography of the target (Wehner 1975) . Values of the sputterir yield of a number of metals and semiconductors have been determined by Laegrid and Wehner (1961) and Rosenberg and Wehner (1962) for bombardment by various noble gas ions with a range of energies. Quantitative aspects of composition-depth profiles in AES using sputter ion etching are discussed by Hall and Morabito (1978).

Commercially available sputter ion guns for depth profiling in AES are usually of the hot filament type, based on the Bayard-Alpert ionisation gauge (figure 3.1). The heated filament produces electrons which are accelerated into the grid with sufficient energy to ionise gas atoms on collision. The ions are accelerated by the anode into the focus electrode, and are then electrostatically deflected onto the target. The current density of the ion beam has a Gaussian distribution and normally produces a crater in the specimen surface of 1 to 2 mm diameter. This type of source produces ions having a narrow spread of energies, with only a small number of multiply charged and neutral species. It is normally operated with argon ions at energies between 1 and 5 KeV, and with current densities of between 100 and 200 μA cm^{-2}. Under these conditions material can be removed at rates between 10 and 40 nm per minute which is adequate for many depth profiling applications.

In order to obtain an accurate and meaningful profile it is desirable that the analysed area should be much smaller than the sputtered area. This demand can be met in AES, but not in ESCA since X rays cannot in general be focussed and large diameter ions beams are required. Such beams may be achieved by scanning the focussed beam over a larger area, but this is accompanied by a much reduced sputtering rate. An alternative approach is to use a cold cathode ion source, such as the twin anode electrostatic ion gun

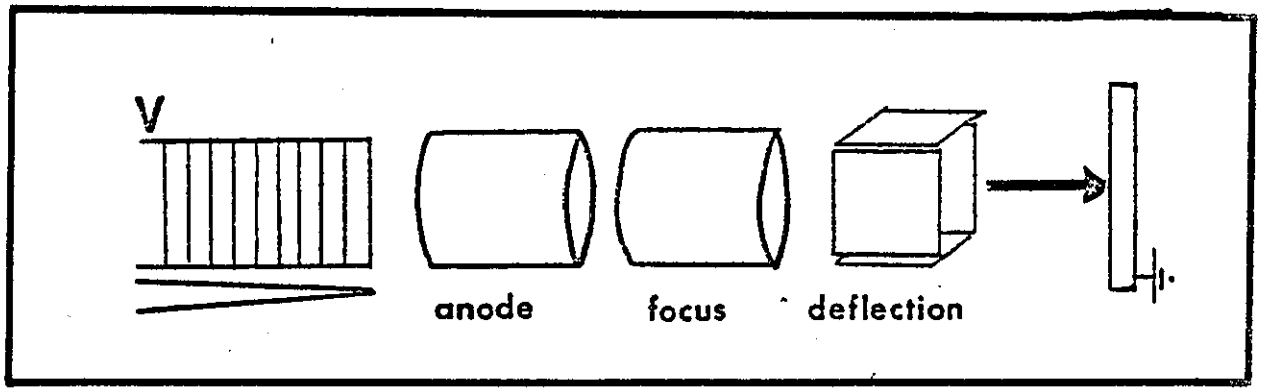

Figure 3.1 Schematic diagram showing the essential features of a hot-filament ion source

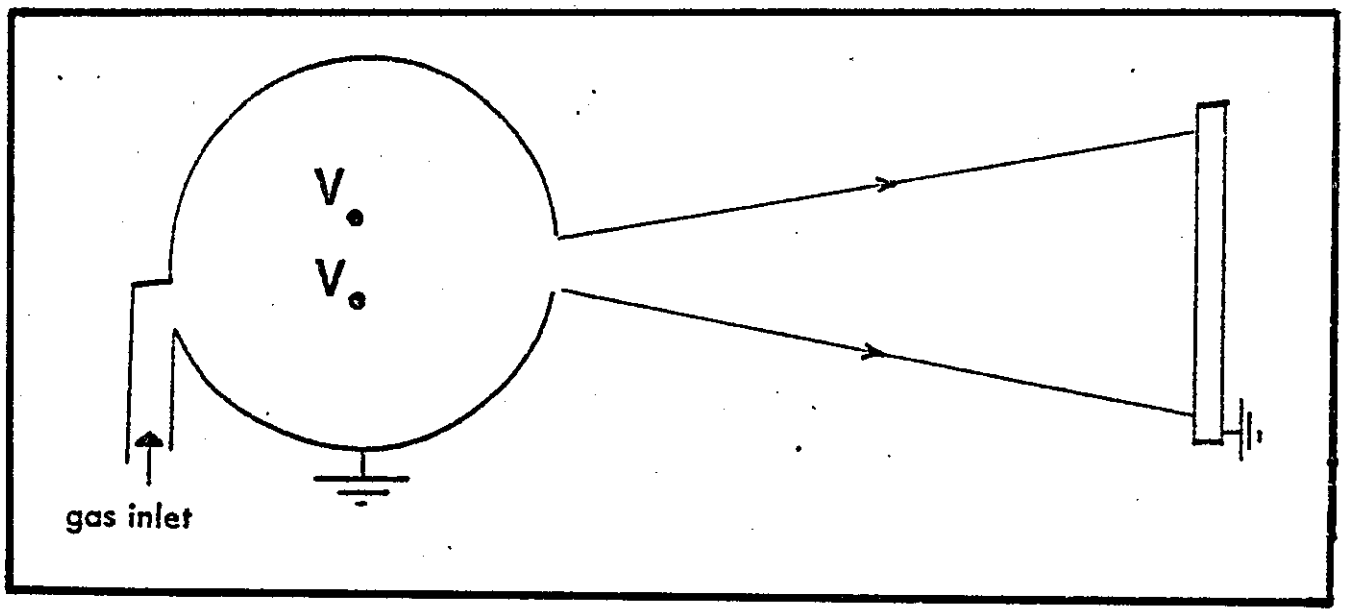

Figure 3.2 Schematic diagram showing the essential features of a cold-cathode ion source

shown in figure 3.2. A discharge is maintained between the anodes, held at a positive potential, and the earthed cathode. The gas species is fed directly into the source so that there is a differential pressure between the source and the specimen chamber. Ions which are formed in the discharge emerge through an exit aperture in the cathode. Sources of this type can produce intense ion currents over a large area. However the ions have a wide energy distribution since their energy depends on the precise position of formation, and a large number of multiply charged ions and neutrals are produced.

For composition-depth profiling in AES, the electron beam can be made at least two orders of magnitude smaller than that of the ion beam and be directed towards the centre of the crater. A schematic diagram showing the relative positions of the ion and electron beams when profiling through a thin film is given in figure 3.3. Composition-depth profiles may be obtained either by sequential ion bombardment and surface analysis using AES, or the analysis may be performed simultaneously. (D.M. Holloway 1975). The latter method possesses an advantage in that surface contamination is greatly reduced. For many applications it is unnecessary to obtain a full spectrum each time and, when the concentration of only a few elements is of interest, it is more efficient to use a multiplexing system. Narrow energy windows are adjusted to cover only relevant peaks, and these are repetitively scanned in sequence. The peak to peak amplitude of the Auger peak is electronically measured and plotted automatically on the Y axis of an X-Y recorder, with sputtering time on the X axis.

3.2 Ion beam artefacts

Although sputtering provides a universal means for obtaining composition-depth profiles, many details of ion etching are unpredictable and are still unexplained. This can lead to several artefacts and impair the depth resolution

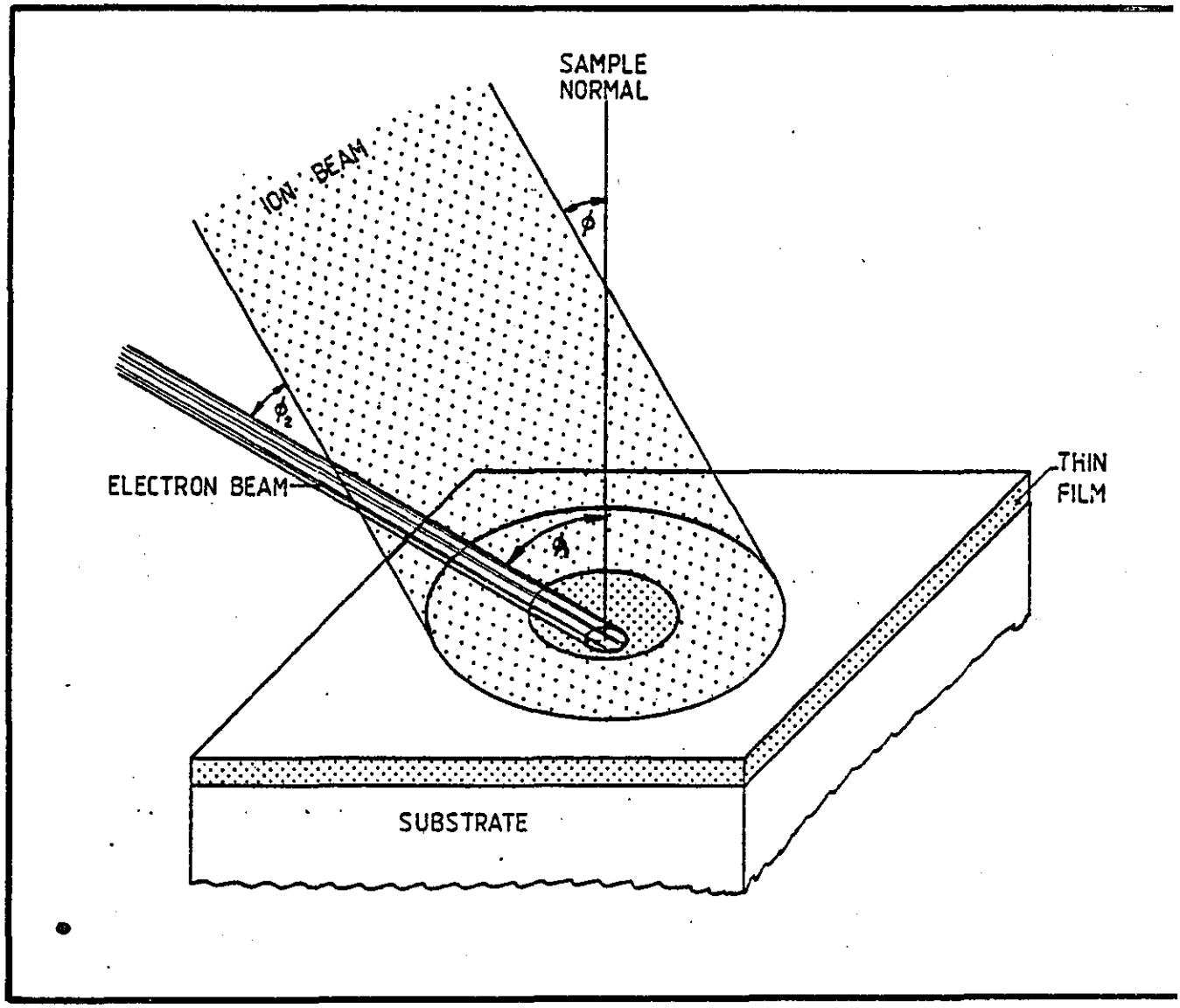

Figure 3.3 The relative positions of the ion and electron beams when depth profiling through a thin film

of the profiles, which deteriorates with increasing depth. The factors which influence the depth resolution in sputter depth profiling may be divided into instrumental or geometrical ones and those due to the sputtering process itself.

3.2.1 Geometrical effects

Geometrical effects arise from a non-uniform ion current distribution, and misalignment of the electron and ion guns (Malherbe et al 1981, Duncan et al 1982). Attempts have been made to correct for such effects analytically (Hoffman 1975, Tsong et al 1980), but they can be almost eliminated by improved experimental techniques. Non-uniformity of the ion beam should not cause a problem so long as its diameter is much greater than that of the electron beam. Redeposition is another problem associated with the crater edge and refers to the sputtering of atoms from the crater wall and their subsequent transfer to the floor of the crater.

3.2.2 The sputtering process

Artefacts of the sputtering process itself have been reviewed by Coburn (1976) and Holloway and Bhattacharya (1981). The elemental composition of a sputter etched crater will in general be different from that of the bulk material due to the substantial differences in the sputtering yields of various elements. The surface coverage of elements with high sputtering yields is decreased and enriched with elements of low sputtering yields (Holloway and Nelson 1979, Tompkins 1979).

Ion bombardment can cause motion of atoms in the specimen material by collisional mixing (Sigmund and Gras-Marti 1980) and radiation-enhanced diffusion (Rivaud et al 1982). Collisional mixing is the collective name for the two separate effects of recoil implantation (Sigmund 1979) and

cascade mixing(Andersen 1979) . Recoil implantation refers to a direct momentum transfer between the bombarding ion and the target atom producing both a shift and a broadening of the profile. Cascade mixing generally refers to indirect processes involving other target atoms, producing primarily a broadening of the initial profile.

3.2.3 Surface topography

The most important factor affecting the depth resolution of sputter depth profiles, particularly for technological and industrial specimens is the presence of surface roughness. Apart from any initial surface roughness of the specimen, sputtering causes the formation of what is generally referred to as ion-induced microtopography (Laty et al 1979) . Naundorf and Macht (1980) found that surface roughness increased as a function of sputtered depth for copper bombarded with various low energy ions. The degree of surface roughness produced was much less in the case of single crystal than polycrystallic specimens. A review of the surface changes which are induced by ion bombardment is given by Navinsek (1976).

The presence of impurities gives rise to local variations in sputtering yield which can lead in extreme cases to the formation of cones (Wehner and Hajicek 1971) . In the case of polycrystalline metals grain boundaries and dislocations become delineated as furrows or pits. Each grain shows characteristic fine etch features, or facets, which reveal the crystalline orientation. As well as any intrinsic defects, ion-induced dislocations (Webber and Walls 1979) can occur even on homogenous and isotropic specimens having a smooth initial surface. These effects do not occur on amorphous materials, or on semiconductors which tend to become amorphous during ion bombardment (Dennis and Hale 1976).

The sputtering yield is a sensitive function of angle and so for a

monodirectional ion beam the etch rate will be different at differently inclined microslopes. This leads to further modification of the surface topography. Smith and Walls (1979) have given a three dimensional theory which accounts for the development of surface topography on amorphous surfaces and leads to some recommendations regarding the optimum conditions for depth profiling. The theory has been extended to include crystalline materials by Smith et al (1981).

Since the sputtering yield is a sensitive function of angle, the formation of ion-induced surface roughness could be suppressed by rotating the specimen. However this is impractical due to the technical difficulties associated with ultra high vacuum, and the limitations of current sample manipulators. Sykes et al (1980) have described a system employing two ion guns, symmetrically inclined to the sample normal, which produced a significant improvement in the depth resolution of profiles through a Ag/Cu multilayer sandwich. This improvement may be attributed to a suppressio of ion-induced microtopography, confirmed using scanning electron microscopy by Makh et al (1982) who also considered the problem theoretically and accounted for the difference in topography observed.

4. Crater-edge profiling

In this form of sputter depth profiling the wall of the crater formed under ion bombardment is used as a taper section through the specimen. Taylor et al (1976) have used the technique to examine the interface region of phosphorous-doped silicon/silicon oxide films. The slope of the crater is determined by the current density of the incident ion beam, which can be measured with a Faraday cup. Taylor et al obtained an angle of 1.3×10^{-3} degrees at the interface for a crater with a maximum depth of about 1200Å. Crater-edge profiling is well suited to high resolution scanning Auger systems and is useful for many semiconductor device applications. For

example, van Oostrom et al (1980) have used the technique for the characterization of epitaxially grown films on GaAs substrates to depths of about 1 μm.

If the current density of the ion beam is assumed to have a Gaussian distribution then the cross-section of the crater should have a similar shape. According to Zalar and Hofmann (1980) the maximum slope for a Gaussian profile is given by

$$\tan \alpha_m = 0.6\left(\frac{Z_o}{x_\sigma}\right) \qquad (3.3)$$

where Z_o is the depth of the crater at the centre and x_σ is the x value corresponding to the standard deviation σ of the Gaussian function. Zalar and Hofmann used a multilayer Ni/Cr sandwich of known thickness to evaluate the slope of the crater. A layer thickness of 11.5 nm was magnified to 60μm on the X scale giving a magnification of $\tan \alpha_m = 1.93 \times 10^{-4}$, so that $\alpha_m = 1.23 \times 10^{-2}$ degrees. This gives a value for x_σ of 0.72mm for Z_o = 230 nm, corresponding to an ion beam diameter (full width at half maximum (FWHM) = 2.35σ).

Although the taper angles for crater-edge profiling appear to be some two orders of magnitude smaller than those involved in conventional angle-lapping or ball-cratering, it must be remembered that much shallower depths are involved. The maximum angle α_m is shown in figure 3.4 as a function of the crater depth Z_o for various ion beam diameters. In the case of an ion beam diameter of 1mm (FWHM) the taper angle reaches 1 degree at a depth of about 12 μm.

5. Taper-sectioning techniques

Taper-sectioning techniques have been used over a number of years for a variety of purposes, including the characterization of surface roughness (Bowden and Tabor 1973). The specimen is electroplated with a layer of

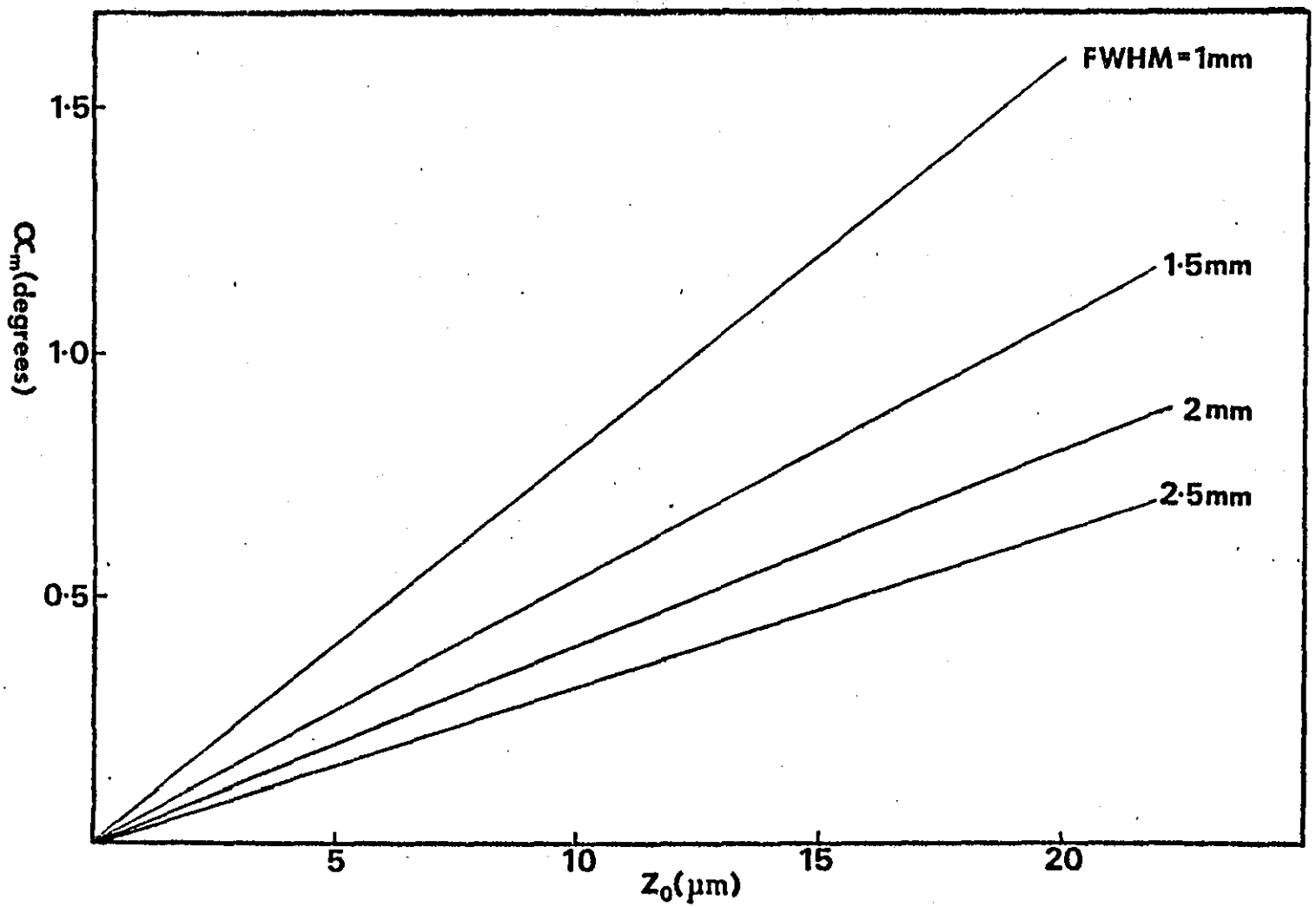

Figure 3.4 The maximum angle α_m of the crater wall in crater-edge profiling as a function of the total depth Z_0 for a range of ion beam diameters

metal of approximately the same hardness, and is then cut and polished at a small angle to the surface. The section may then be examined by optical or electron microcsopy. Angles used in this case are relatively large, typically 6 degrees, which produces a magnification of ten times.

Similar angle lapping techniques have been used in combination with electron probe microanalysis (EPMA) for the examination of composition gradients. Hutchins (1974) gives an example of a 3 degree lap used in the characterization of a flux-grown crystal. The chief drawback of this approach is the poor depth resolution of the EPMA due to the relatively large depth, the order of 1 μm, to which X-rays are excited. It is desirable to make this depth as small as possible by using low accelerating voltages and soft X-rays for the analysis.

Another important application of angle lapping is its use in combination with the spreading resistance technique (Mazur and Gruber 1981) for the determination of the depth distribution of dopants in silicon. To obtain the best resolution the taper angle should be as small as possible. Severin et al (1975) have described a lapping and polishing jig which can achieve angles of less than 0.1 degrees. The measurement of such small angles is difficult, but is normally carried out using some form of optical interference technique (Tong et al 1972).

5.1 Angle lapping and Auger electron spectroscopy

Tarng and Fisher (1978) combined the angle lapping technique with Auger electron spectroscopy, using a taper of 0.5 degrees for the analysis of thick insulating multilayers. A similar approach has also been used by Chubb et al (1980) in the characterization of single and multilayer coated carbide cutting tools. The geometry of an ideal angle lapped specimen is shown in figure 3.5. The specimen is lapped and metallographically polished at a small angle $\emptyset$ to the surface to reveal the entire depth to be

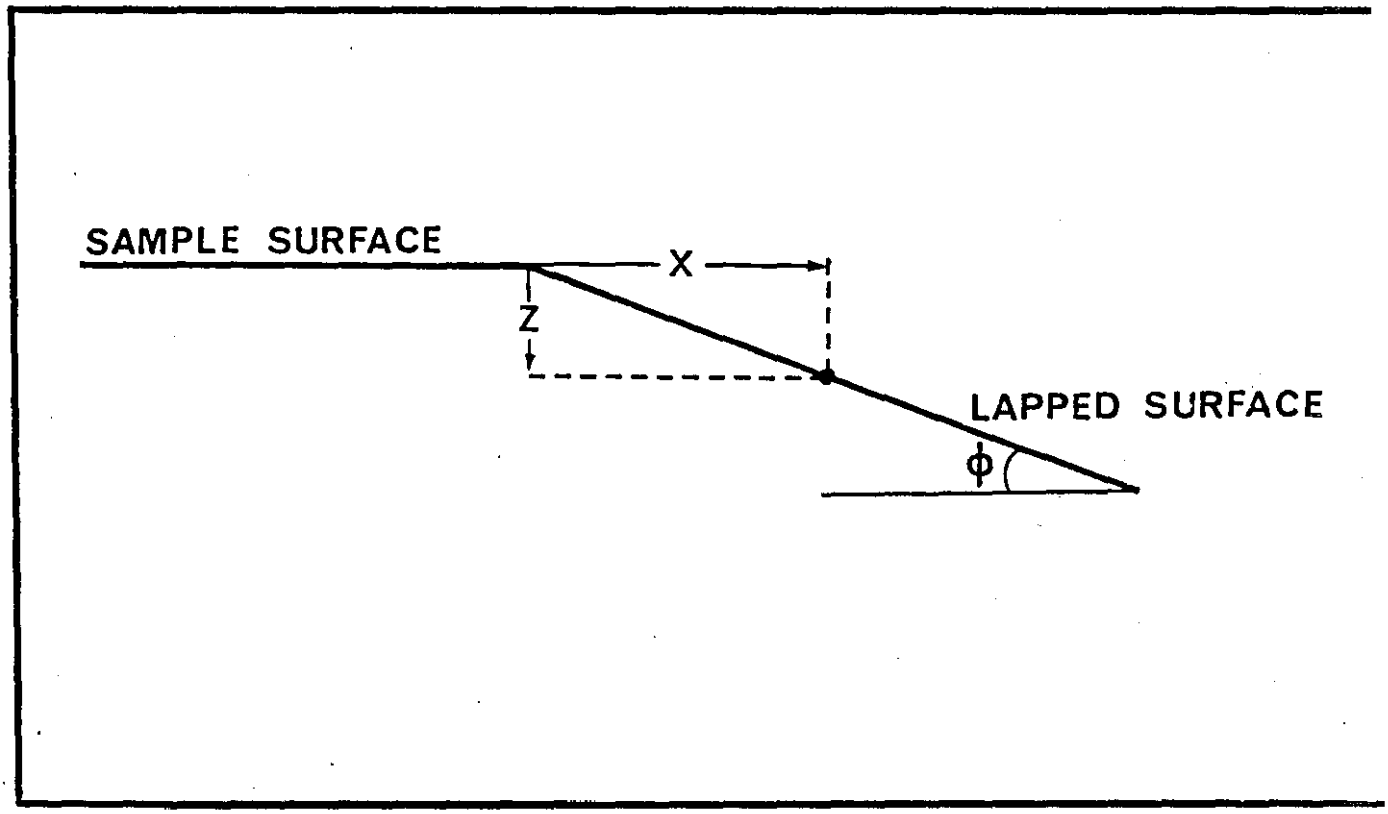

Figure 3.5 A schematic diagram illustrating the geometry of an angle-lapped surface

profiled. The depth at any point on the taper is x tan ϕ where x is lateral distance from the edge. The taper effectively provides a magnification of the revealed region of cotan ϕ. The production of the small angles required for depth profiling, 0.5 degrees or less, is not routine and cannot be measured readily. An important disadvantage of the technique is that it is, in general, limited to perfectly flat samples.

Moulder et al (1979) have described a technique whereby thick film structures are cut and polished perpendicular to the surface, giving a cross-section of the specimen. However, as the section is not magnified at all, it is necessary to use a very fine electron beam in the subsequent analysis.

5.2 Ball-cratering

Happ and Shockley (1956) described a forerunner of the technique which involved the cutting of a cylindrical groove for the measurement of the depth of diffused layers in silicon. A cylinder is rotated against the specimen in the presence of a fine abrasive to produce a groove of well defined geometry. The method was evaluated by McDonald and Goetzberger (1962) and compared with conventional angle lapping techniques.

Ball-cratering provides a means for producing a spherical crater in the specimen surface and was first reported by Thompson et al (1979). It was used in combination with Auger electron spectroscopy to obtain a composition-depth profile of a TiN coating on a steel substrate. Walls et al (1979) further illustrated the usefulness of the technique, and recognised the advantages of combining ball cratering with sputter ion etching for the analysis of deep interfaces.

5.2.1 Geometry

The principle of the technique is illustrated in figure 3.6. A rotating bearing steel ball coated in fine diamond paste is used to abrade a spherical crater in the sample surface. The ball rests in the V-shaped groove of a hardened steel shaft and is made to rotate against the specimen which is mounted on an inclined table, the angle of which controls the load. The mass of a 3 cm diameter steel ball is 110 grams, giving loads on the specimen typically in the range 20 to 70 grams force.

The spherical geometry of the crater (figure 3.7) allows the depth d to be determined simply from a measurement of the diameter, since

$$\left(\frac{D}{2}\right)^2 = d(2R-d) \qquad (3.4)$$

$$\frac{D^2}{4} = 2Rd-d^2$$

Therefore

$$d = \frac{D^2}{8R} \qquad (3.5)$$

if $R \gg d$ where R is the radius of the ball.

Ball cratering is a useful means for measuring the thickness of a thick film or surface coating. The thickness t is given by

$$t = \frac{D^2 - D_s^2}{8R} \qquad (3.6)$$

where D_s is the diameter of the revealed substrate region.

The spherical geometry of the crater is illustrated in figure 3.8 which shows an interference micrograph of a typical crater. For a spherical surface the radius of the dark fringes r is related to the fringe number

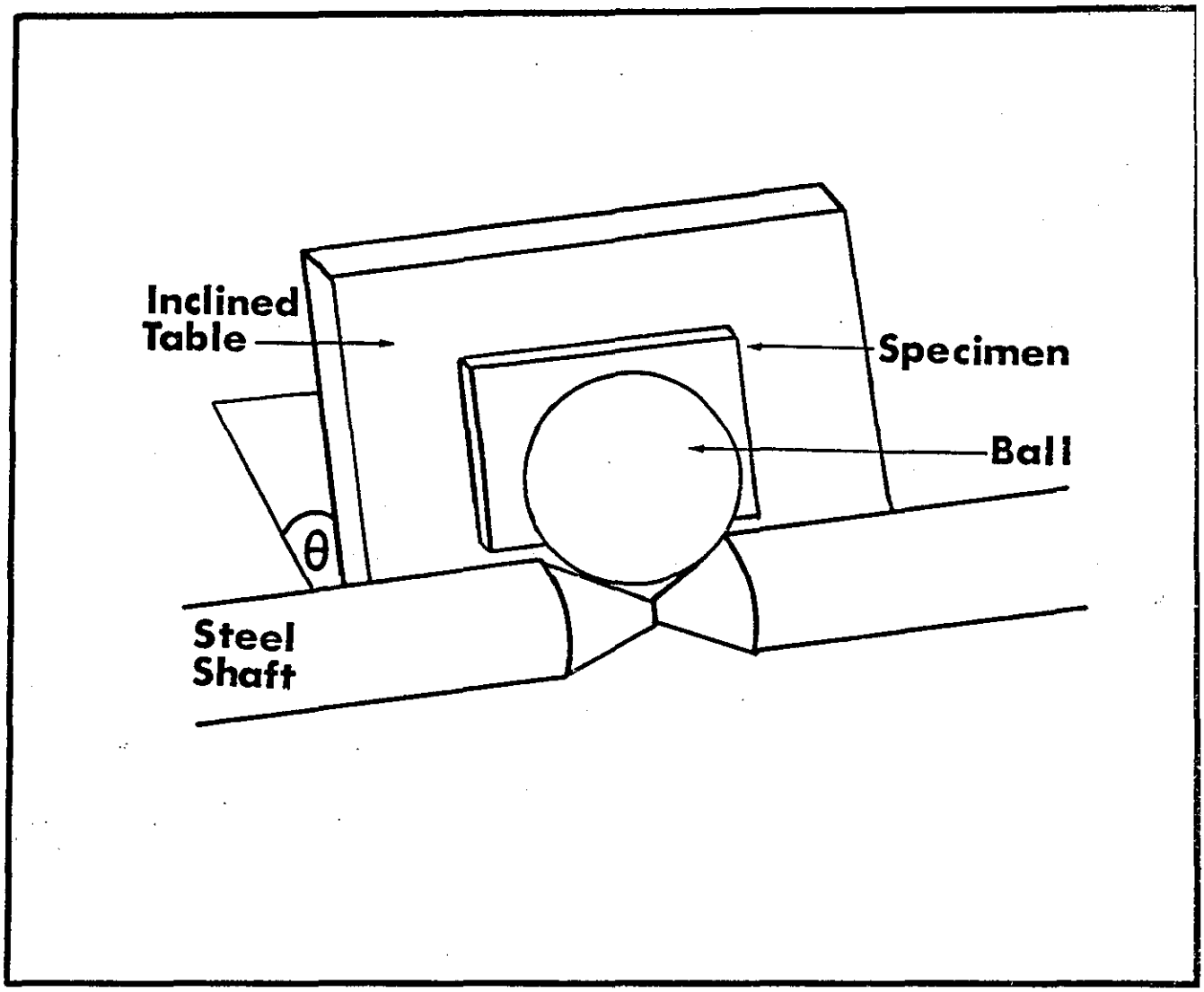

Figure 3.6 A schematic diagram showing the essential features of the ball-cratering instrument

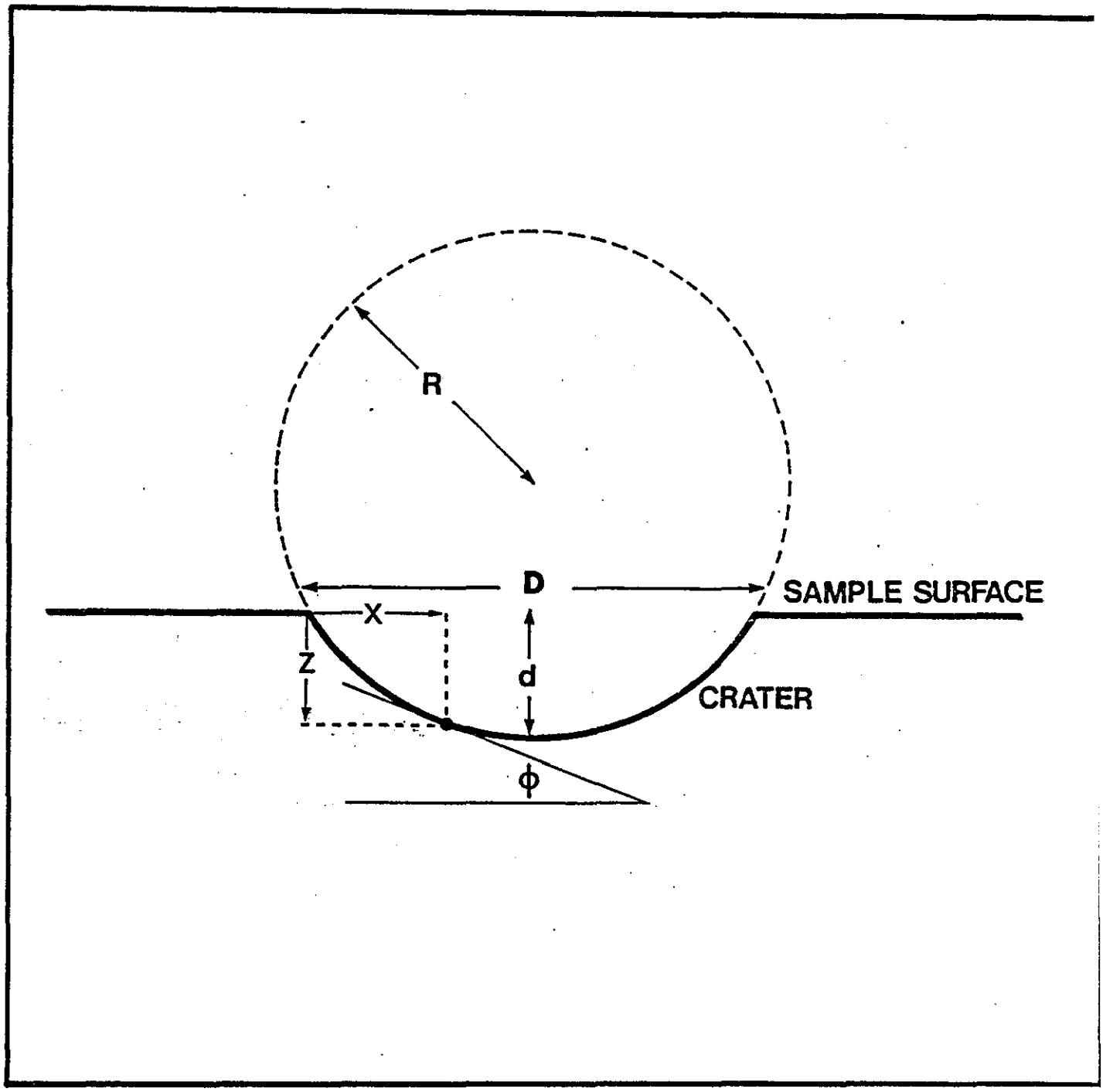

Figure 3.7 A schematic diagram illustrating the spherical geometry in ball-cratering

n by the equation

$$r^2 = n R \lambda \qquad (3.7)$$

where R is the radious of curvature of the surface, and λ is the wavelength of light used.

The corresponding plot of r^2 against n, shown in figure 3.8, is found to be a straight line, and confirms the sphericity of the crater.

5.2.2 Composition-depth profiling

Combining the ball-cratering technique with Auger electron spectroscopy enables composition-depth profiles to be obtained. The probing electron beam may be electrostatically scanned across the crater to give elemental linescans, or full spectra can be taken at a series of positions on the crater wall. Although the gradient of the taper is not constant as in simple angle-lapping, the depth at the point of analysis may still be found by measuring the lateral distance x from the crater edge.

$$\begin{aligned} x(D-x) &= Z\,(2R-d-(d-Z)\,) \qquad (3.8) \\ &= Z\,(2R-2d+Z) \\ &= 2Z(R-d) + Z^2 \end{aligned}$$

For small z, $\quad Z = \dfrac{x(D-x)}{2(R-d)} \qquad (3.9)$

The gradient $\tan \phi$ at depth z is given by

$$\tan \phi = \frac{D-2x}{2(R-d)} \qquad (3.10)$$

The angle ϕ is shown as a function of the lateral distance $(\frac{D}{2} - x)$ from the centre of the crater in figure 3.9 for various values of the ball radius R. Over this range the angle increases almost linearly, and for a

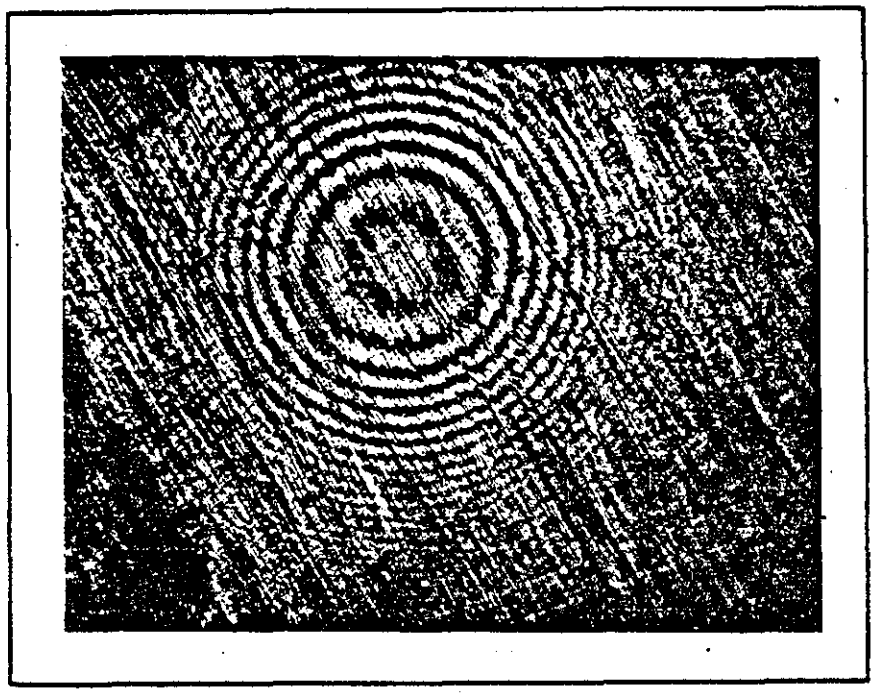

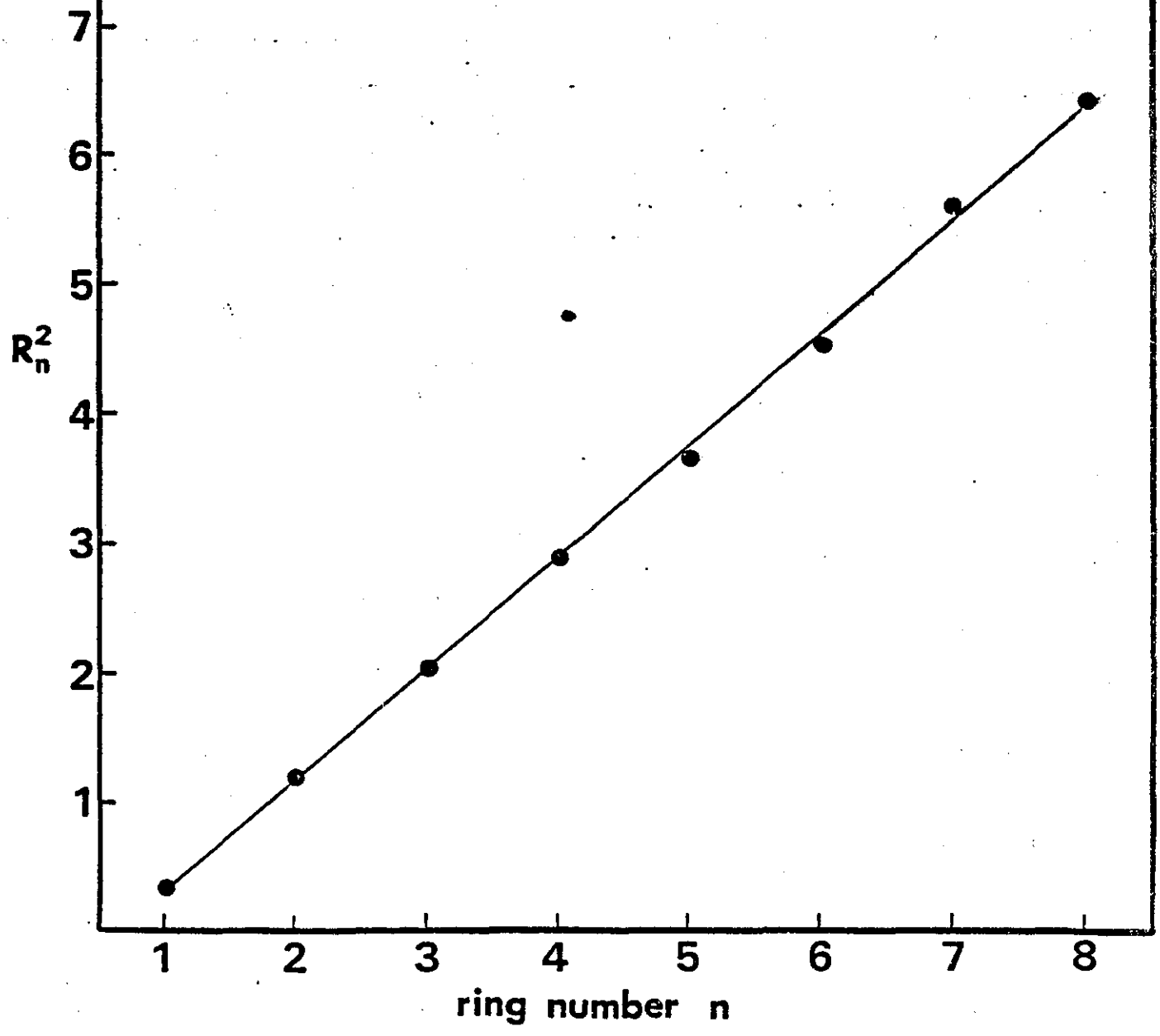

Figure 3.8 An interference micrograph of a typical crater surface together with the corresponding plot of the square of the ring radius as a function of the ring number

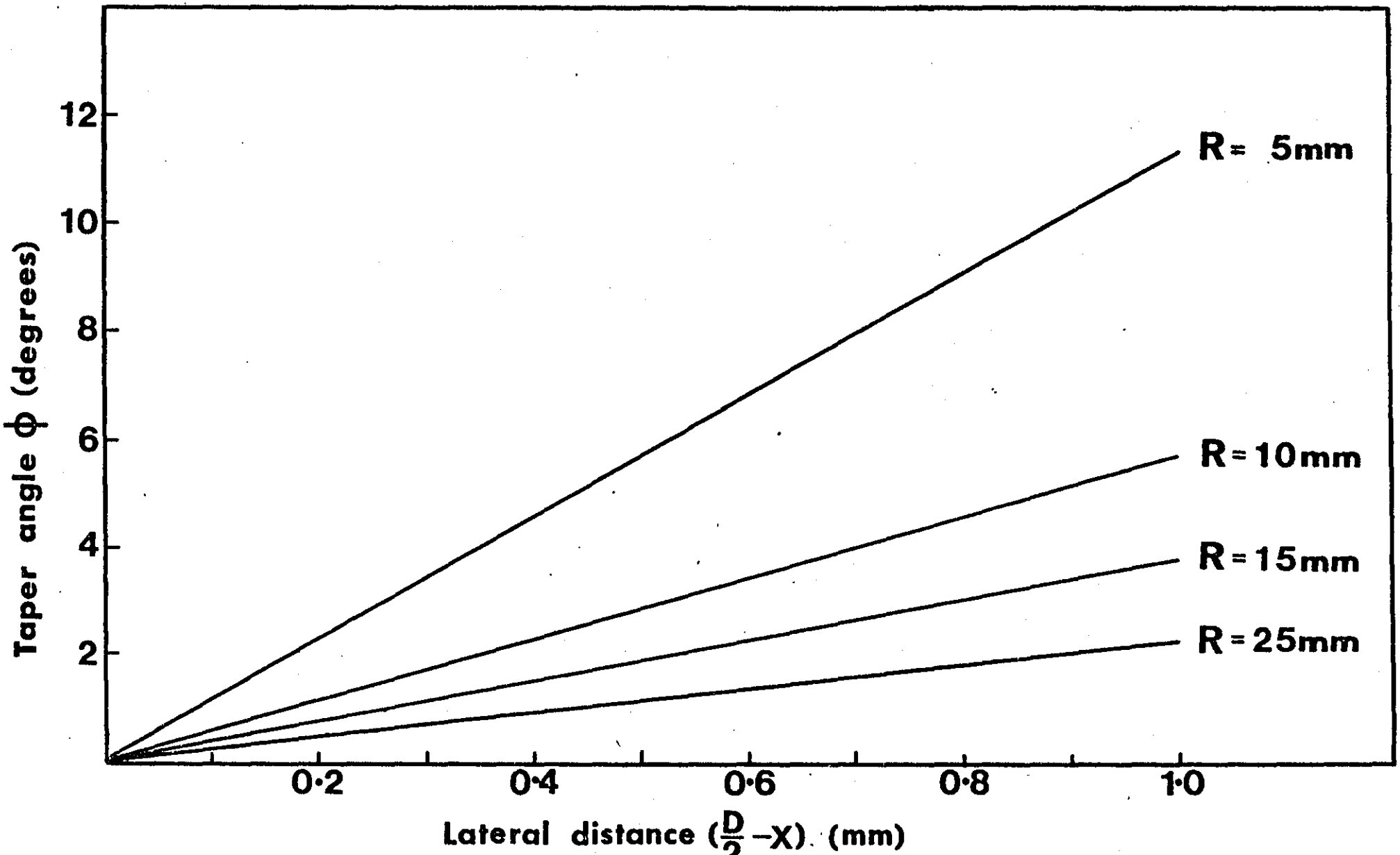

Figure 3.9 The dependence of the taper angle ϕ with distance from the centre of the crater in ball-cratering for a range of ball sizes

30 mm diameter ball is less than 1 degree within 0.2 mm of the centre.

The special geometry of ball cratering gives it an advantage over the ordinary angle lapping technique since the gradient at the base of the crater becomes vanishingly small. During depth profiling it can be arranged for a coating-substrate interface, or some other region of specific interest, to be located towards the centre to give the maximum magnification, and correspondingly the best depth resolution.

6. Discussion

The combination of ion etching and surface analytical techniques is the most widely used means for obtaining composition-depth profiles. However there are several artefacts of the sputtering process which give rise to the formation of surface microtopography and impair the depth resolution. This, together with the relatively slow rate of material removal, makes sputter ion etching unsuitable for profiling to depths of more than a few microns. Profiles to greater depths are best achieved using taper-sectioning techniques in combination with Auger electron spectroscopy. The principles of these techniques have been described, with emphasis on ball cratering, and the means for obtaining composition-depth profiles have been outlined. The particular geometry of ball-cratering gives it several advantages over conventional angle lapping techniques. The precise position of analysis can be chosen more accurately, it can be used on curved surfaces, and the gradient at the base of the crater becomes vanishingly small.

Chapter 4 DEPTH RESOLUTION

1. Introduction

The definition of depth resolution which is used in sputter depth profiling forms the basis of that which will be used to characterise profiles obtained using taper sectioning techniques. In view of this the theoretical models for sputtering are first reviewed, and the other factors which affect the depth resolution of sputter depth profiles are mentioned. The main contributions to the depth resolution in profiles obtained with taper-sectioning techniques are then discussed. A model system is used for a series of experiments aimed at defining the relative importance of these contributions in profiles obtained using ball cratering and Auger electron spectroscopy.

2. Sputter depth profiles

2.1 The sequential layer sputtering model

The dependence of depth resolution on sputtered depth can be estimated from the sequential layer sputtering (SLS) model proposed by Benninghoven (1970, 1976). This states that the probability of sputtering is the same for all atoms in any layer which have become exposed during sputtering, and that the sputtering yield is the same for all layers independent of composition. The contribution to the depth resolution, at depth Z, due to the sputtering process has been derived by Hofmann (1976)

$$\Delta Z_s = 2(az)^{\frac{1}{2}} \qquad (4.1)$$

where a is a measure of the layer thickness. This equation is only applicable for $\frac{z}{a} \gtrsim 8$.

When sputtering through a sharp interface the SLS model predicts a profile having the shape of a Gaussian error function. The broadening of the interface (ΔZ) is defined as twice the standard deviation of the Gaussian. This corresponds to the width between the intensity at 84% of the maximum signal and that at 16%.

Hofmann (1977) showed that the depth resolution as given by the SLS model agreed well with a number of experimental results obtained by different authors, for example Ho and Lewis (1976), Mathieu et al (1976) and Hofmann and Zalar (1976). However it now seems that this agreement may have been fortuitous since equation 4.1 does not incorporate the contributions to the depth resolution of other factors such as knock-on effects and topographical changes. It is likely that such agreement occurs because the result is coincidentally a good description of the combined effects in sputtering (Seah and Lea 1981) .

Roll and Hammer (1978) obtained results for multilayer films which obeyed the empirical formula

$$Z = \alpha + \beta Z^{\frac{1}{2}} \qquad (4.2)$$

According to Roll and Hammer the additional constant term α was due to the initial roughness of the interface. Hofmann and Zalar (1979b) also found a deviation from equation 4.1 at small z, but they attributed this to the depth independent contribution of the Auger electron escape depth.

2.2 Criticisms of the SLS model

Wittmaack and Schulz (1978) have presented evidence against the sequential layer sputtering model such as the results of Hofer and Liebl (1975) who found that Δz remained approximately constant with depth after an initial increase. Wittmaack and Schulz concluded that the parameter 'a' in

equation 4.1 could not be regarded as a constant, and that it decreased with depth. This indicates that bombardment induced atomic mixing and the original surface roughness play important roles. However the results of Hofer and Liebl and the later ones of Hofer and Martin (1978) were obtained with rather higher energy ($\sim$ 10 KeV) ions than those used in the compilation of Hofmann, and so do not satisfy the requirements for 'soft' sputtering implicit in the SLS model.

Werner (1982) proposed a relation of the form

$$\Delta z = \alpha + \beta z^{\gamma} \qquad (4.3)$$

where α accounts for the intrinsic specimen contribution to the depth resolution due to effects which are present at z=o or are independent of depth, including initial surface roughness. β includes all instrumental effects, and the development of surface roughness as a result of processes such as preferential sputtering. Werner concluded then an 'ad hoc' compilation of the results of different authors is inappropriate since different values of α, β and γ may exist depending on the specimen composition and the instrumental set up.

2.3 Modifications to the SLS model

The main assumptions of the SLS model have been considered by a number of authors in order to improve the model. The sputtering yield of each individual event is not constant, but is only on average equal to the measured sputtering yield. Shimizu (1979) suggested that since the sputtering process consists of two mechanisms, ion bombardment and sputtering, it should be treated as a conditional probability. He incorporated the sputtering yield into equation 4.1 such that

$$\Delta Z = 2 \left[aZ (1 + y) \right]^{\frac{1}{2}} \qquad (4.4)$$

where y is the sputtering yield. For the assumption of soft sputtering

$(y \rightarrow o)$ the above equation reduces to that of Hofmann.

Erlewein and Hofmann (1980) incorporated the effects of atomic migration into the SLS model, and predicted that there was a tendency for Δz to become constant at greater depths.

In the original SLS model the probability of sputtering was considered to be independent of atomic position. However it is clearly influenced by the occupancy of neighbouring sites, and is dependent on the binding energy. A atomic coordinate dependent sputtering rate has been incorporated into the SLS model by Seah et al (1981), who also found that the depth resolution remained constant for more than 10 atomic layers.

We may conclude from the above that the modified SLS contribution to the depth resolution does not increase as the square root of depth, but is constant and may in practice be dominated by instrumental, topographical and atomic mixing effects.

2.4 Other contributions to the depth resolution

In addition to the contribution Δz_s from the basic sputtering process, there are a series of other factors which contribute to the total depth resolution in a real system. Ion bombardment also causes a certain amount of roughening of the surface, and there are knock-on and ion mixing effects. The initial roughness of the specimen surface, the finite depth resolution of AES due to the escape depth of electrons, and a number of instrumental effects also determine the magnitude of the depth resolution (Hofmann 1980, 1981). The measured depth resolution Δz is a function of all these different contributions ΔZ_i. If they are mutually independent then they may be added according to the general error law by a quadratic sum (Hofmann 1977).

$$\Delta Z = \left[\sum_{i=1}^{n} \Delta z_i^2 \right]^{\frac{1}{2}} \qquad (4.5)$$

Seah and Lea (1981) have examined the depth resolution of composition-depth profiles obtained by ion sputtering for single and multilayer films on real substrates. They found that the observed broadening depends on the orientation of the surface peaks as well as the magnitude of the roughness. The broadening also depends on the orientation of the ion beam, and the best resolution is obtained at normal incidence. The broadening of the interface is given by the quadratic sum of the sputter broadening and that due to the initial roughness of the interface, Δz_I (Lea and Seah 1981)

$$\Delta Z = \left[(\Delta Z_s)^2 + (\Delta Z_I)^2 \right]^{\frac{1}{2}} \qquad (4.6)$$

Carter et al (1982) have reviewed theoretical models of surface topography development and atomic mixing, and describe some new approaches. It is shown that the depth resolution is a complex function of depth, and that both broadenings and shifts are to be expected. They conclude that, in general, the relationship of the depth resolution with depth cannot be expressed in a simple mathematical form.

3. Taper sectioning techniques

The definition of depth resolution used to characterise composition-depth profiles obtained with taper sectioning techniques follows from that which has been applied to sputter depth profiles. Again it is measured according to the degree of broadening of an initially sharp interface. The two major contributions are that due to the roughening caused by the mechanical lapping process used in producing the taper, and a geometrical term arising from the finite diameter of the electron beam. If Δz_B is the contribution of the electron beam diameter and ΔZ_R is that due to mechanical roughening then

$$z = \left[(\Delta z_B)^2 + (\Delta z_R)^2 \right]^{\frac{1}{2}} \qquad (4.7)$$

Taper sectioning techniques possess an important advantage over ion

etching in that the depth resolution is independent of depth. Although a small amount of sputtering is always necessary to remove the top few layers of contamination, the term due to the sputtering process ΔZ_s is insignificant compared to those mentioned above.

3.1 Geometrical contribution

At any position on the taper the electron beam of diameter b gives rise to secondary electrons from a depth ΔZ_B given by

$$\Delta Z_B = b \tan \phi \qquad (4.8)$$

where ϕ is the taper angle (figure 3.3). The intensity of the electron beam has a Gaussian distribution, and to be consistent the diameter is defined as twice the standard deviation from the position of maximum current density.

The angle ϕ is not a constant in ball cratering (figures 3.5and 3.6) and the electron beam contribution to the depth resolution depends on the precise position of analysis. However this does not present too much of a problem in practice, since ϕ can be expressed (equation 3.9) in terms of the lateral distance from the crater edge.

3.2 Experimental determination

The purpose of this series of experiments is to investigate the principal factors controlling the depth resolution in ball cratering, and to compare the measured resolution with that predicted from the sum of the contributions of the individual factors (Brown et al 1981) . A model system consisting of a hard chrome coating, electrodeposited on to a polished mild steel substrate, was chosen for this investigation. Electroplated coatings of a suitable thickness ($\geqslant 5\ \mu m$) can be produced routinely, and

they provide a sharp interface with a minimum of intermixing. The mild steel substrate was metallographically polished prior to deposition of the coating using various grades of silicon carbide paper followed by 6 μm, 1 μm and finally 0.25 μm diamond polishing wheels. Attempts were made to deposit a number of metals on to the polished substrate but there were problems with most due to poor adhesion. Hard chrome was found to have suitable mechanical properties and strongly adhered to the substrate. The precise thickness of the coating is unimportant but 5 to 10 μm was thought to be suitable. It was found to be 6 μm thick when measured with the ball cratering instrument. An optical micrograph of a ball crater through the electrodeposited hard chrome coating is shown in figure 4.1.

The contribution of the electron beam diameter to the depth resolution depends on the position of the point of analysis on the crater wall. To investigate the effects of surface roughness it was decided to fix this position so that the interface in each case was at a height of 3 μm above the base of the crater. A series of craters was produced in the hard chrome/mild steel specimen to a total depth of 9 μm, using a 30 mm diameter ball and three grades (6 μm, 1 μm and 0.25 μm) of diamond paste.

3.2.1 Auger analysis

Analyses were performed in a varian 10 KeV scanning Auger electron spectrometer. The specimens were cleaned ultrasonically using a suitable solvent, propan-2-ol, before being inserted in the vacuum chamber. Surface contamination was removed prior to analysis by sputtering with 3 KeV argon ions at a current density of 75 μA cm^{-2}. The length of time required for cleaning was typically 1 to 5 minutes.

Composition-depth profiles were obtained by means of elemental linescans across the diameter of the crater. The electron beam energy used was 5 KeV

Figure 4.1 An optical micrograph of a ball crater through an electrodeposited hard chrome coating (thickness 6μm) on a polished mild steel substrate.

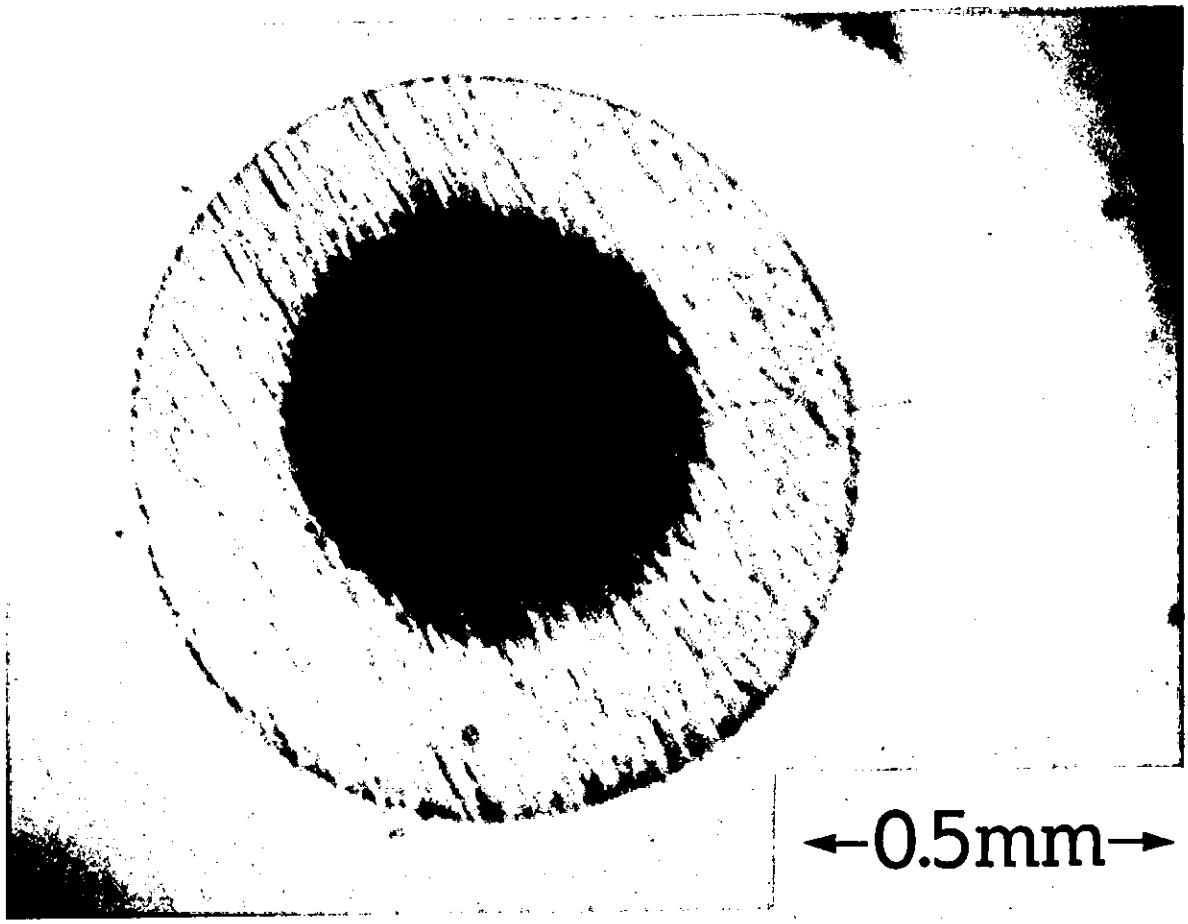
0.5mm

and the beam current 0.5 μA, giving an electron beam diameter of 10 μm. This was measured by performing a linescan across a knife-edge, and measuring the observed broadening (figure 4.2). The electron beam diameter was taken to be the lateral distance over which the signal decreased from 84% to 16% of its maximum, corresponding to twice the standard deviation for a Gaussian beam. Elemental linescans for chromium and iron across the interface region of a typical crater are shown in figure 4.3. The horizontal distance Δx over which the chromium signal decreases from 84% to 16% is indicated.

It is important that the linescans are performed along the diameter of the crater. The use of a scanning Auger spectrometer allows a secondary electron image of the crater to be seen on a T.V. monitor, enabling the position of the electron beam to be located fairly accurately. Figure 4.4 shows the effect of performing linescans along a series of chords of the crater. The diameter corresponds to the linescan where the interface is positioned at the furthest left of this series.

Linescans are normally performed orthogonally to the unidirectional grooves formed by the wear process. However large scratches were sometimes observed in the case of the hard chrome/ mild steel coatings. The effect of this on the depth profile can be seen in the linescan in figure 4.5 (a). Performing the linescan parallel to the direction of the grooves resulted in figure 4.5 (b) which has a more regular shape. The width of the interface, however, and consequently the depth resolution obtained, is the same in each case.

3.2.2 Results

The lateral distance Δx is converted to a depth resolution by means of the equation

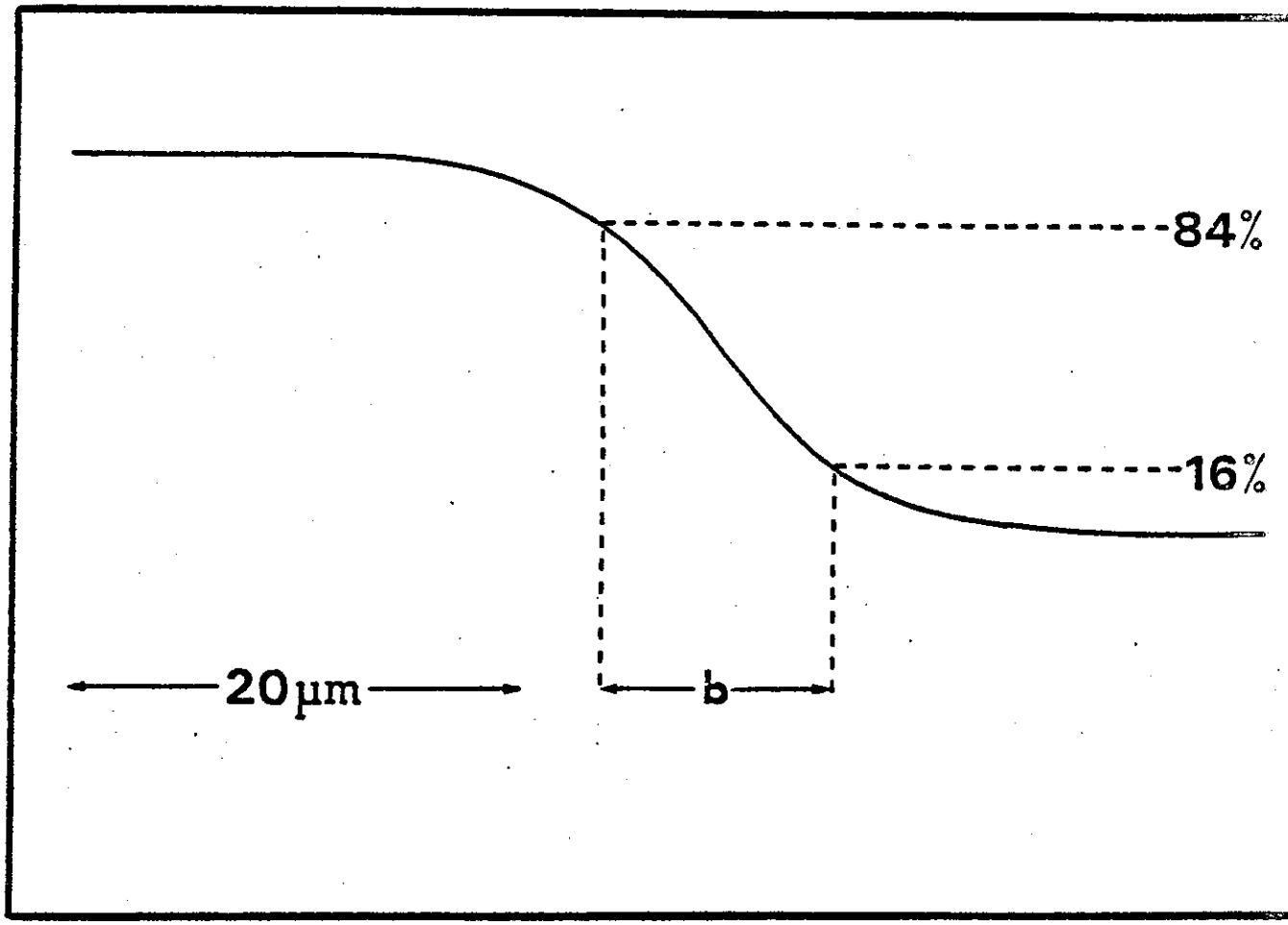

Figure 4.2 An elemental linescan for iron performed across a knife-edge, enabling the electron beam diameter to be determined

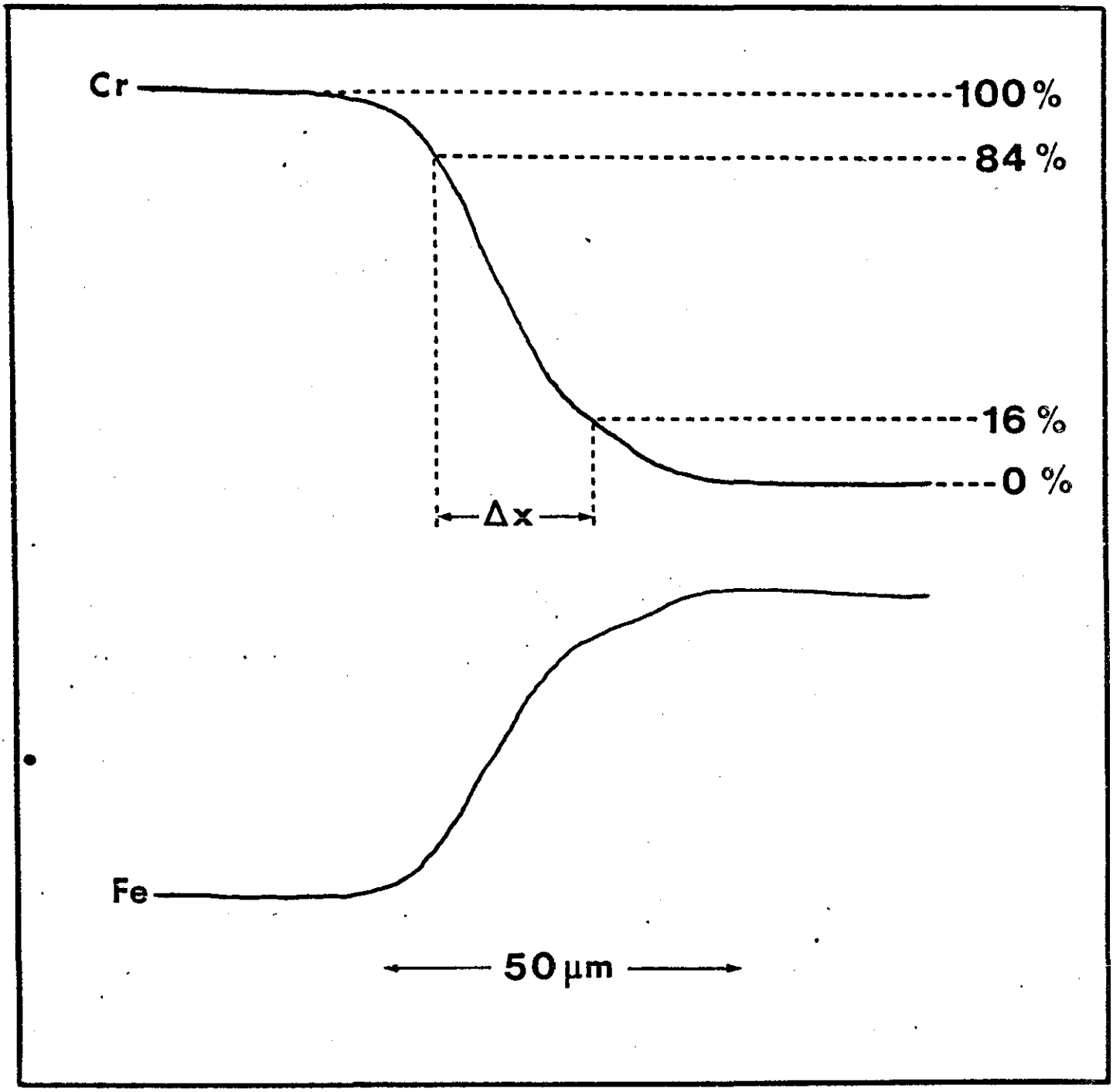

Figure 4.3 Elemental linescans for chromium and iron across the interface region of a hard chrome coating on mild steel illustrating the measurements used to determine depth resolution

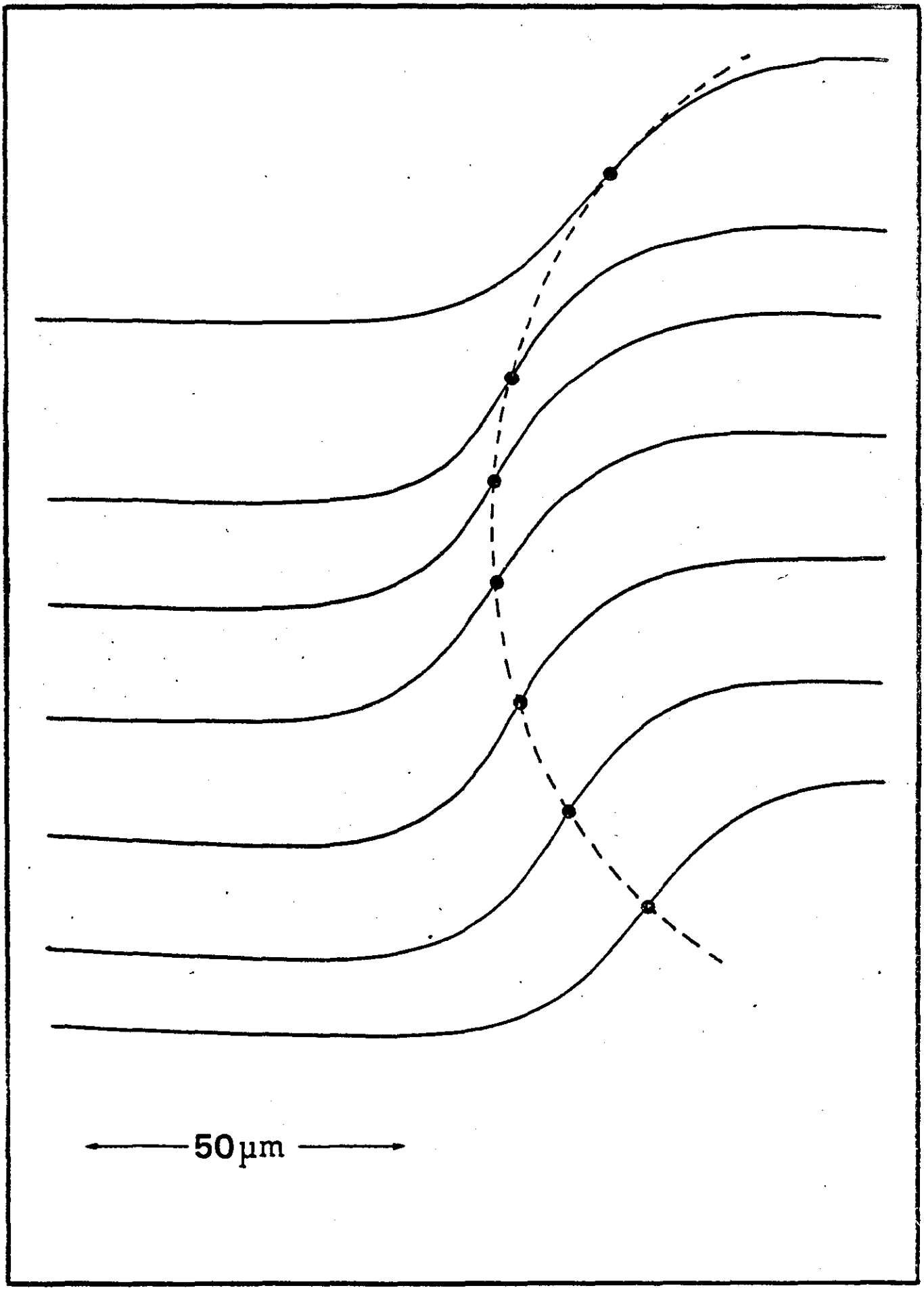

Figure 4.4 Elemental linescans for chromium along a series of parallel chords of the crater. The diameter corresponds to the linescan where the interface is positioned at the furthest left of this series

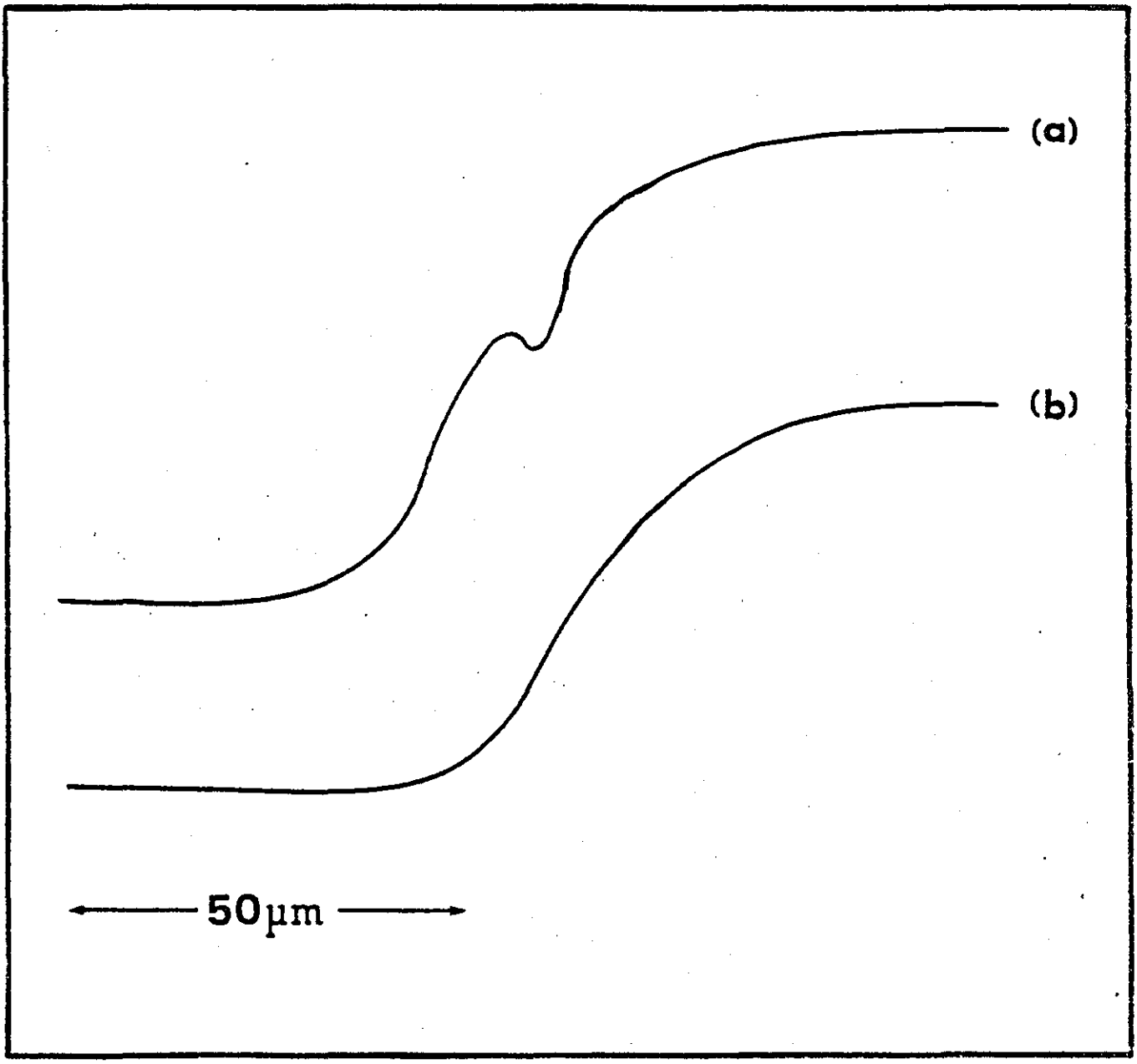

Figure 4.5 Elemental linescans for chromium along perpendicular diameters of the crater (a) orthogonally and (b) parallel to the unidirectional grooves formed by the wear process

$$\Delta z = \Delta x \tan \phi \qquad (4.9)$$

where ϕ is the slope of the crater wall at the point of analysis. For this series of craters the position of the interface was fixed at 3 μm above the base of the crater. This gives a value for $\tan\phi$ of 0.02. Values of the depth resolution obtained with each grade of diamond paste used are given in table 4.1.

The depth resolution in ball cratering can be predicted from equation 4.7 which takes into account the broadening caused by the finite diameter of the electron beam, and that due to the surface roughness produced by the wear process. For real samples there is an additional term due to the initial interface roughness Δz_I. Equation 4.7 now becomes

$$\Delta Z = \left[(\Delta Z_B)^2 + (\Delta Z_R)^2 + (\Delta Z_I)^2 \right]^{\frac{1}{2}} \qquad (4.10)$$

The initial interface roughness, obtained from a Talystep profile of the polished mild steel substrate prior to deposition of the coating, was 25 nm.

The geometrical contribution to the depth resolution ΔZ_B is given by equation 4.8 in terms of the electron beam diameter b and the gradient $\tan\phi$ of the crater at the point of analysis. In this case $b = 10\,\mu$m and $\tan\phi = 0.02$ so that the value of Z_B is $0.20\,\mu$m.

The surface roughness produced by the wear process in ball cratering was measured using a Talystep instrument, having a stylus tip radius of 12.5 μm. Profiles across the mild steel substrate region are shown in figure 4.6 for each grade of diamond paste used. The contribution of the surface roughness ΔZ_R to the depth resolution was defined as twice the standard deviation (2σ) of the surface from the mean position. Values obtained from figure 4.6 were 0.70, 0.20 and 0.025 μm for 6, 1 and 0.25 μm diamond paste respectively. In each case the roughness was much less than the diamond particle size.

DIAMOND PASTE SIZE (μm)	RMS ROUGHNESS ΔZ_R (μm)	INTERFACE ROUGHNESS ΔZ_I (μm)	ELECTRON BEAM CONTRIBUTION ΔZ_B (μm)	DEPTH RESOLUTION	
				EXPERIMENTAL ΔZ (μm)	PREDICTED ΔZ (μm)
0.25	0.025	0.025	0.20	0.27 ± 0.08	0.20
1	0.20	0.025	0.20	0.51 ± 0.16	0.28
6	0.70	0.025	0.20	1.07 ± 0.22	0.73

Table 4.1 The measured roughness of the interface and crater surface, the calculated sampling depth due to the finite size of the electron beam, together with a comparison of predicted and experimentally determined depth resolution

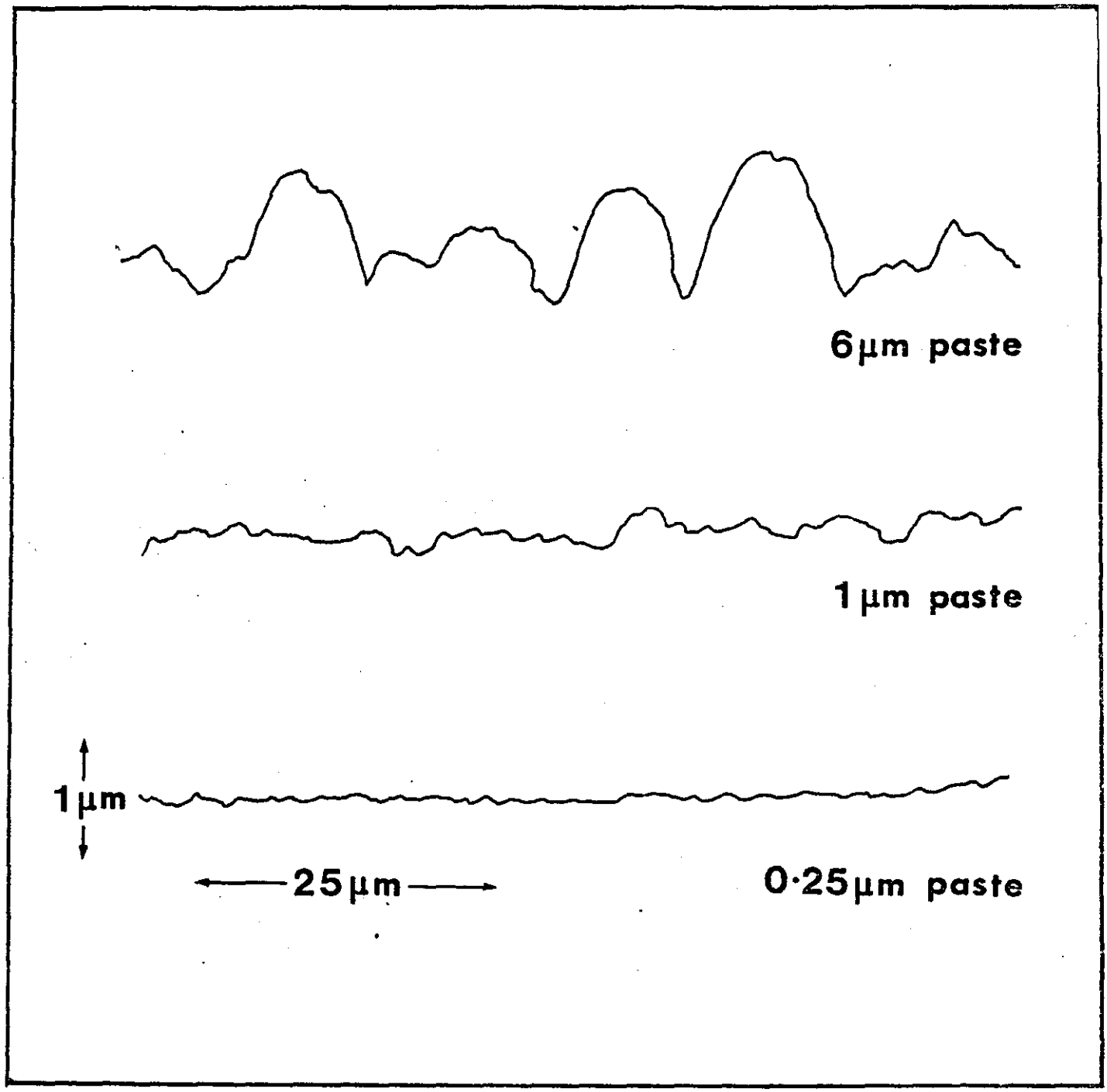

Figure 4.6 Talystep profiles of craters formed on mild steel using various grades of diamond paste

Predicted values of the depth resolution, calculated from equation 4.10, for each grade of diamond paste are given in table 4.1 where they may be compared with the experimental values.

3.2.3 Discussion of results

Although there is good agreement, the predicted values of depth resolution are consistently less than the experimental values. There are two factors which may account for this discrepancy. First, the Talystep will tend to underestimate the magnitude of surface roughness when the periodicity is less than the size of the stylus tip, the error becoming greater as the size of diamond paste is decreased. Secondly, when the periodicity of the surface roughness becomes large in comparison with the electron beam diameter the peak to peak magnitude of the roughness may become more important. In the case of 6 μm diamond paste, for example, the electron beam diameter is comparable with the periodicity of the surface roughness and it is likely that the relevant measure of surface roughness is between the 2σ and peak to peak values.

For craters produced using 6 μm diamond paste the surface roughness of the crater is the major contribution to the depth resolution. When finer diamond paste is used, however, the contribution of the 10 μm diameter electron beam becomes more significant, and it is the limiting factor for the 0.25 μm paste.

Chapter 5 THE WEAR PROCESS IN BALL CRATERING

1. Introduction

One of the most important factors affecting the depth resolution of composition-depth profiles obtained using ball cratering is the surface topography developed in the crater. The ultimate surface finish is determined by the nature of the wear processes involved. These processes depend on the operating conditions, including the abrasive size used, and the mechanical properties, particularly the hardness, of the specimen material. In view of this a survey of the likely wear mechanisms is presented, and a series of experiments is undertaken in order to determine the relative importance of these mechanisms.

Ball cratering is a good means for measuring the wear rate, and enables the value of the wear coefficient to be determined. This can provide useful information concerning the nature of the wear mechanisms occurring in each case. The worn surface is examined using the scanning electron microscope and stylus measuring techniques.

2. Mechanisms of wear

Wear is generally classified into four main categories (Rabinowicz 1965). These are adhesive wear, abrasive wear, corrosive wear and surface fatigue wear. Other processes such as fretting and erosion are sometimes classified as types of wear (Eyre 1978) , but the former occurs as the result of the combination of other wear mechanisms while erosion by impinging particles is not strictly a form of mechanical wear.

Adhesive wear is the most common form of wear and occurs whenever one material is slid over the surface of another or is pressed against it. Abrasive wear occurs when a rough hard surface slides against a softer

surface to produce a series of grooves. Corrosive wear can occur when sliding takes places in a corrosive environment. It does not occur unless the sliding materials react chemically with the atmosphere or lubricant in which they operate. Surface fatigue wear can take place during a repeated sliding or rolling process. Repeated loading and unloading cycles may lead to the formation of subsurface cracks, eventually causing the break-up of the surface and the production of large wear particles. It can only occur when the other forms of wear are very low, otherwise the surface material will be continuously removed before it can become fatigued.

The two dominant wear mechanisms as far as ball-cratering is concerned are abrasive wear and adhesive wear. Abrasive wear arises primarily as a result of the diamond paste introduced between the ball and the specimen, while adhesive wear occurs to some extent in all systems where two solids are in contact with each other.

2.1 Adhesive wear

When one material slides against the surface of another local plastic deformation takes place at the contacting asperities, and adhesion occurs at a certain proportion of these contacts. The junctions rupture at their weakest point, resulting in material transfer or the formation of loose wear particles. This situation is illustrated in figure 5.1. However the creation of wear particles is a relatively rare event, and the separation of the contacting surfaces is most likely to occur at the interface.

From studying the results of many experiments, carried out mainly with unlubricated metals, the laws of adhesive wear can be expressed empirically as follows (Halling 1976)

1. The volume of wear is proportional to the distance of sliding L
2. The volume of wear is proportional to the applied load W

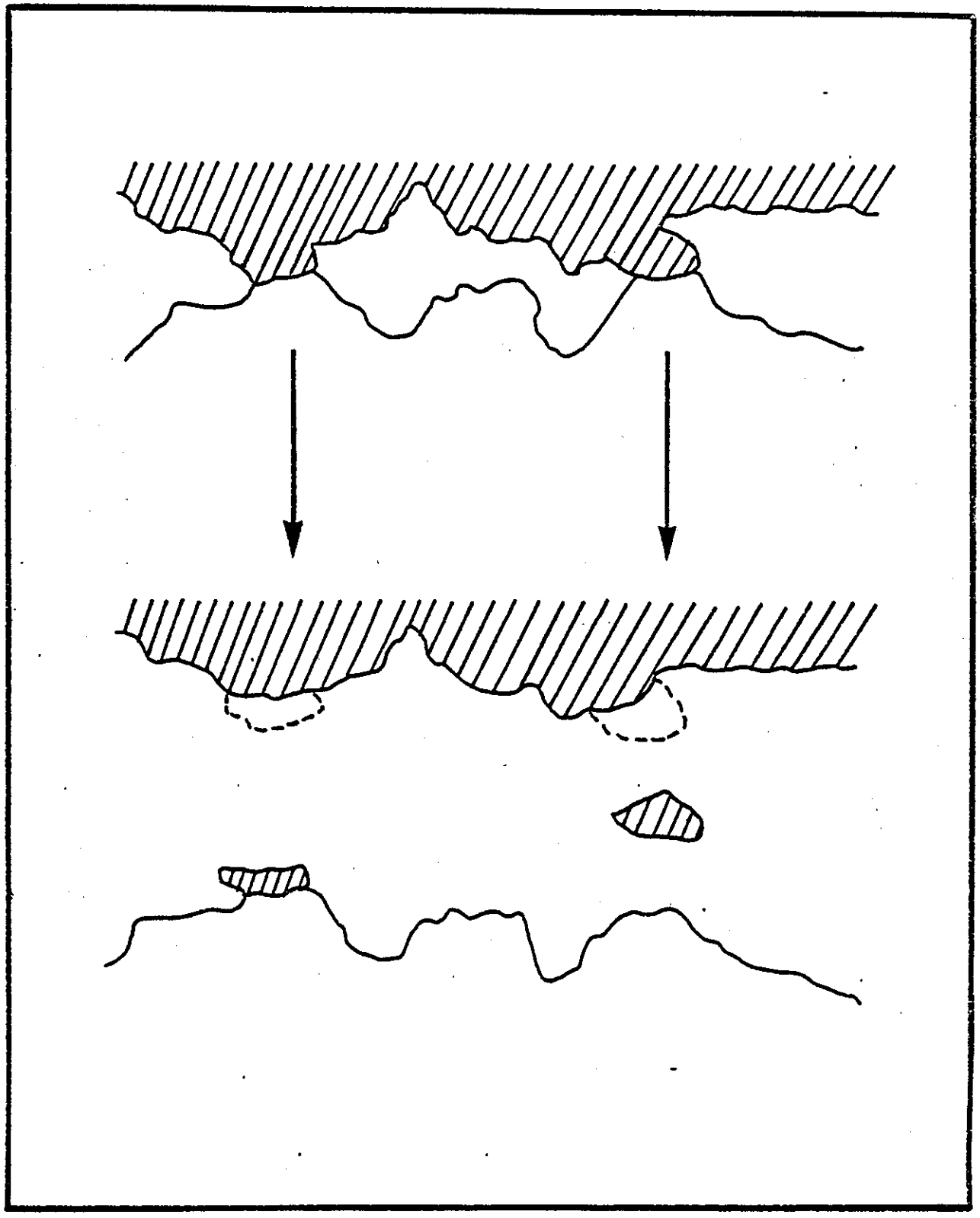

Figure 5.1 A schematic diagram of the adhesive wear process which results in material transfer or the formation of loose wear particles

3. The volume of wear is inversely proportional to the hardness H of the softer material.

These laws may be expressed in the form

$$V = C \frac{W}{H} L \qquad (5.1)$$

where C is a non-dimensional constant.

Archard (1953) derived the above equation by considering a model for the sliding process. He assumed that when two asperities come into contact to form a junction there is a constant probability K that a wear fragment will be formed. The constant of proportionality in equation 5.1 is now replaced by K/3 so that

$$V = \frac{K}{3} \frac{W}{H} L \qquad (5.2)$$

where K is the adhesive wear coefficient, usually referred to as the Archard constant.

Typical values of the wear coefficient for metals under clean and lubricated conditions are given in Table 5.1 (Rabinowicz 1965). Lubrication prevents or minimises the contact between the sliding surfaces, reducing the number of asperities in contact and so reducing the probability of creating a wear particle.

2.2 Abrasive wear

When a rough hard surface slides against that of a softer material the hard asperities dig into the softer surface to produce a series of grooves. This process, which is generally referred to as two body abrasive wear, is made use of in grinding with abrasive paper. If hard particles such as diamond are introduced between the two sliding surfaces then the

Condition	Like metals	Unlike metals
Clean	5×10^{-3}	2×10^{-4}
Poorly lubricated	2×10^{-4}	2×10^{-4}
Average lubrication	2×10^{-5}	2×10^{-5}
Excellent lubrication	$2 \times 10^{-6} - 10^{-7}$	$2 \times 10^{-6} - 10^{-7}$

Table 5.1 Typical values of the adhesive wear coefficient for metals under clean and lubricated conditions (Rabinowicz 1965).

process is known as three body abrasive wear. This latter form of abrasive wear is made use of in lapping and polishing, and occurs in ball-cratering where diamond paste is used to produce the crater.

A similar equation to that which applies to adhesive wear may be derived (Rabinowicz 1965)to describe abrasive wear, with an abrasive wear coefficient K_{abr} replacing the Archard constant K. Values of K_{abr} are generally in the range 10^{-1} to 10^{-2} for two body abrasive wear, and about on order of magnitude smaller, 10^{-2} to 10^{-3}, for the three body case. This compares with values in the range 10^{-2} to 10^{-7} for the adhesive wear coefficient.

3. Polishing

Although polishing is an important subject, and has been extensively studied, it is not well understood and no wholly satisfactory mechanism has been devised (Rabinowicz 1970) . Polishing normally refers to the use of very small abrasive grains, the order of 5 μm or less, on an elastic backing or cloth, to produce a smooth, reflecting surface. The most obvious explanation for the polishing process is that the use of finer and finer abrasive particles leads to the formation of progressively narrower grooves in the surface. According to this explanation polishing is simply an extension of abrasive wear, but on a smaller scale.

However early this century Sir George Beilby (1921) put forward an alternative theory, proposing that polishing occurs as a result of material being smeared over the surface to eliminate surface features and produce a smooth surface. A surface formed in this way will have a different structure from the bulk and Beilby proposed that an amorphous-like layer was produced. A mechanism for the formation of this Beilby layer was put forward by Bowden and Hughes (1937), who noted that very high temperatures can be produced by

frictional heating at the contacting asperities. They suggested that this could lead to a softened or molten layer, enabling material from the high points on the surface to flow into neighbouring depressions. The main evidence to support the Beilby layer was that wear tracks or other topographical features could not be seen on polished surfaces. However, it now appears that this was mostly due to the limitations of the microscopical techniques available at the time.

Later work of Samuels (1956, 1967) showed that the amorphous Beilby layer does not generally form, and that polishing is closely related to the ordinary abrasive wear process. However, the mechanism of material removal is not quite the same due to the presence of the elastic backing or cloth. This appears to play an important role in producing the highly reflecting surfaces observed but the precise polishing mechanisms are still not well understood.

Although fine diamond paste ($\leq 6\mu m$) is used in ball-cratering, the steel ball provides an inelastic backing and so the mechanism for material removal is likely to be predominantly abrasive wear, rather than polishing.

4. The wear coefficient and the measurement of wear

The wear coefficient is a useful parameter, since its value can provide valuable information concerning the type of wear occurring. The quantities of load W and hardness H are generally known, or can be easily measured, so that the value of K in a particular case can be found using equation 5.2 from measurements of the wear volume. The amount of material removed is generally obtained by weighing, mechanical gauging using a micrometer, or by means of optical examination. A disadvantage of most of the conventional techniques is that the specimen must be removed, which means that the volume of wear cannot normally be monitored during the course of an experiment.

4.1 Measurement of wear in ball cratering

Ball cratering is a very convenient means for the measurement of wear. The wear volume can be found simply from a measurement of the crater diameter and the ball is self-centring so that the measurements can be performed without removing the specimen. Equation 5.2 can be re-arranged so that

$$\frac{dV}{dL} = \frac{K}{3}\frac{W}{H} \qquad (5.3)$$

and the wear coefficient is given by

$$K = \frac{3H}{W}\frac{dV}{dL} \qquad (5.4)$$

It is generally more convenient to monitor the volume of wear as a function of time, rather than of sliding distance. In this case we may write

$$K = \frac{3H}{W}\left(\frac{dV}{dt}\right)\left(\frac{dt}{dL}\right) \qquad (5.5)$$

The volume of material removed in ball cratering is simply that of a spherical cap, and the geometry is illustrated in figure 5.2. Consider a disc of radius x and thickness δy at an arbitrary distance y from the centre of the ball. The volume of this disc is given by

$$\delta V = \pi x^2 \delta y \qquad (5.6)$$

For a crater of depth d, the volume is given, in the limit as $y \to o$, by

$$V = \pi \int_{-R}^{-(R-d)} x^2 dy \qquad (5.7)$$

Since the equation of a circle is $x^2 + y^2 = R^2$, we can substitute for x so that

$$V = \pi \int_{-R}^{-(R-d)} (R^2 - y^2)\, dy$$

$$= \left[R^2 y - \frac{y^3}{3} \right]_{-R}^{-(R-d)}$$

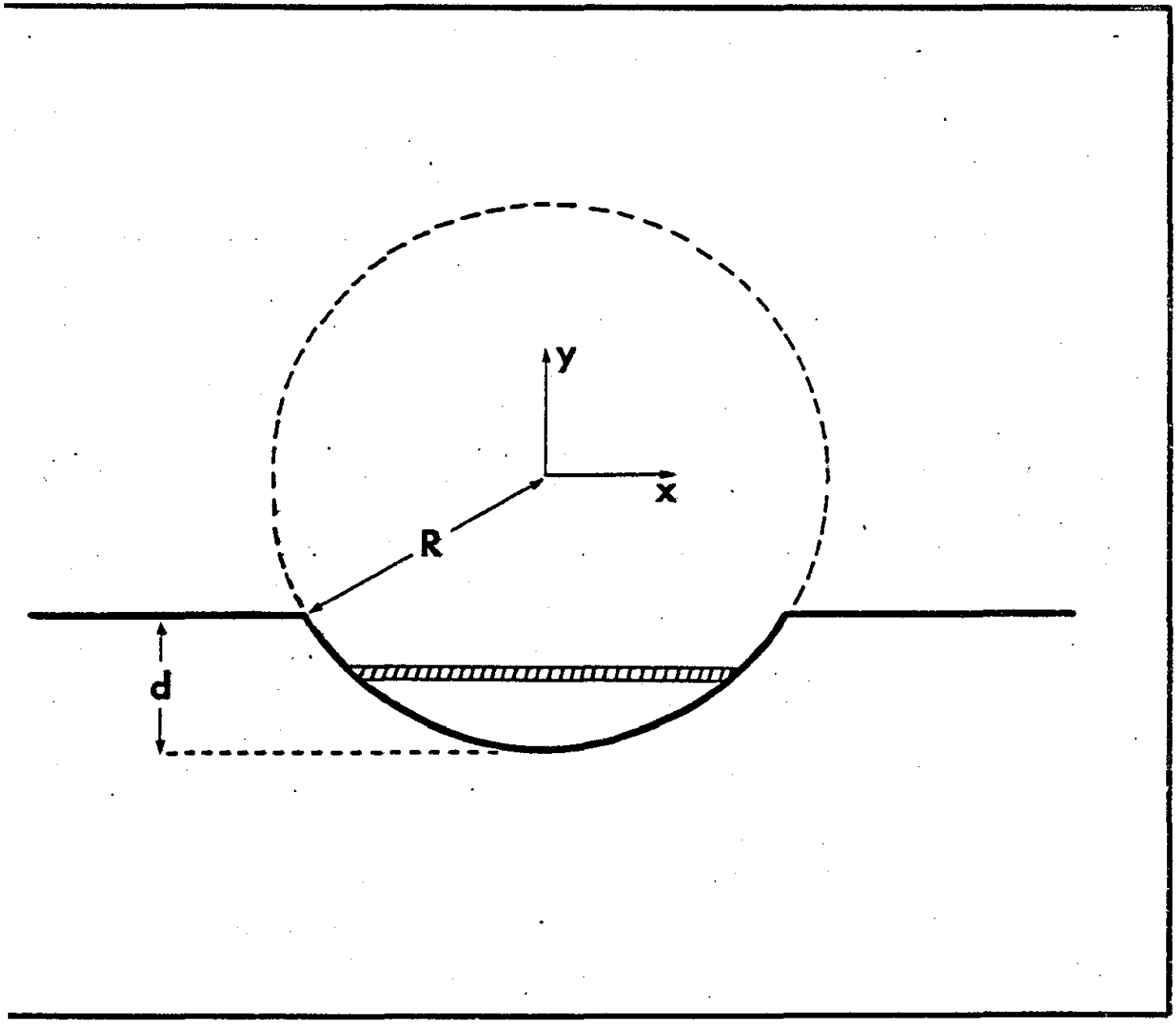

Figure 5.2 The geometry of a spherical cap, illustrating the volume of material removed in ball cratering

Therefore $V = \pi d^2 (R - \frac{d}{3})$ (5.8)

The depth d of the crater is normally very much less than the ball radius R so that the above equation becomes

$$V = \pi d^2 R \quad (5.9)$$

4.1.1 Measurement of load

The load imparted by the ball on the specimen, when the inclined table is at a given angle, can be measured by means of a strain gauge (figure 5.3) The strain gauge consists of a transducer fixed to a sheet of aluminium formed into a stiff spring which takes the place of the specimen. This transducer, together with an identical one as a standard, forms part of a bridge, and changes in resistance are detected by a galvanometer. The calibration of the galvanometer, for angles of 70 and 80 degrees of the specimen table, is shown in figure 5.4. For a standard 30mm diameter bearing steel ball the load on the specimen was found to be 60 grams at 70 degrees, and 37 grams at 80 degrees.

4.1.2 Dependence of the wear rate on abrasive size

In order to show the effect of diamond paste on the wear rate in ball cratering, the wear volume for a copper-beryllium alloy (hardness 420 $kgmm^{-2}$ Vickers) is shown as a function of time in figure 5.5 for a variety of conditions. The wear rate is dependent on the size of diamond paste used and the rate for 6 μm diamond (2×10^{-5} $mm^3 s^{-1}$) exceeds that for 1 μm diamond (9×10^{-6} mm^3 s^{-1}). In both these cases the diamond paste and lubricant were renewed after each reading and, apart from an initial effect, the wear rate is constant.

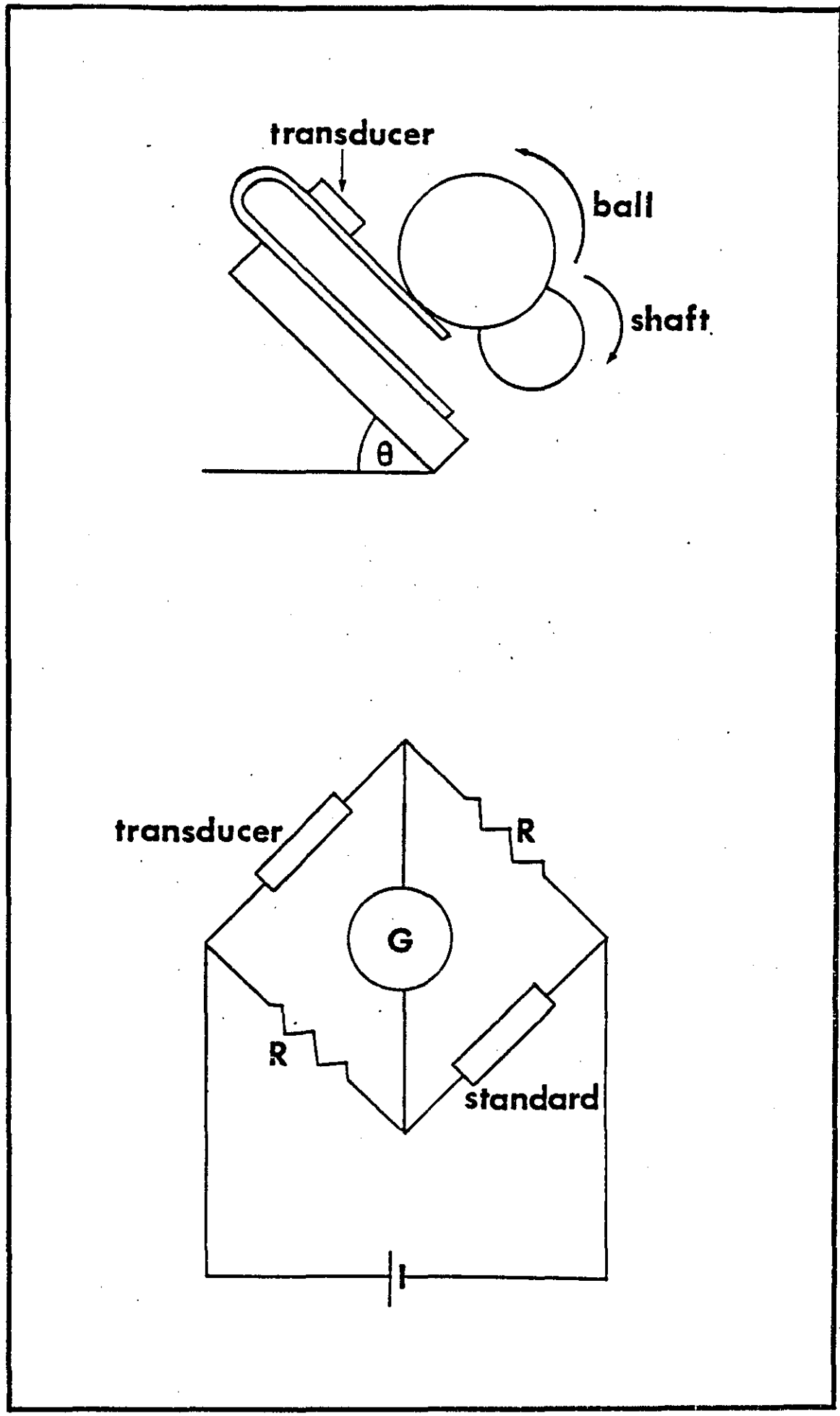

Figure 5.3 A schematic diagram illustrating the essential features of the strain gauge used to determine the load on the specimen in ball cratering

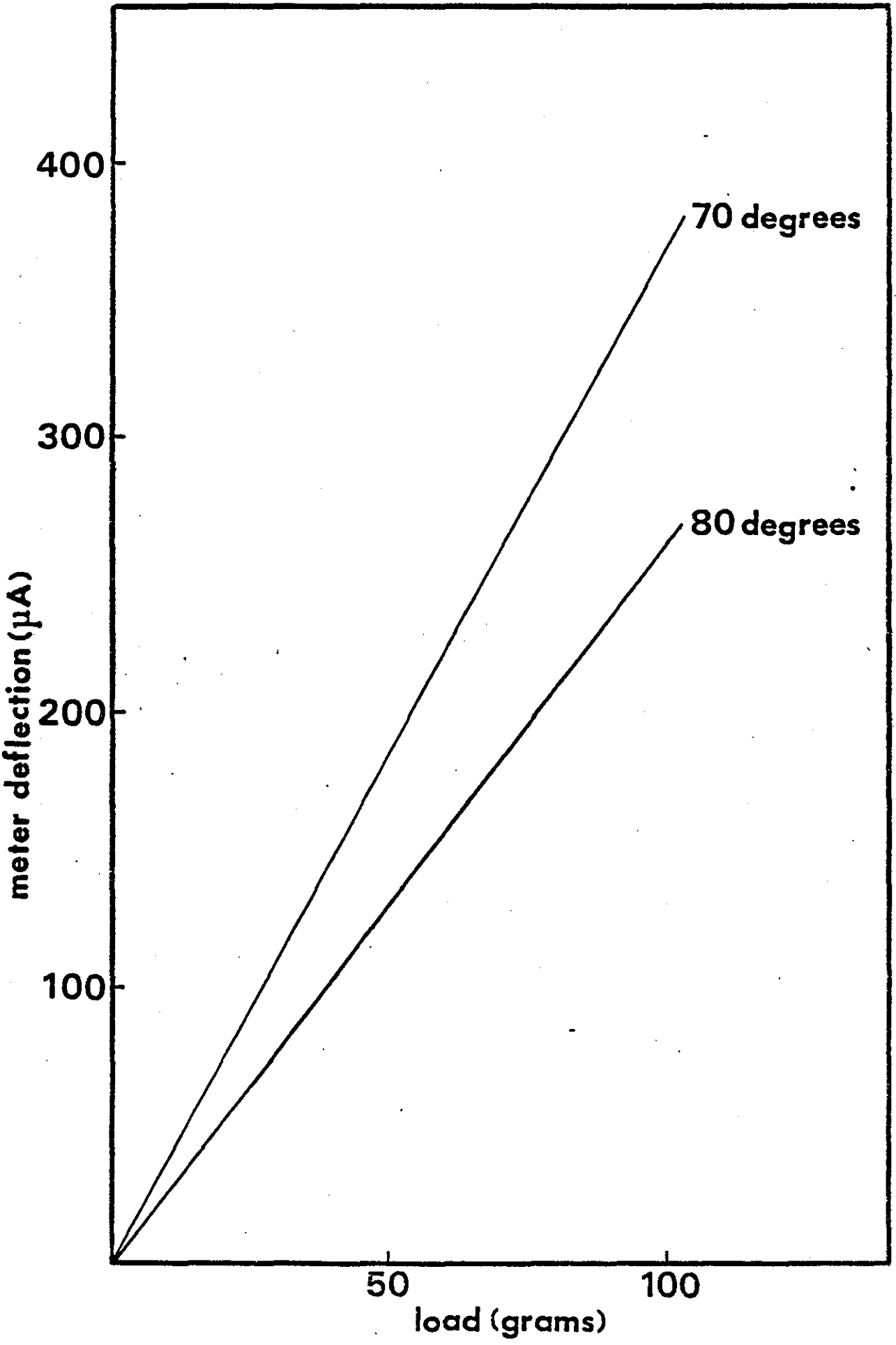

Figure 5.4 Calibration of the strain gauge galvanometer for angles of inclination of 70 and 80 degrees of the specimen table.

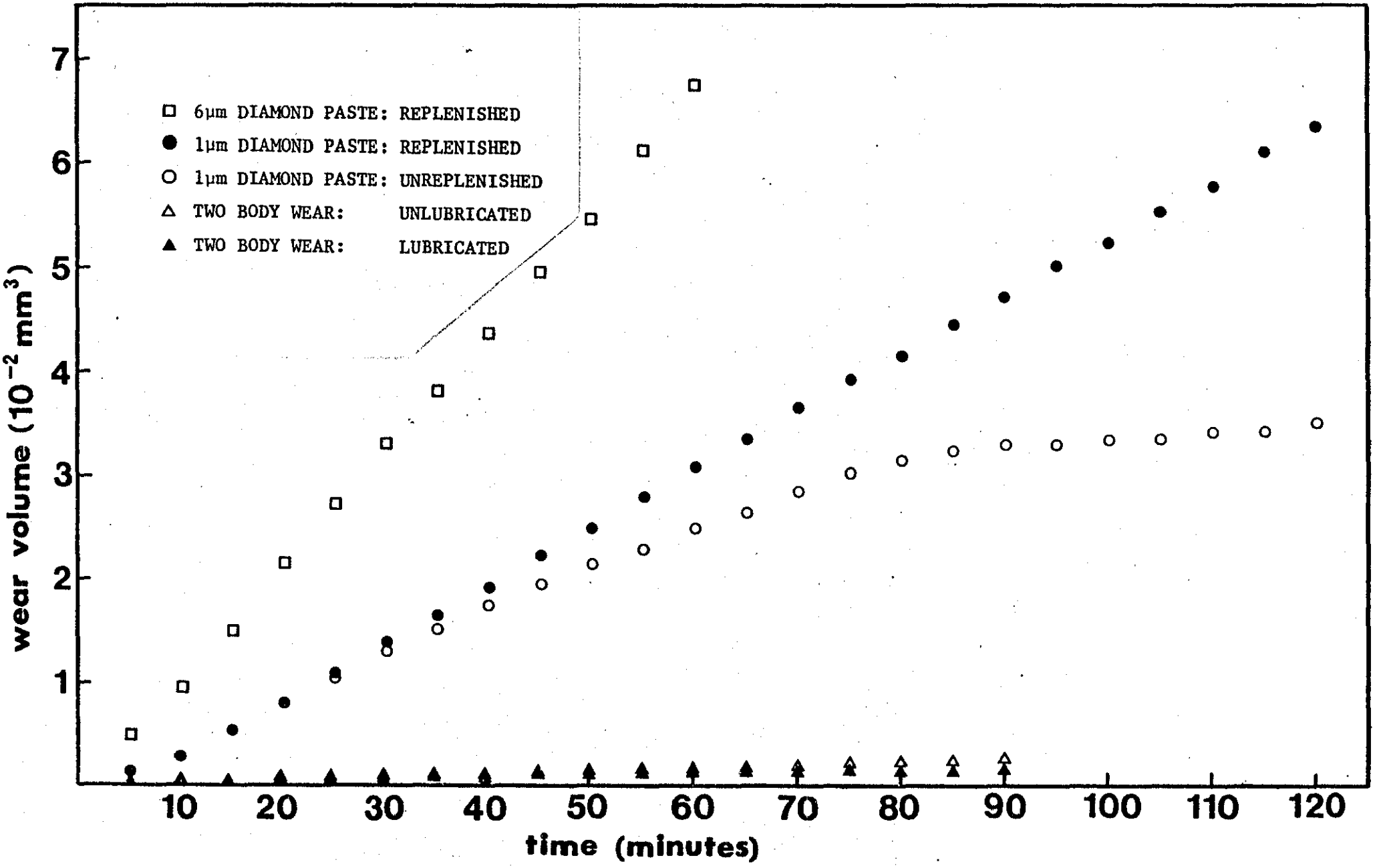

Figure 5.5 The wear volume as a function of time for a copper-beryllium alloy (hardness 420 kg mm^{-2}) for a range of conditions

Figure 5.5 also shows the effect of not replenishing the diamond abrasive, in the case of 1 μm paste. The wear rate decreases as the abrasive is displaced, and eventually the gradient tends towards that for lubricated two body wear (also shown).

4.1.3 Dependence of the wear rate on specimen hardness

Wear rates were measured for a series of metals and alloys with a range of hardness (7 to 1600 $kgmm^{-2}$) and the results are presented in table 5.2. Results were obtained for two body wear, under both lubricated and unlubricated conditions, and for three body wear using 1 μm and 6μm diamond paste (Walls et al,1982) .

The wear rate for two body wear tends to decrease as the hardness of the specimen increases, and the use of lubricant generally reduces the wear rate by an order of magnitude. The relationship between the wear resistance, which is the reciprocal of the wear rate, and hardness for the unlubricated case is shown graphically in figure 5.6. The wear coefficient was calculated in each case and the results are presented in table 5.3. It remains fairly constant over the entire hardness range, particularly under unlubricated conditions where it lies between 2 and $6x10^{-4}$, indicating that the wear mechanism is similar in all cases. Values are consistent with those generally obtained for adhesive wear (table 5.1).

The wear rates in the case of three body wear, where diamond paste is introduced, do not show a clear dependency on hardness, and the values obtained are within the same order of magnitude throughout the entire hardness range. However, values of the wear coefficient K range from $6x10^{-5}$ in the case of lead to 10^{-1} for the hardest materials. This is shown graphically in figure 5.7, for 1 μm diamond, and indicates that the wear mechanism is dependent on the hardness of the specimen. In the case of the harder

Wear rate $(\frac{dv}{dt})$ $mm^3\ S^{-1}$

Material	Hardness	Three body wear (Diamond Paste)		Two body wear (No diamond Paste)	
		1μ	6μ	lubricated	unlubricated
Lead	7	4×10^{-6}	7×10^{-5}	4×10^{-6}	2×10^{-5}
Aluminum	45	5×10^{-6}	3×10^{-5}	4×10^{-6}	3×10^{-6}
Copper	66	4×10^{-6}	2×10^{-5}	3×10^{-7}	2×10^{-6}
Mild steel	106	1×10^{-6}	4×10^{-6}	4×10^{-7}	2×10^{-6}
Brass	120	6×10^{-6}	6×10^{-6}	1×10^{-6}	2×10^{-6}
Cu/Be	420	9×10^{-6}	2×10^{-5}	1×10^{-7}	6×10^{-7}
Stellite	800	2×10^{-5}	2.5×10^{-5}	3×10^{-8}	3×10^{-7}
Tungsten	1600	1×10^{-5}	3×10^{-5}	9×10^{-9}	1×10^{-7}

Table 5.2 Values of the wear rate obtained in ball cratering for a series of metals with a range of hardness. Results are presented for two body wear under both lubricated and unlubricated conditions, and for three body wear using 1μm and 6μm diamond paste

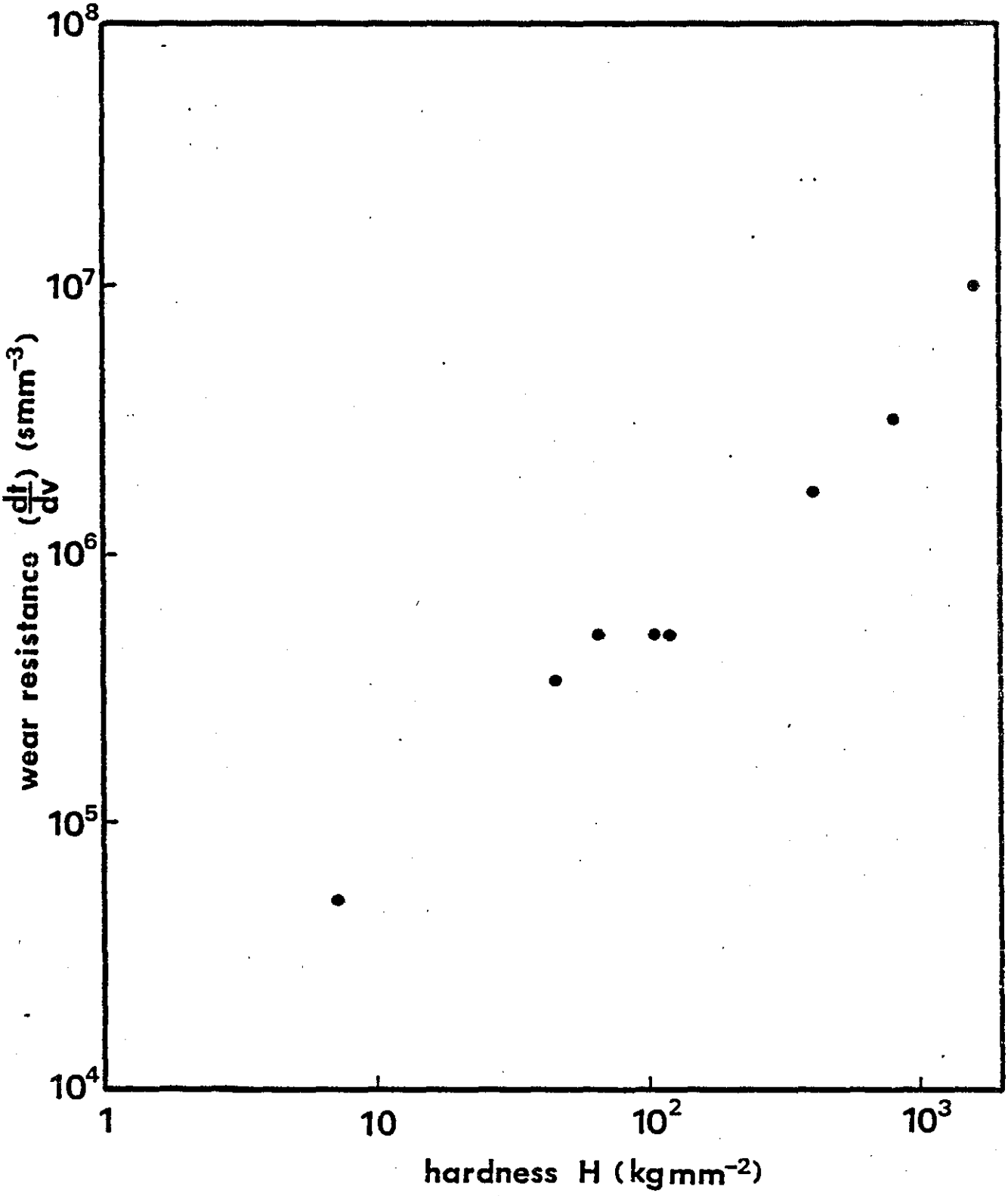

Figure 5.6 The relationship between wear resistance and hardness for unlubricated two body wear

Wear coefficient k

Material	Hardness	Three body wear (Diamond Paste)		Two body wear (No Diamond)	
		1μ	6μ	lubricated	unlubricated
Lead	7	6×10^{-5}	9×10^{-4}	6×10^{-5}	2×10^{-4}
Aluminum	45	6×10^{-4}	3×10^{-3}	3×10^{-4}	3×10^{-4}
Copper	66	6×10^{-4}	3×10^{-3}	3×10^{-5}	2×10^{-4}
Mild steel	106	3×10^{-4}	9×10^{-4}	9×10^{-5}	3×10^{-4}
Brass	120	1×10^{-3}	1×10^{-3}	3×10^{-4}	6×10^{-4}
Cu/Be	420	8×10^{-3}	2×10^{-2}	1×10^{-4}	6×10^{-4}
Stellite	800	3×10^{-2}	3×10^{-2}	6×10^{-5}	6×10^{-4}
Tungsten	1600	3×10^{-2}	1×10^{-1}	3×10^{-5}	3×10^{-4}

Table 5.3 Values of the wear coefficient obtained in ball cratering under two and three body wear conditions

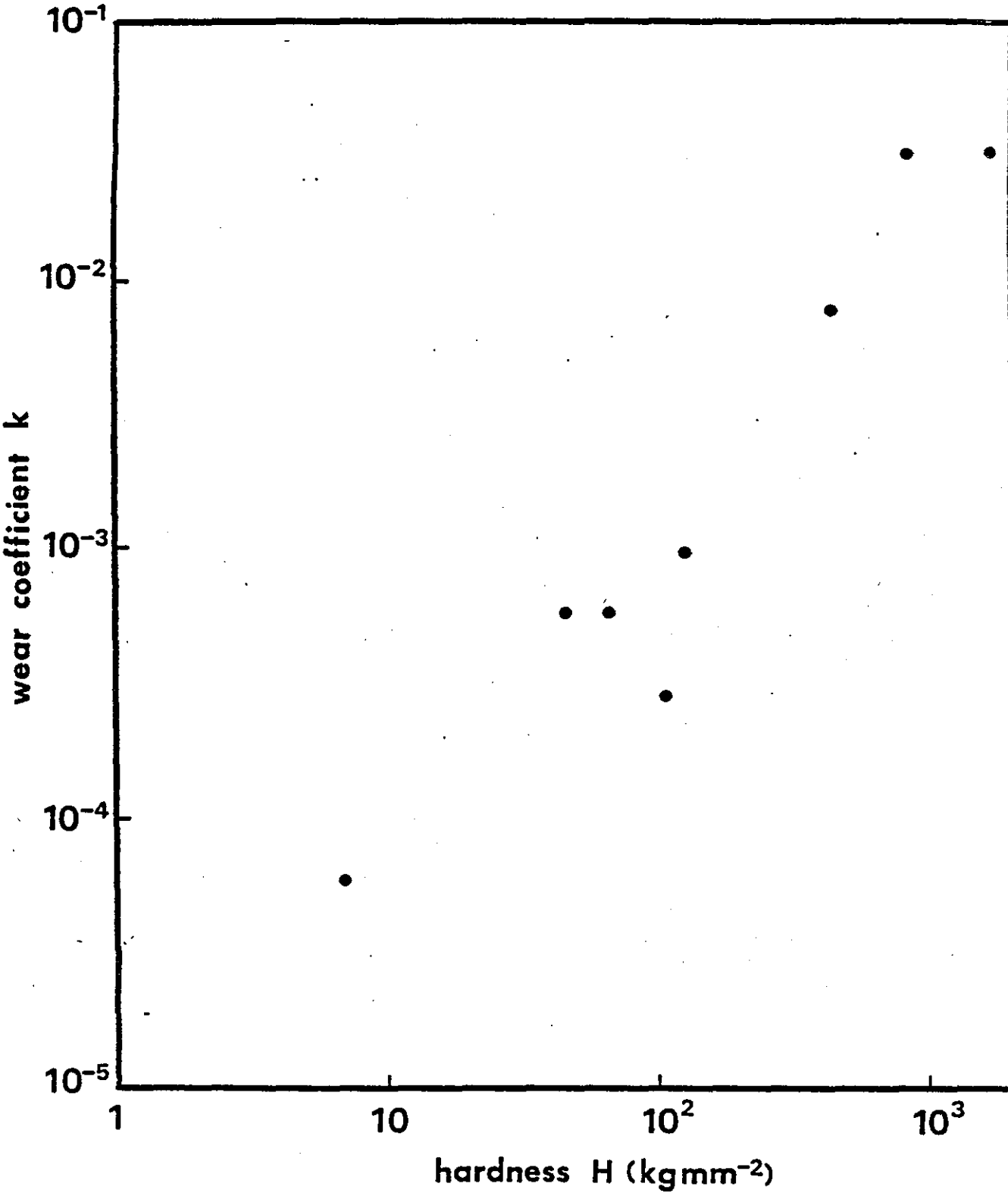

Figure 5.7 The relationship between the wear coefficient and hardness for three body wear using 1 μm diamond paste

materials the magnitude of K is consistent with values generally associated with abrasive wear, but values obtained for the softer materials suggest that there is an adhesive component present.

5. Scanning electron microscopy

Further evidence concerning the nature of the wear mechanisms in ball cratering was obtained from observations using the scanning electron microscope. The appearance of craters produced in the copper-beryllium alloy using 6 μm and 1 μm diamond paste is shown in figure 5.8. The periodicity and magnitude of the surface roughness is consistent with the grade of diamond paste used, but the general appearance is similar indicating that the same wear mechanism operates in each case.

Figure 5.9 shows the appearance of craters obtained with 1 μm diamond paste for a series of metals and alloys having a range of hardness. The well-defined parallel grooves present in the case of copper-beryllium (hardness 420 $kgmm^{-2}$) are typical of those produced under abrasive wear conditions. For the harder materials such as stellite (800 $kgmm^{-2}$) the wear tracks are narrower since the diamond particles do not penetrate as far into the surface of the specimen. The tracks become even narrower in the case of tungsten (1610 $kgmm^{-2}$), and cracks are present in a direction perpendicular to that of the wear tracks. This appearance is typical of that produced in brittle materials, and indicates the occurrence of brittle fracture which is a form of surface fatigue wear.

The mild steel specimen (106 $kgmm^{-2}$) has wear tracks which are rather less well-defined than those found in copper-beryllium, although the grooves are still clearly visible. There is a certain amount of surface roughening superimposed on the wear tracks, possibly caused by local plastic deformation due to the greater ductility of mild steel. The wear tracks in aluminium

Figure 5.8 A comparison of the wear tracks in craters formed in the copper-beryllium alloy using (a) 6 μm and (b) 1 μm diamond paste.

a

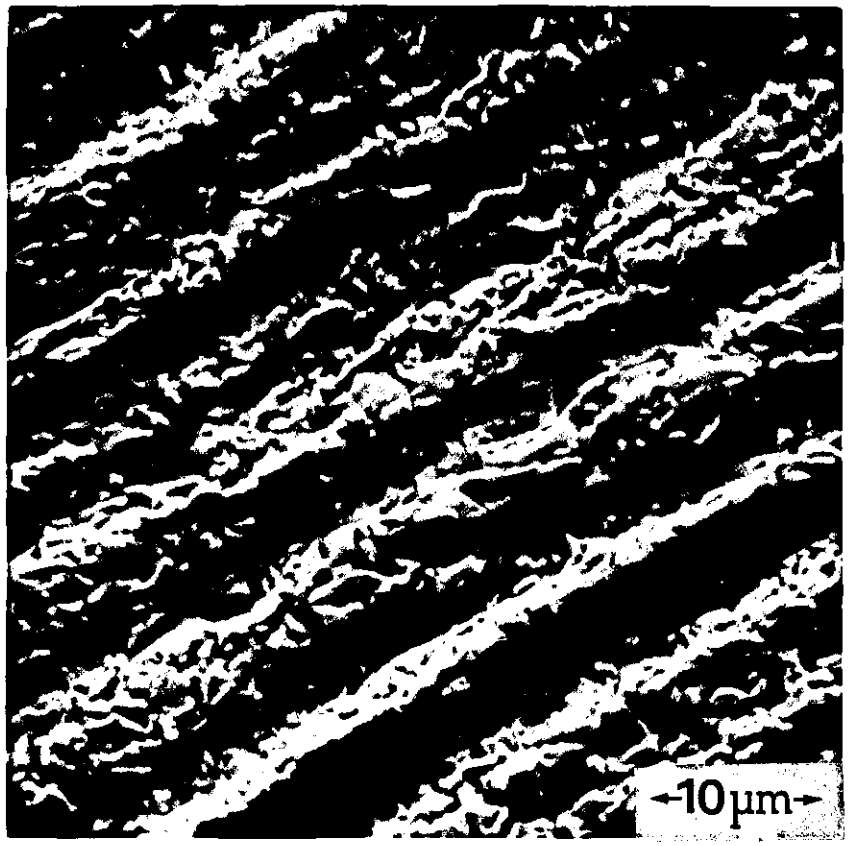

b

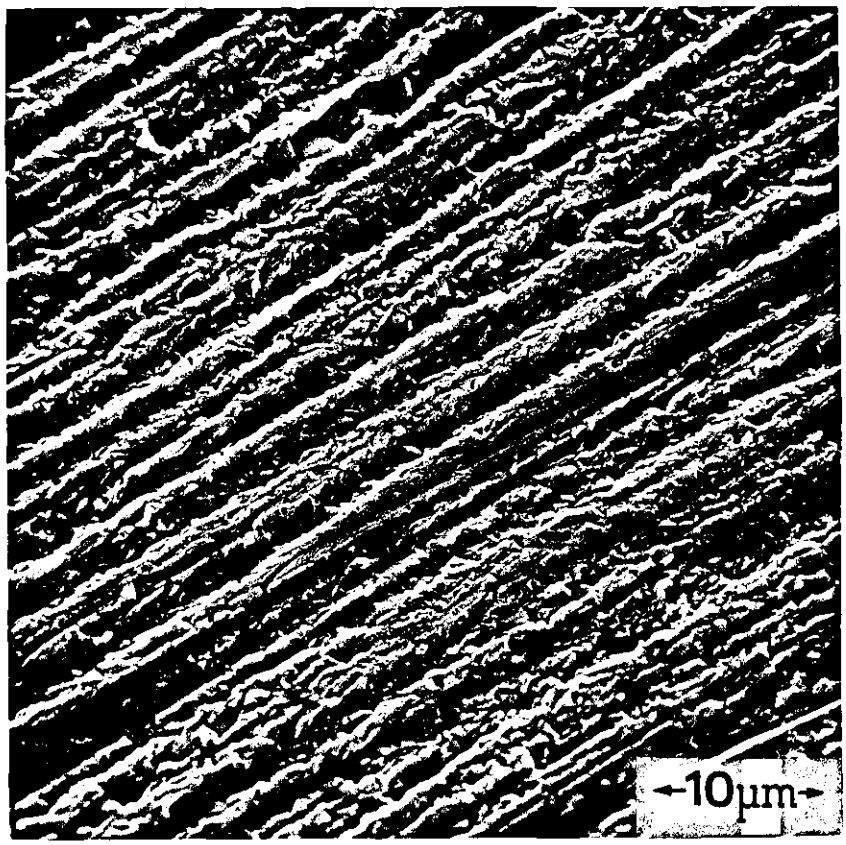

Figure 5.9 The appearance of the wear tracks obtained using 1μm diamond paste for a series of metals with a range of hardness

(a) tungsten (hardness 1610 kg mm^{-2})

(b) stellite (800 kg mm^{-2})

(c) copper-beryllium (420 kg mm^{-2})

(d) mild steel (106 kg mm^{-2})

(e) aluminium (45 kg mm^{-2})

(f) lead (7 kg mm^{-2})

a

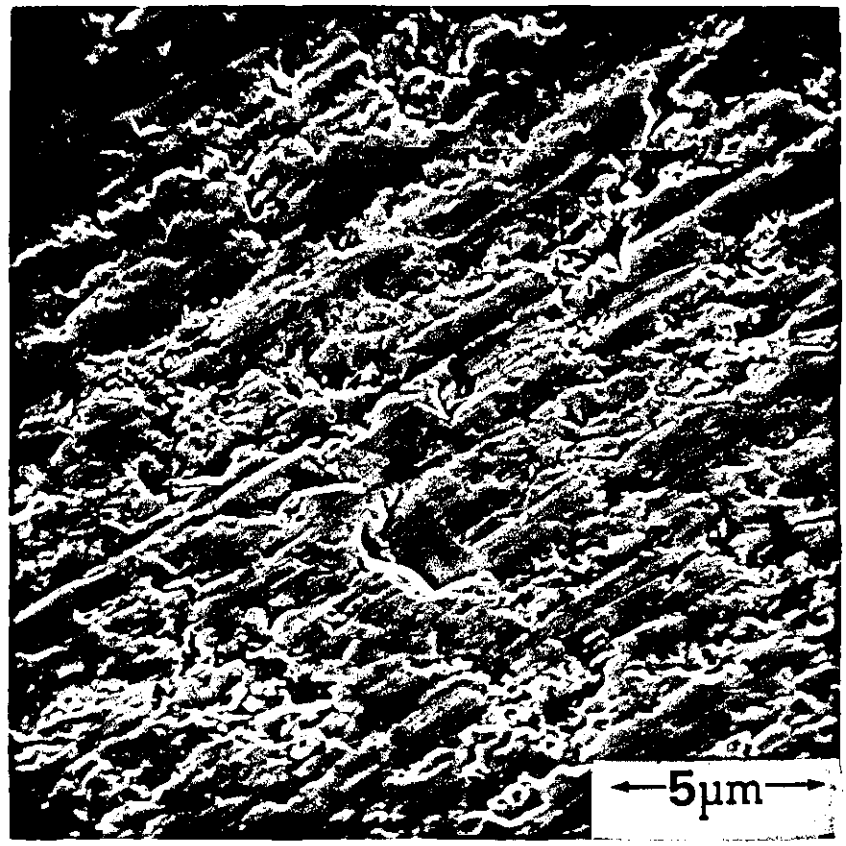

b

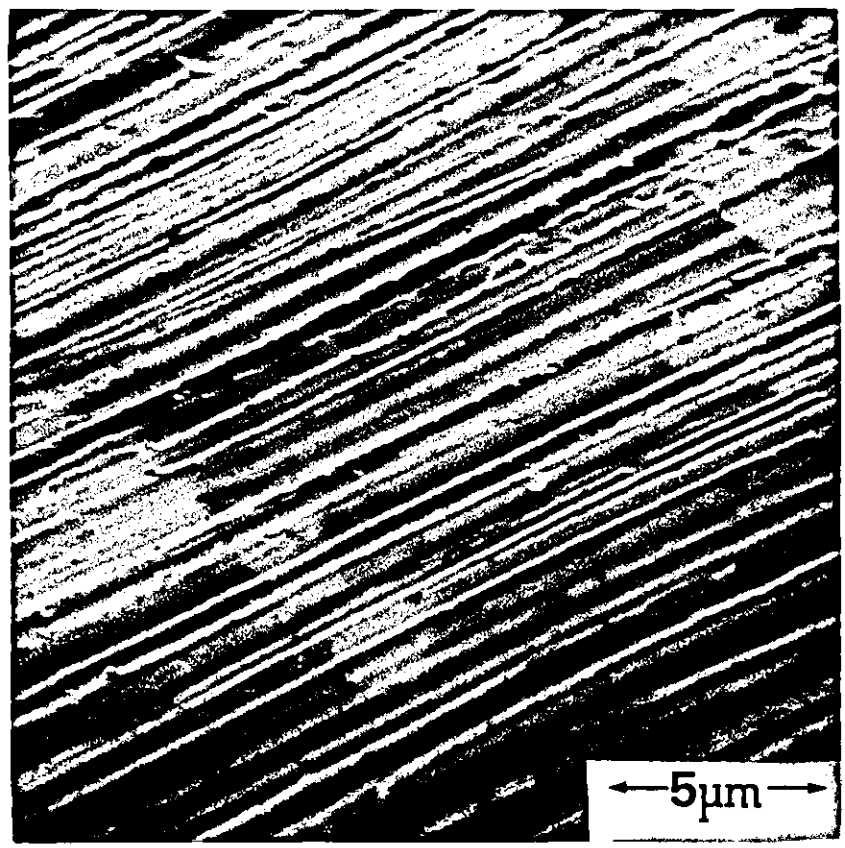

c

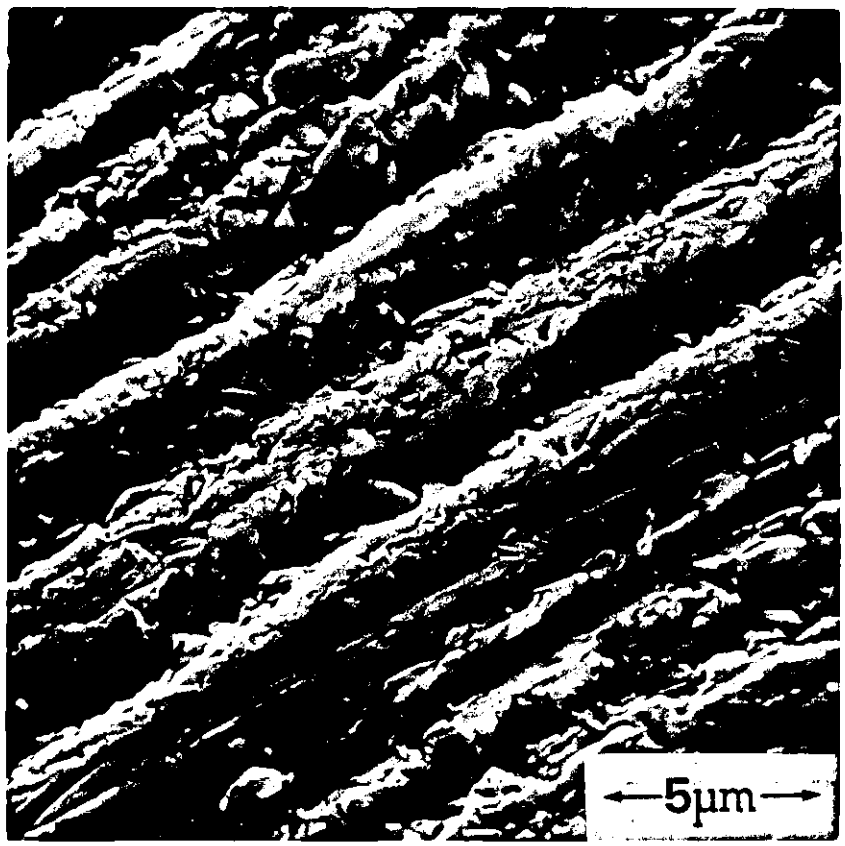

d

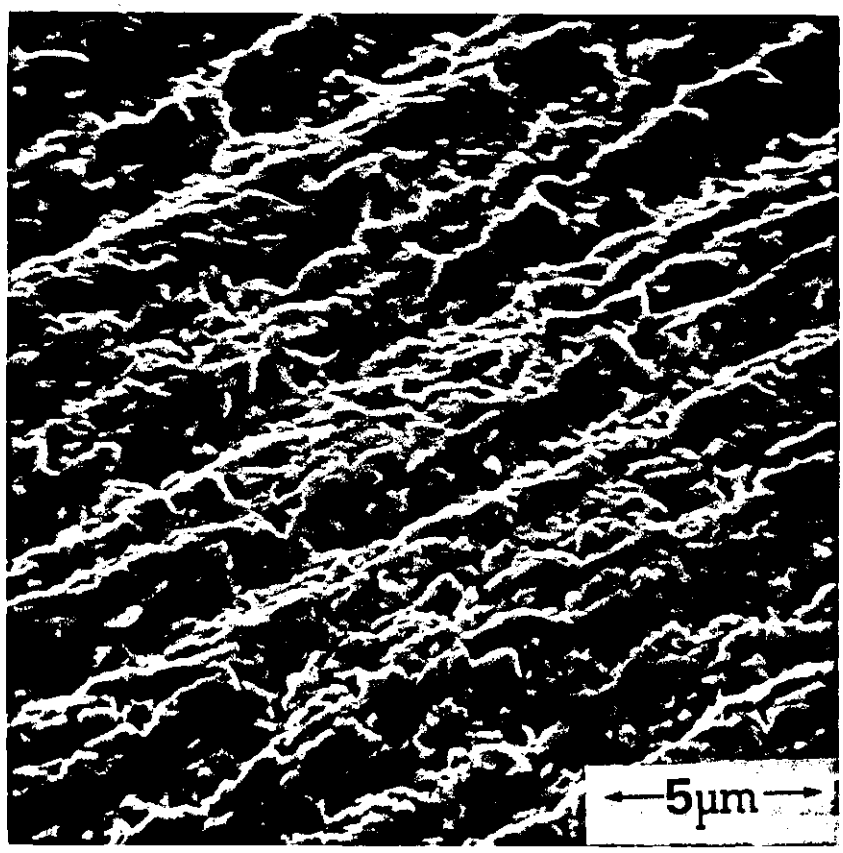

e

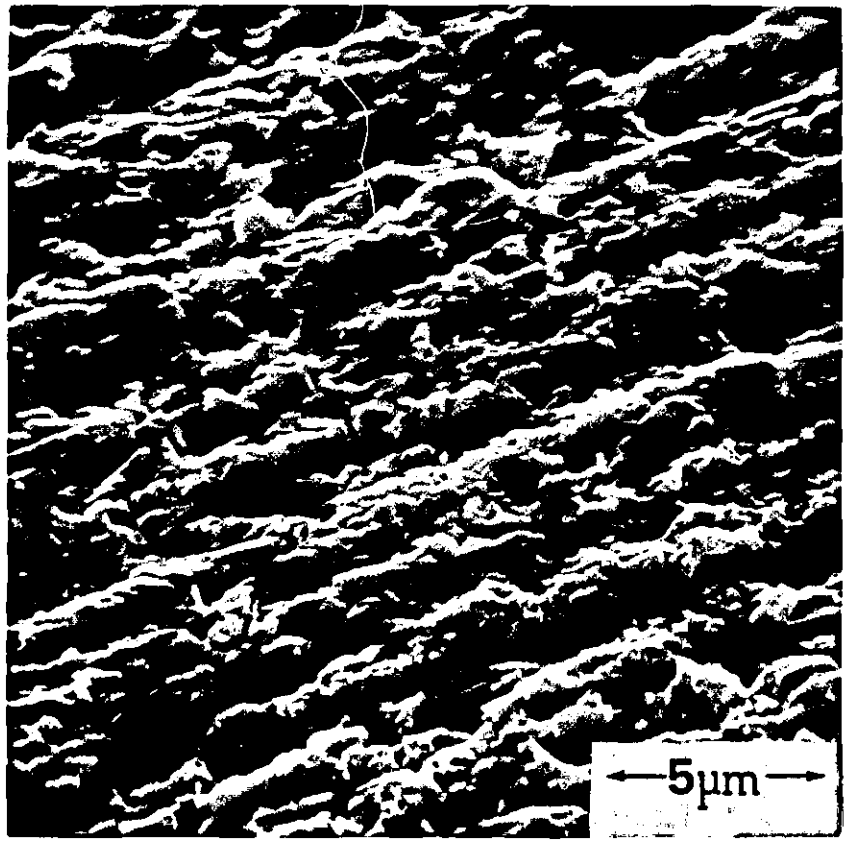

f

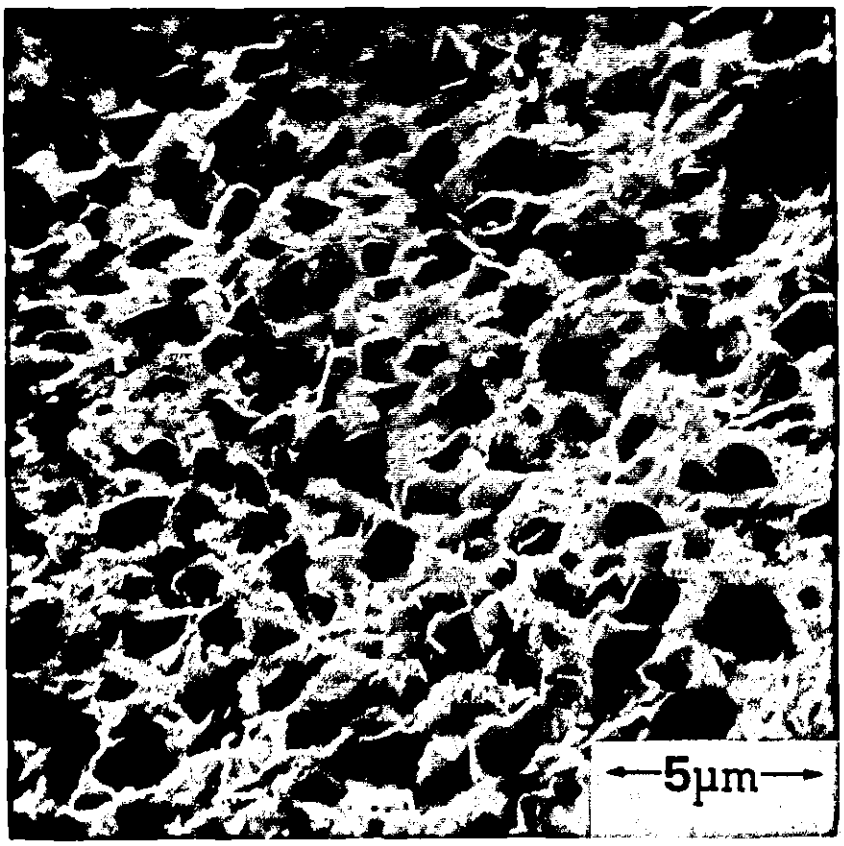

(45 $kgmm^{-2}$) show the same effect, but to a greater degree. However the worn surface of lead (7$kgmm^{-2}$) has a totally different appearance, and the grooves are no longer present. This suggests that a different wear mechanism is taking place, and is consistent with the results of the wear rate measurements. In addition it appears that particles of diamond have become embedded in the specimen surface. This impaction of diamond may have an effect on the wear rate, and provide further explanation for it being rather less than might be expected.

6. Investigation of surface topography using stylus profilometry

A stylus profilometer (Talystep 1, stylus radius 12.5 μm) was used to examine the surface topography produced in ball cratering for a series of metals with a range of hardness. The resulting profiles of craters formed using 1 μm diamond paste are shown in figure 5.10. The roughness generally decreases with increasing hardness as the diamond particles form shallower indentations in the harder materials. However the roughness is less than expected for the metals with a hardness below about 100 $kgmm^{-2}$. This could be due to the presence of local plastic deformation as a result of the greater ductility of these metals. This explanation for the effect, which is greatest in lead, is supported by the evidence of the scanning electron micrographs discussed earlier. The occurrence of such plastic deformation would tend to modify and suppress the topography formed by the abrasive wear mechanism.

The influence of hardness on the surface topography is evident in the case of surface coatings where the hardness is different from that of the substrate. Figure 5.11 shows a Talystep profile of the inteface region for the example of an electrodeposited hard chrome coating on a mild steel substrate. The difference in amplitude of the surface roughness can clearly be seen. The roughness produced in the substrate region (hardness 106 $kgmm^{-2}$),

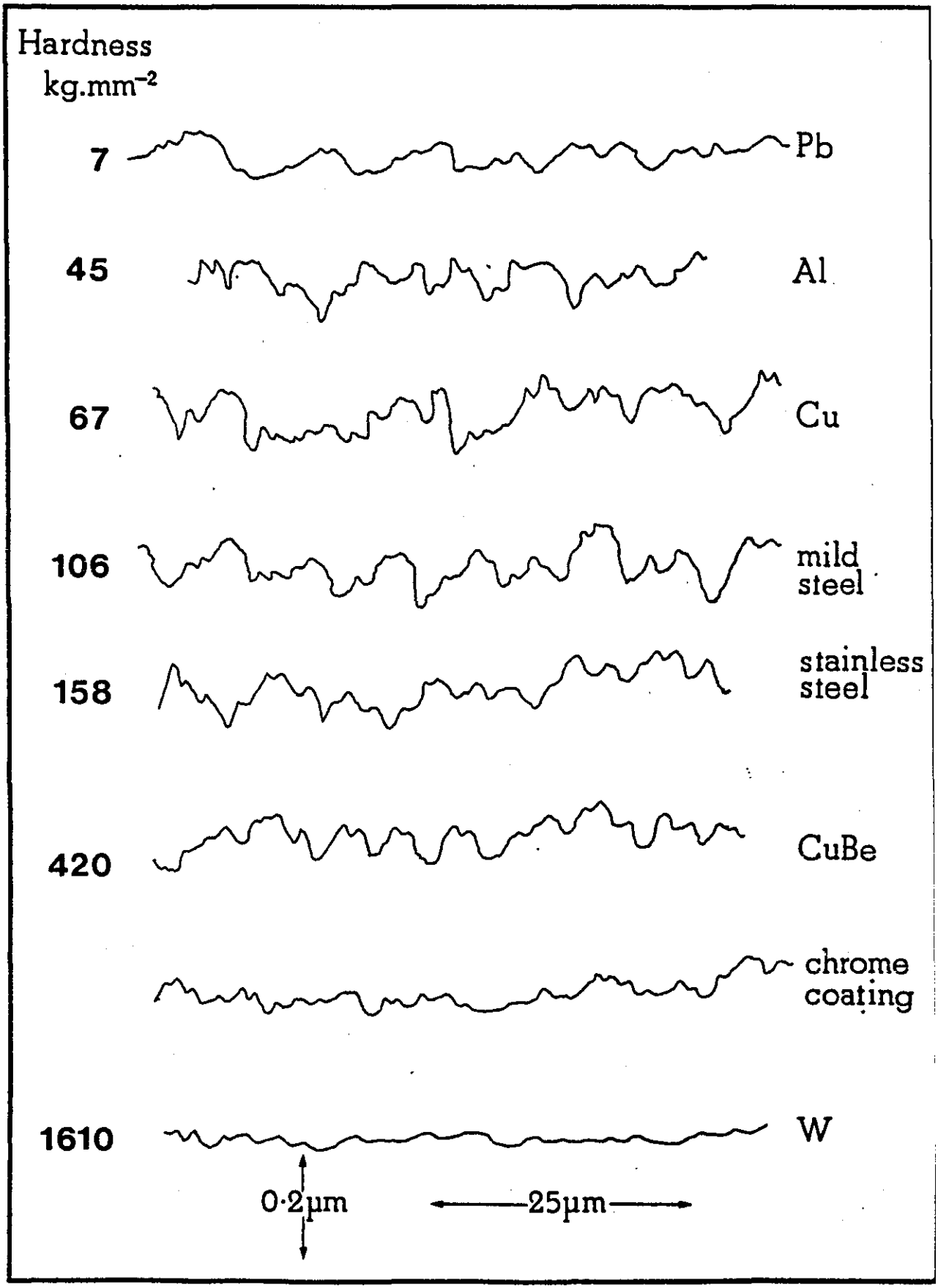

Figure 5.10 Talystep profiles of craters formed using 1µm diamond paste in a series of metals with hardnesses in the range 7 to 1600 kg mm^{-2} (Vickers)

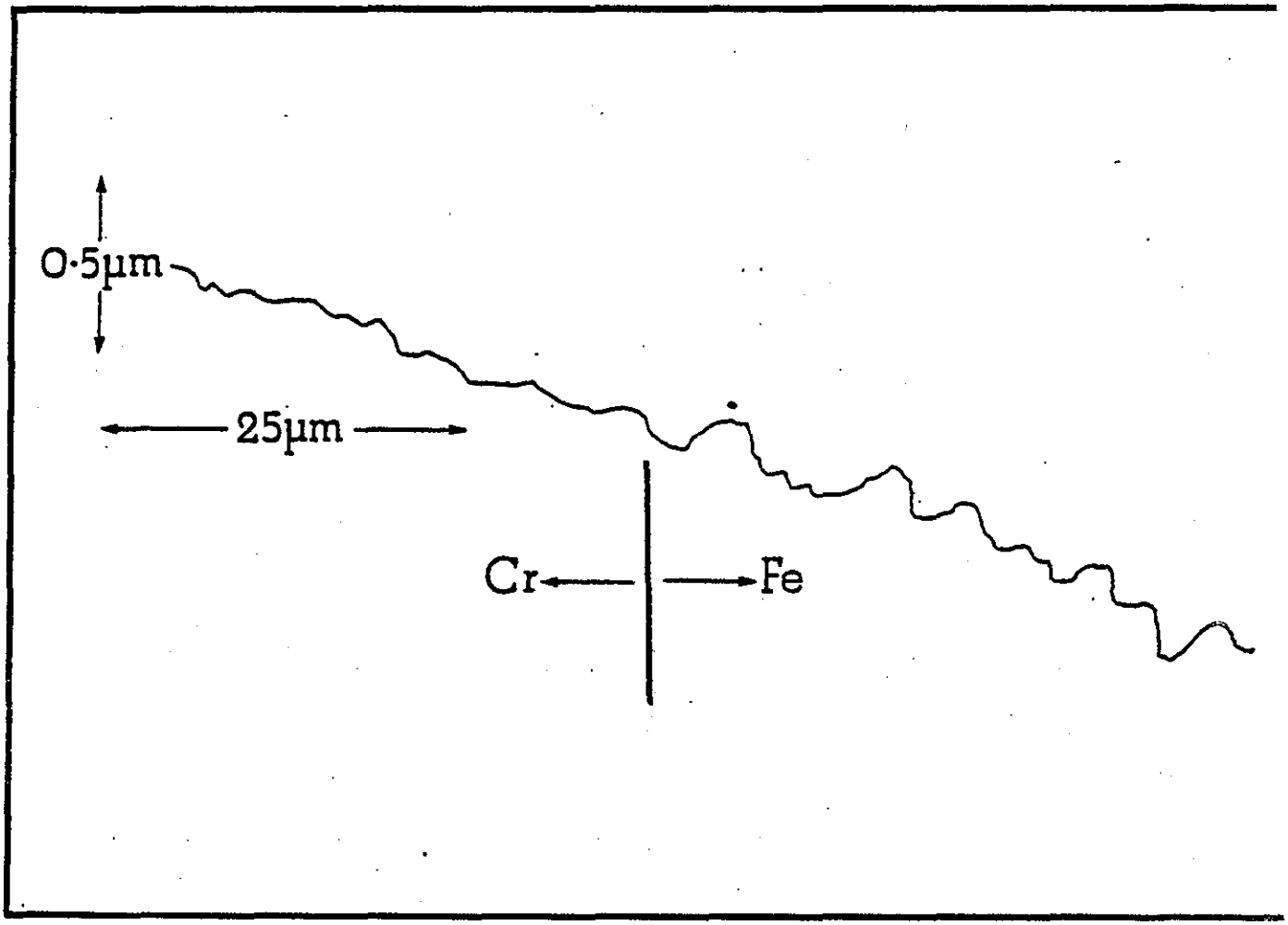

Figure 5.11 A Talystep profile of the interface region for an electrodeposited hard chrome coating on a mild steel substrate

as measured by twice the standard deviation (2σ) of the surface from its mean position, is 0.20μm. A much smoother surface (2σ= 0.06μm), however is produced in the hard chrome coating (hardness approximately 1000 kg mm^{-2}).

6.1 Effect of ball-cratering on the surface topography of the ball

Figure 5.12 shows the effect of producing a crater using 1μm diamond paste in a mild steel specimen of hardness 106 kg mm^{-2}. This is much less than that of the ball, which is made from bearing steel, and has a hardness of about 900 kg mm^{-2}. Three Talystep profiles are given in figure 5.12, showing the initial topography of the ball, the topography of the crater and the final topography of the ball. As might be expected the surface roughness produced in the crater itself (2σ= 0.20μm) is considerably greater than that of the ball (2σ= 0.02μm), which remains largely unchanged.

Figure 5.13 shows the topography produced for a tungsten specimen of hardness 1610 kg mm^{-2}, which is greater than that of the ball. A relatively smooth crater is obtained in this case (2σ= 0.03μm), but the ball has become considerably rougher. The roughness produced on the ball is 0.09 μm, compared with its initial value of 0.01 μm. This demonstrates that wear is a two way process and occurs on both the specimen and the ball. The amount of wear on each surface depends on their relative hardness.

Similar Talystep profiles are shown in figure 5.14 for a crater formed in an electrodeposited hard chrome coating. This has a hardness of about 1000 kg mm^{-2} which is of the same order as that of the ball. In this case the roughness obtained on the ball (2σ= 0.06μm) is comparable with that produced in the crater, which is also 0.06μm.

7. Discussion

The surface topography produced in ball cratering under a variety of

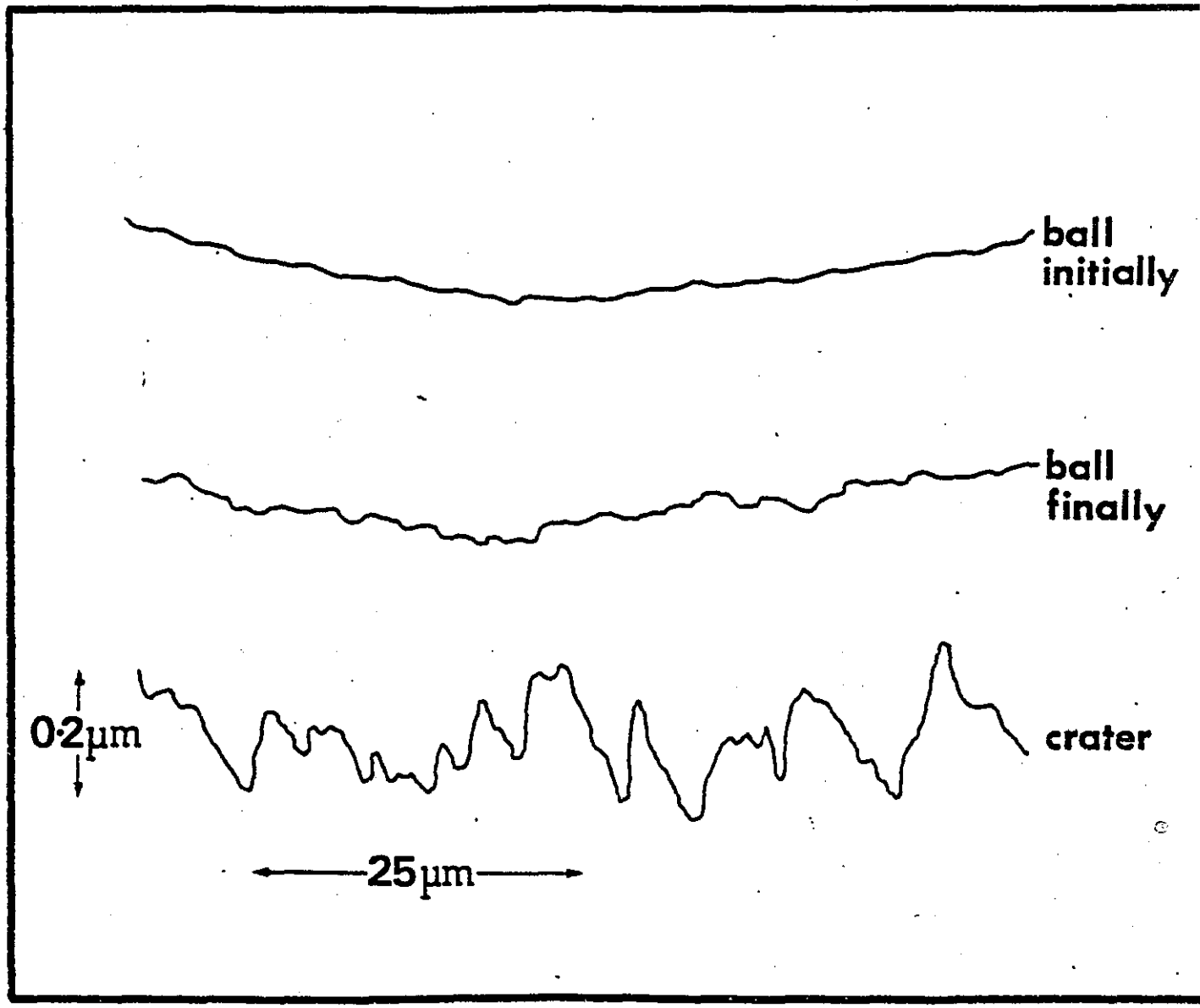

Figure 5.12 The effect of producing a crater using 1μm diamond paste in a mild steel specimen of hardness 106 Kg mm^{-2} . Talystep profiles are shown illustrating the initial topography of the ball, the topography of the crater and the final topography of the ball

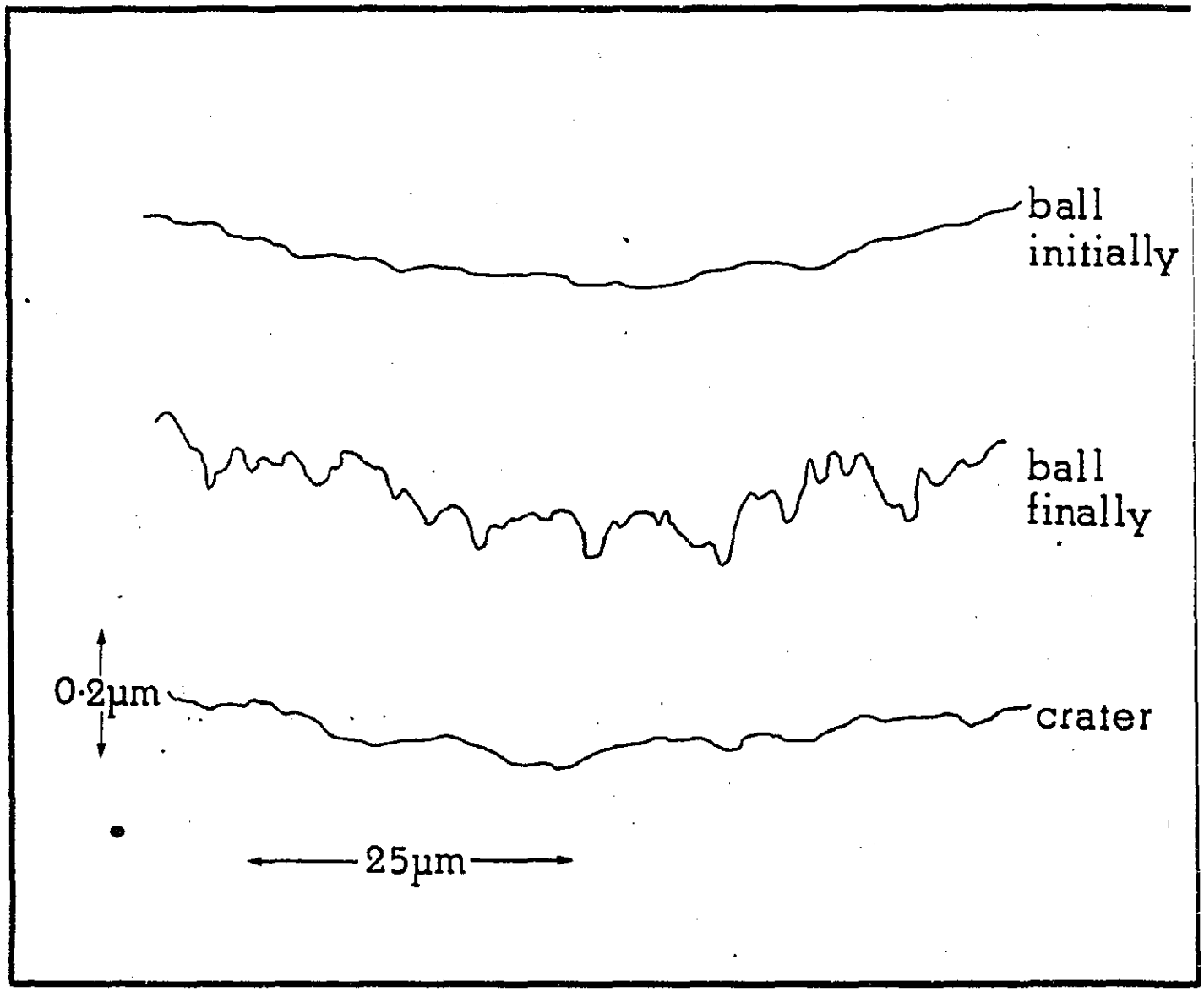

Figure 5.13 Talystep profiles showing the topography of a crater formed in a tungsten specimen (hardness 1610 Kg mm^{-2}) and on the ball itself using 1μm diamond paste

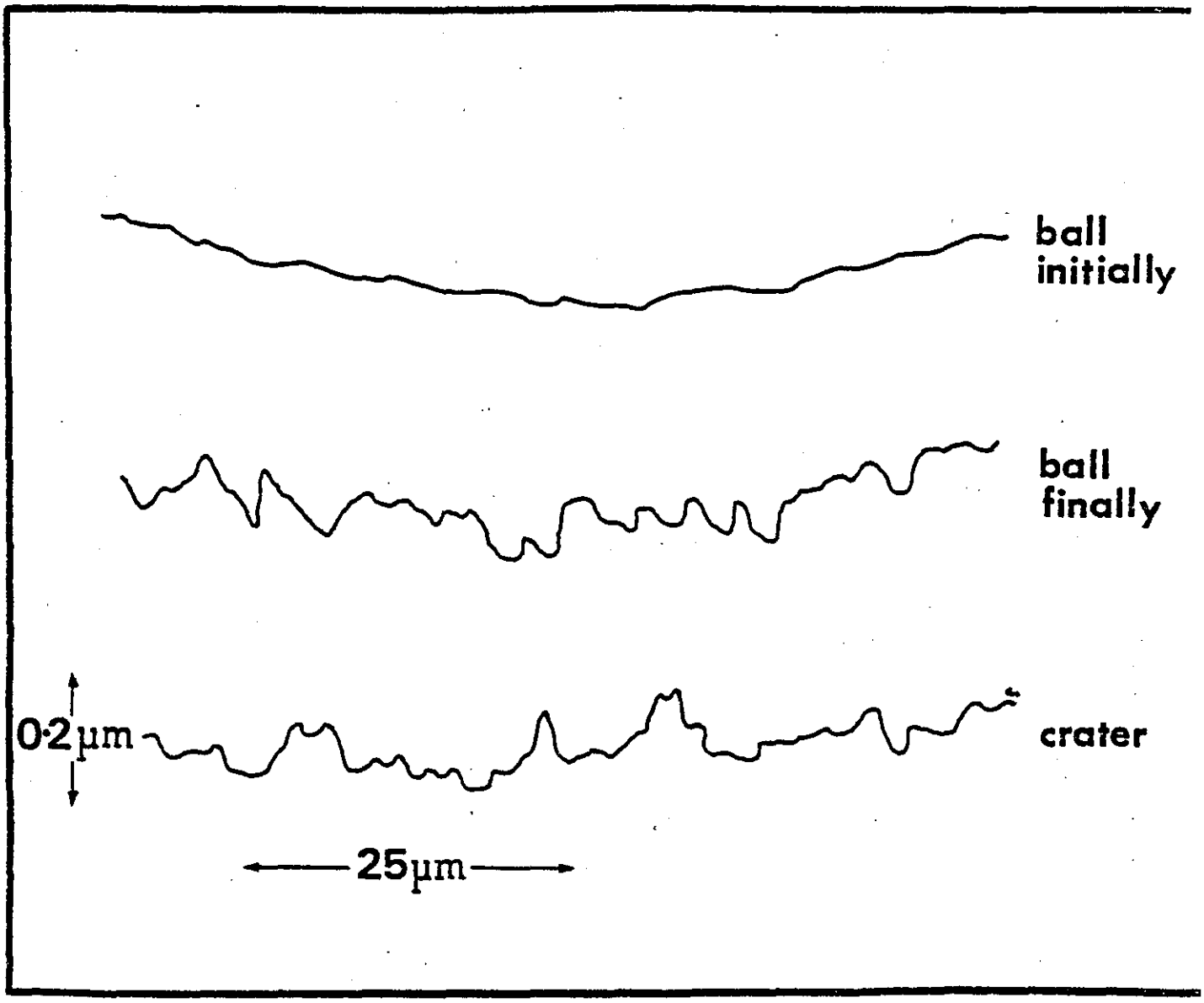

Figure 5.14 Talystep profiles showing the topography of a crater formed in an electrodeposited hard chrome coating (hardness approximately 1000 kg mm^{-2}) using 1μm diamond paste, together with the initial and final topography of the ball.

operating conditions has been examined for a series of metals with a range of hardness. Evidence from the scanning electron microscope and the values of the wear coefficient indicate that the material is removed by abrasive wear for hard metals (> 150 kg mm^{-2}). In the intermediate range (40-150 kg mm^{-2}) the mechanism is still predominantly abrasive, but the appearance of the wear tracks indicates a contribution from the adhesive wear mechanism. For the softest materials such as lead (7 kg mm^{-2}) the value of the wear coefficient and the lack of well-defined wear tracks indicate that the wear process is predominantly adhesive. Thus difficulties may arise in the softest materials since the adhesive wear mechanism may lead to material transfer, and the impaction of diamond and wear debris in the sample surface. However, in practice these effects may often be minimised by careful use of low loads and slow rotation speeds.

Chapter 6 APPLICATIONS

1. Introduction

Auger electron spectroscopy and other surface analytical techniques provide information concerning the chemical composition of the top few atomic layers of the surface. Some information concerning the depth distribution of elements can be found by using variations in the escape depth of the emitted electrons. This, non-destructive, method is limited to a total depth of about 5 nm, but is useful for studies of oxidation, adsorption and surface segregation. Profiles to greater depths are usually obtained using a combination of sputter-ion etching and Auger electron spectroscopy. This method has provided useful information concerning the depth distribution of elements in a range of thin films and surface treatments (Holloway 1975, Walls 1981). These include those produced by vapour deposition and ion plating(Walls et al 1978), while the layered structures of certain electroplated specimens such as tinplate and tin free steel have also been examined (Johannessen et al 1980) . However the use of this technique is generally limited to depths of less than 1 μm, and there are a number of applications for which composition-depth profiles to much greater depths are required. Profiles to such depths are best achieved by the use of taper-sectioning techniques. In the following examples ball-cratering, in combination with Auger electron spectroscopy, is shown to provide valuable information on the composition of a range of industrially important surface coatings and treatments.

2. Electroplated coatings

Zinc coatings formed by electrodeposition are industrially important for the protection of steel surfaces (Gabe 1978) . The appearance of a ball crater through a commercially available electroplated zinc coating on

mild steel is shown in figure 6.1. The crater was developed to a total depth of 48 μm using a 30 mm diameter ball. The total diameter of the crater was 2.40 mm and that of the revealed substrate region 1.34 mm. This gives a value for the coating thickness of 33 μm.

Composition-depth profiles were obtained using a combination of elemental linescans, and full Auger analysis at specific points on the crater wall. A linescan showing the variation of the total secondary electron current enabled the precise position of the crater edge to be determined. This is important in calibrating the depth scale for the elemental linescans. Alternatively the crater edge can be located by coating the specimen with a thin film of gold prior to ball cratering (Thompson et al 1979).

A series of linescans for the selected elements of zinc, iron, chromium and oxygen is shown in figure 6.2. These linescans show the distribution of elements through the specimen, but are not generally used to provide quantitative information. However they are useful in selecting the most appropriate positions for point analysis. In this example full Auger spectra were obtained from the 14 points indicated in figure 6.2. These spectra provided quantitative information which was used to construct the composition-depth profile with a linear depth scale shown in figure 6.3. There is a relatively thin chromate treatment present at the surface, detectable to a depth of about 5 μm. This treatment is used to prevent oxidation and atmospheric discolouration (Williams 1972). The interface between the zinc coating and the steel substrate is very sharp which is typical of coatings produced by electrodeposition. Sputter-ion etching may be combined with ball cratering to provide a more detailed examination of this interface region. Positioning the ion beam at point 'X' in figure 6.1 enables a conventional sputter depth profile to be carried out from this position. The use of this procedure exploits the advantages of both techniques.

Figure 6.1 An electron micrograph showing the appearance of a ball crater through a commercially available electroplated zinc coating on a mild steel substrate.

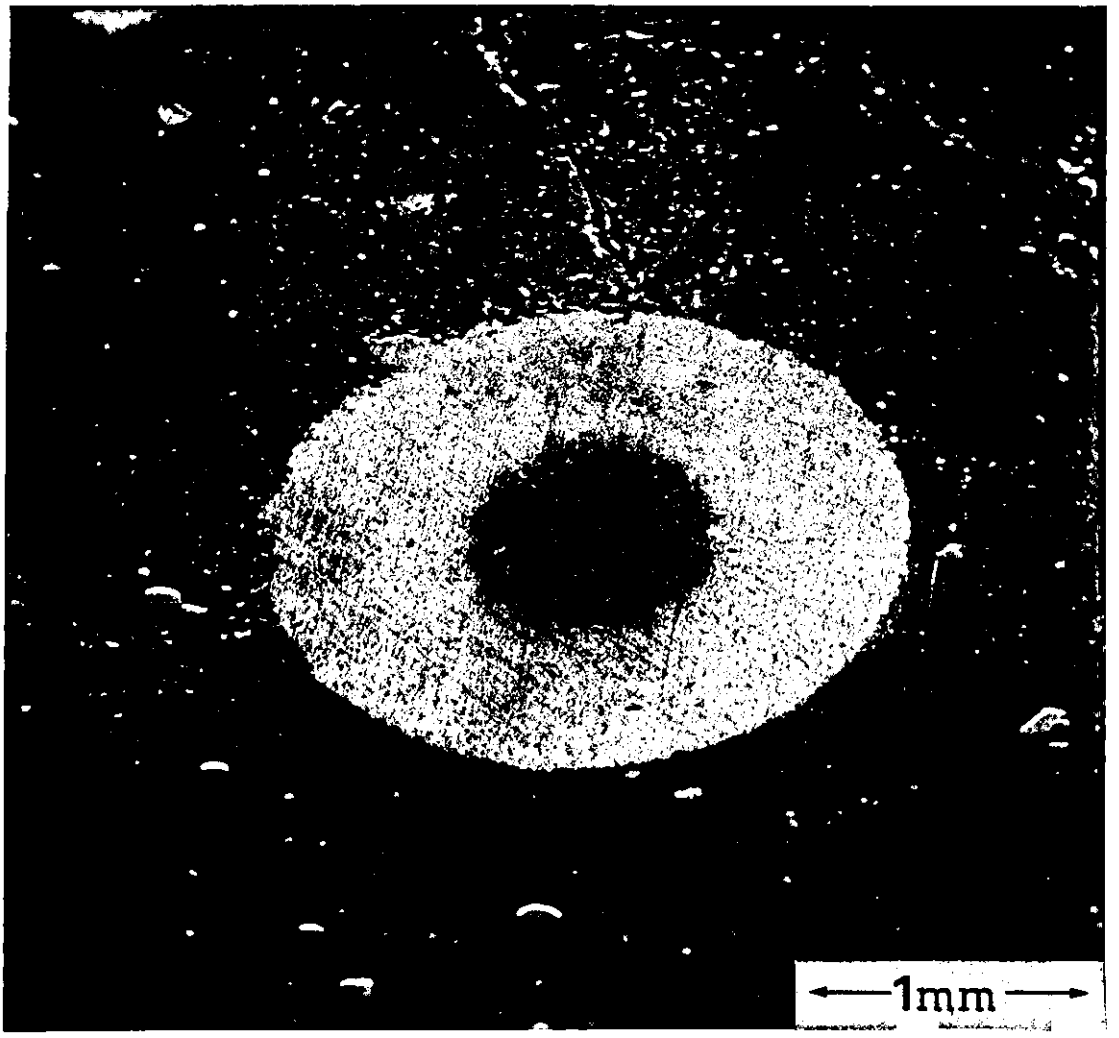
1mm

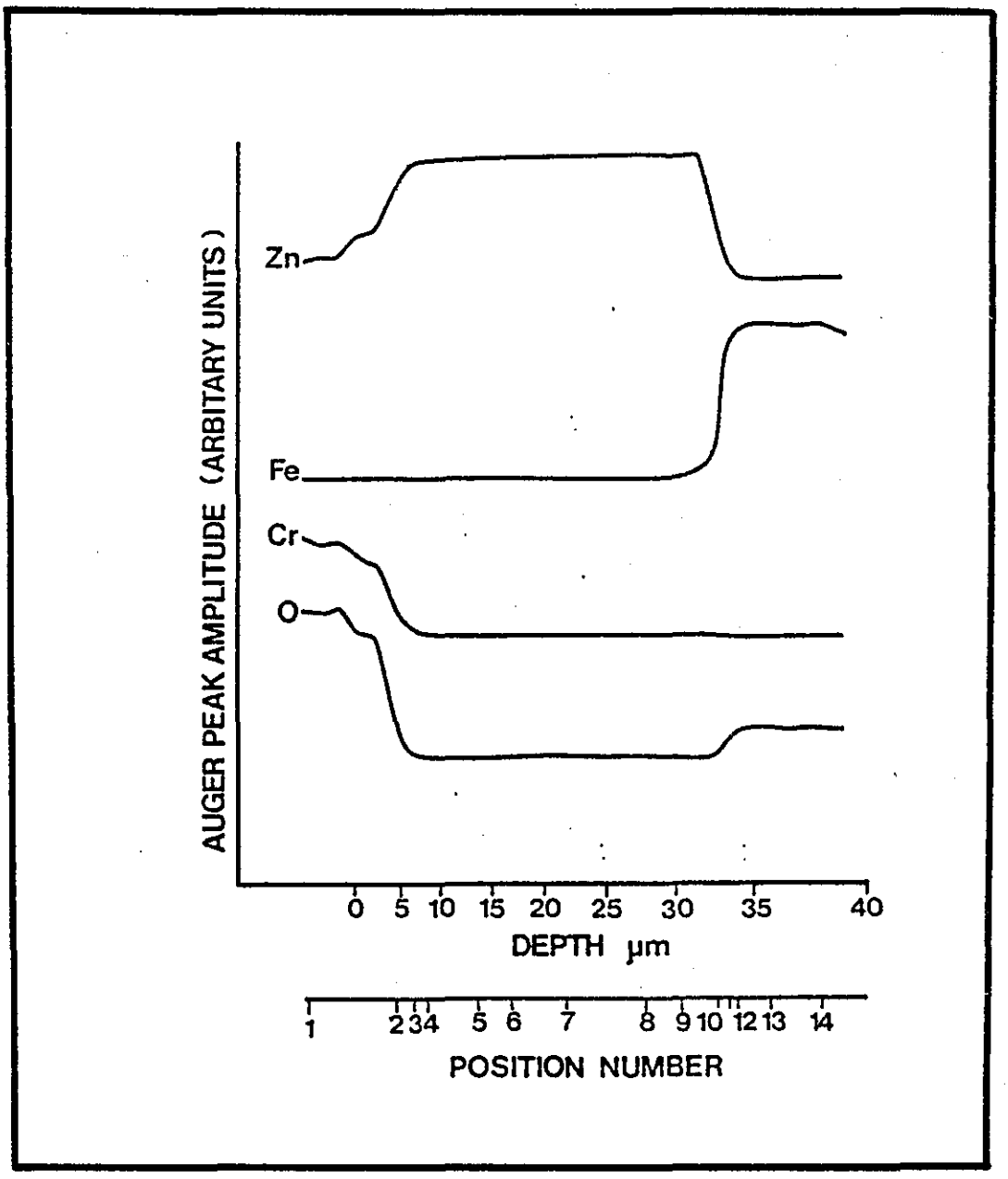

Figure 6.2 Elemental linescans for zinc, iron, chromium and oxygen showing the distribution of elements through the specimen shown in figure 6.1

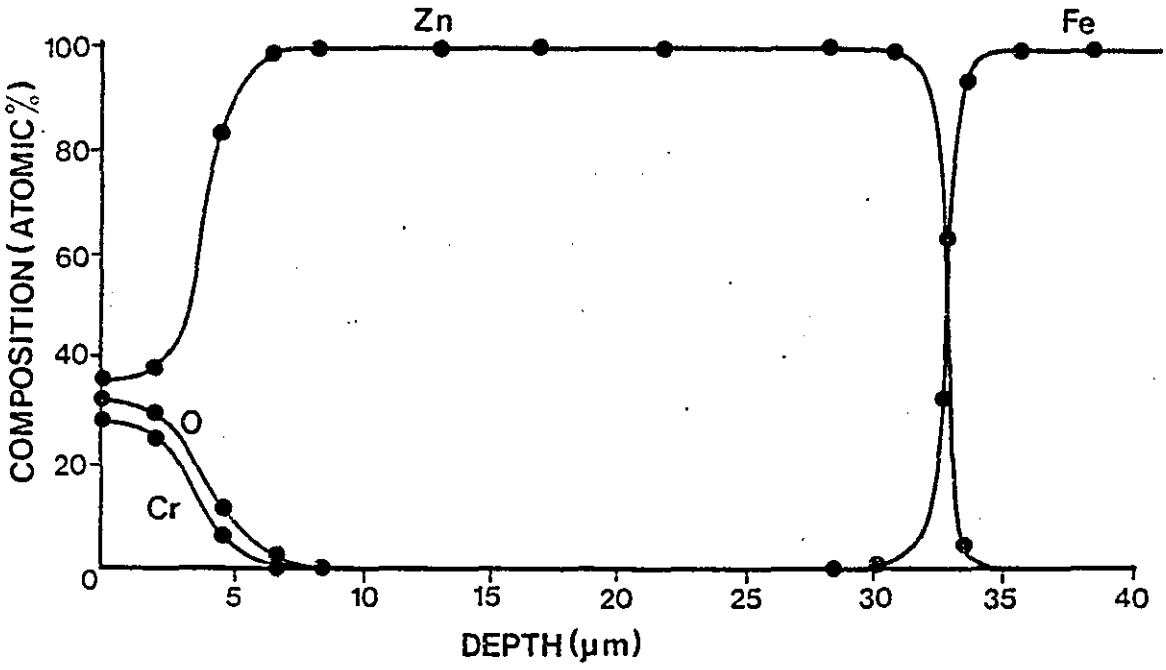

Figure 6.3 A composition-depth profile with a linear depth scale obtained from a series of Auger spectra at the 14 positions indicated in figure 6.2

3. Ion plated coatings

Ion plated coatings (Mattox 1973) have excellent adhesion and the technique is becoming increasingly important for producing high quality coatings for wear resistance and materials protection. A system of current interest is the use of mixed aluminium/aluminium oxide to protect mild steel components (Ahmed and Teer 1982). Flat steel samples were polished and ultrasonically cleaned with detergent before being inserted into a vacuum chamber at a pressure of 3×10^{-5} Torr. The steel substrates were cleaned by sputtering with 2 keV argon ions at a pressure of 10^{-2} Torr. The argon pressure was then reduced to 10^{-3} Torr and the substrate bias voltage was set to the required value. Aluminium was thermally evaporated on the substrate in the desired pressure of oxygen, which was admitted to the chamber in pulsed intervals. The substrate was water cooled so that the temperature never exceeded 250°C.

Ball craters were produced in the specimens with a 30mm diameter ball using 1μm diamond paste and a rotation speed of 24 r.p.m. The appearance of a crater formed in an ion plated sample is shown in figure 6.4. A close up of the interface region is shown in figure 6.5. This specimen was obtained in an atmosphere of 1×10^{-3} Torr of argon and 5×10^{-3} Torr of oxygen, with a bias of 3kV on the substrate. The corresponding composition-depth profile is shown in figure 6.6. The data for this profile was obtained by a combination of linescan techniques and point analysis, and the depth scale was converted from spherical to linear geometry. The profile clearly shows the variation of oxygen content through the coating, and it peaks near the interface. Examination of the crater in figures 6.4 and 6.5 indicates a corresponding region which appears to have a different composition to the rest of the coating. The relative strengths of the aluminium Auger peak in the oxide position (51eV) and the metal position (68eV) suggest that the oxygen is entirely in the form of Al_2O_3. The increased oxide contribution at

Figure 6.4 An electron micrograph showing the appearance of a ball crater through an ion plated aluminium/aluminium oxide coating on a steel substrate.

Figure 6.5 An electron micrograph showing a close-up of the interface region of the above specimen

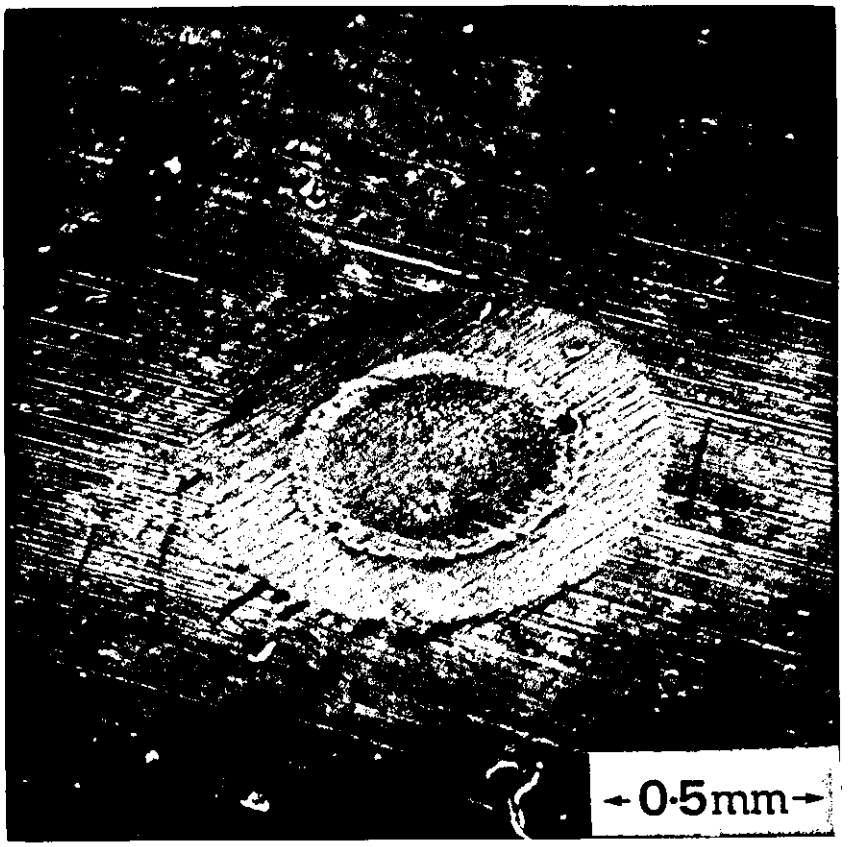
0·5mm

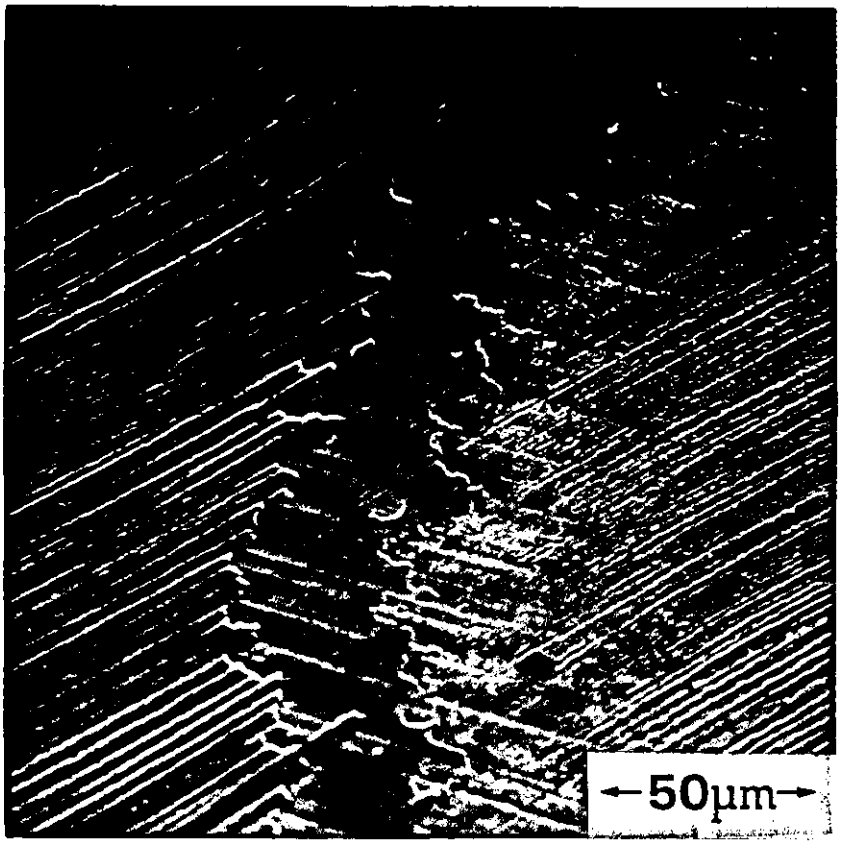
50μm

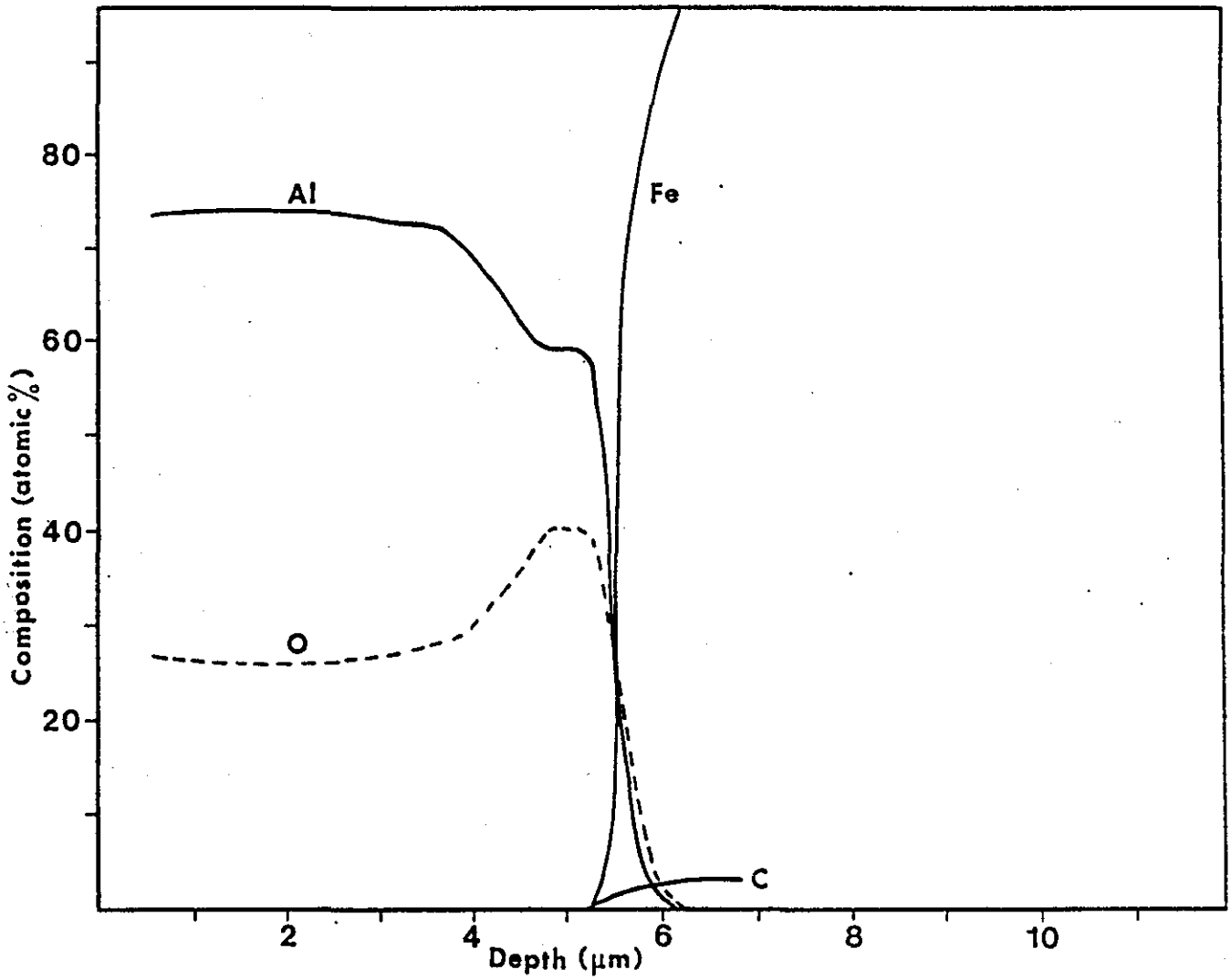

Figure 6.6. The corresponding composition-depth profile of the ion plated specimen shown in figures 6.4 and 6.5. The specimen was produced in an atmosphere of 1 x 10^{-3} Torr argon and 5 x 10^{-3} Torr oxygen.

the interface is probably due to an increased partial pressure of oxygen during the initial stages of deposition.

Figure 6.7 shows the corresponding depth profile for an ion plated specimen produced under similar conditions except that the oxygen pressure was lower at 1×10^{-3} Torr. Although the coating is thicker, 8.5μm compared to 5.5μm, the profile shows the expected decrease in the oxide composition. The provision of profiles such as these can help to predict and control the free metal/oxide ratio in the coating as a function of the oxygen partial pressure.

4. Nitrocarburised surface treatments

Nitrocarburizing is an important industrial process used for hardening steels and improving their tribological properties. Nitrogen and carbon can be introduced into the surface of ferrous metals by a number of methods including gaseous diffusion, ion implantation and chemical salt bath techniques. The precise amounts of carbon and nitrogen and the depth to which they penetrate are important in determining their service performance.

Ball cratering, in combination with Auger electron spectroscopy, is well suited to the analysis of such treatments since composition profiles to depths of up to 20μm are often required. The electron probe microanalyser is not a good technique for this application as it is relatively insensitive to the low atomic number elements such as carbon and nitrogen. A composition-depth profile for a specimen of an EN8 steel which has been nitrocarburized using a chemical salt bath treatment is shown in figure 6.8. Quantitative analysis was achieved using a Fe_3N standard and the results are presented in the form of weight per cent to facilitate comparison with the Fe/C/N phase diagram (Bell 1975). The composition is consistent with that for the ε carbonitride phase, and the levels of nitrogen and carbon are such that this phase

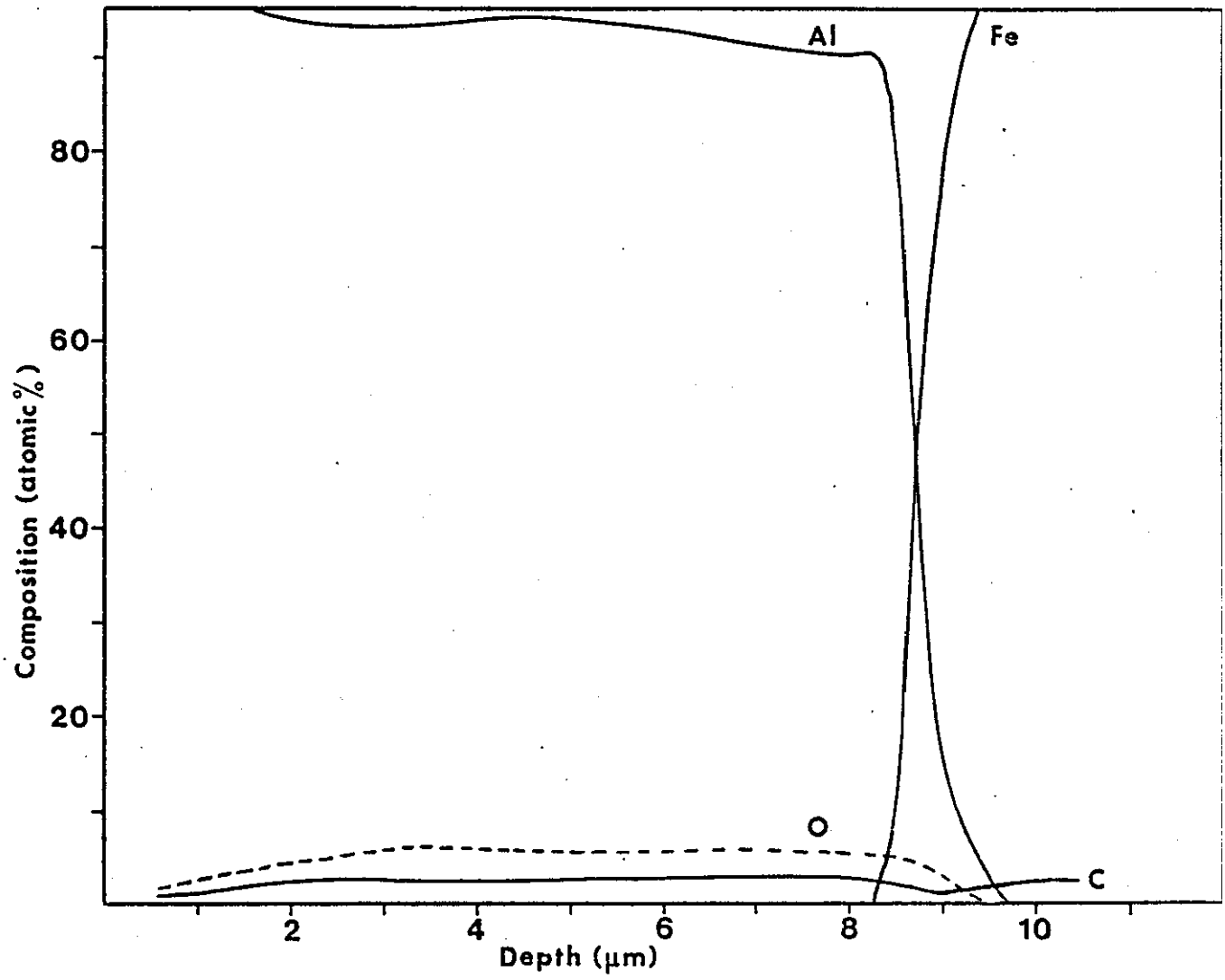

Figure 6.7 A composition-depth profile of an ion plated specimen produced in an atmosphere of 1 x 10^{-3} Torr argon and 1 x 10^{-3} Torr oxygen

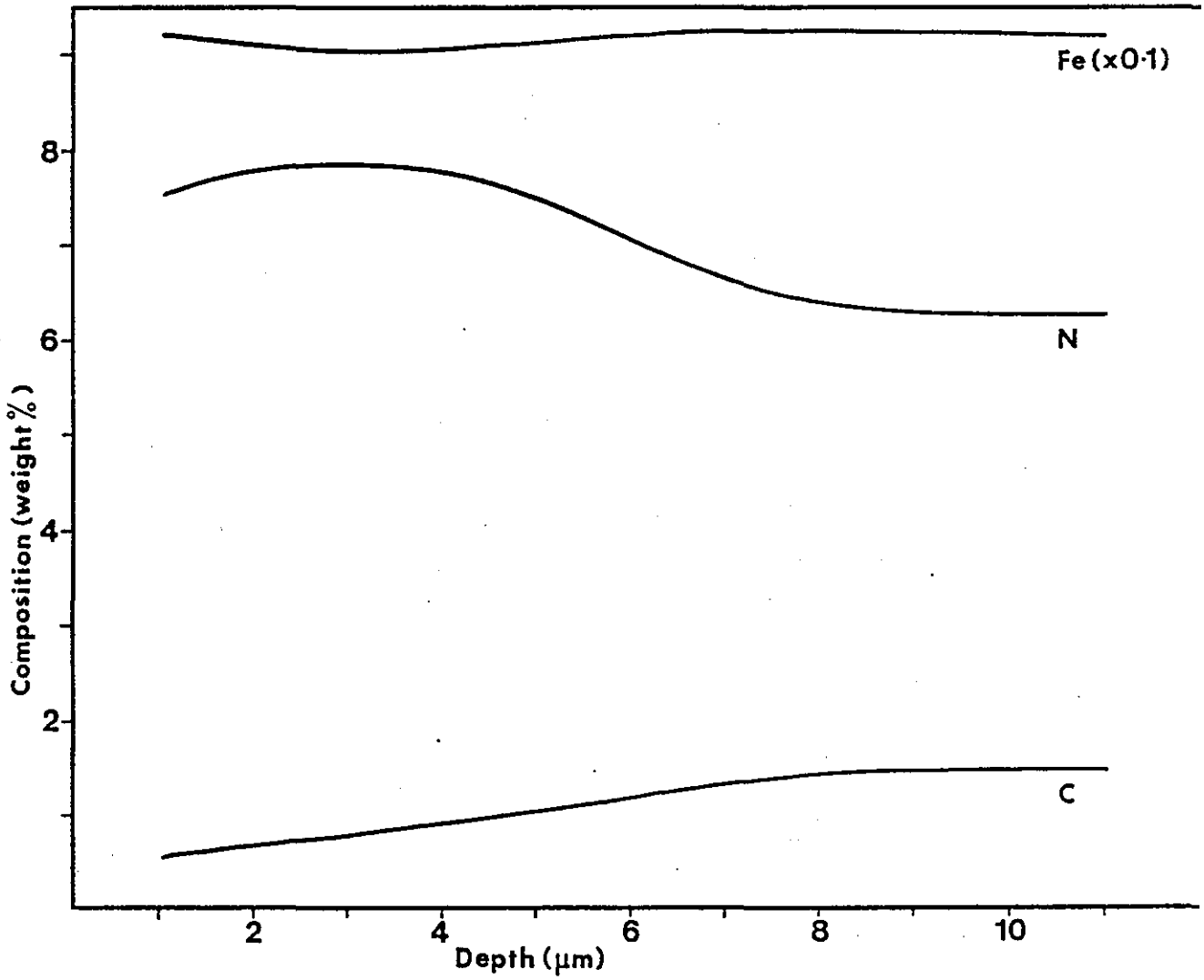

Figure 6.8 A composition-depth profile for a nitrocarburised steel specimen

penetrates to at least 10 μm beneath the surface. As a result the specimen should possess the desired chemical and tribological properties, and is taken from a treatment with a reliable service history.

In contrast, a composition-depth profile for a second sample of a nitrocarburised treatment is shown in figure 6.9. Although the near surface composition is consistent with the ϵ phase, the concentration of nitrogen decreases rapidly beyond about 4μm. It is likely that the γ and γ' phases, which have less desirable tribological properties, are also present at these depths.

5. Discussion

In the preceding examples, ball cratering has been shown to provide a convenient means for composition-depth profiling to depths of up to 50 μm. However there is no particular maximum depth up to which the technique is applicable, and it may in theory be used to any reasonable depth. The minimum depth is determined by that beyond which the depth resolution in ball cratering is superior to that obtained with sputter ion etching. This depends on factors which are a function of the particular specimen under investigation such as the initial surface topography. However, as a general rule, ball cratering gives better results at depths greater than about 1 μm.

The composition-depth profiles were obtained by means of point to point analysis down the walls of the crater using Auger electron spectroscopy. Elemental linescans across the crater diameter are useful for an initial examination, but are seldom used for quantitative analysis. More detailed information concerning the composition in the vicinity of a deep interface, as in the example of the electroplated zinc coating, can be obtained by combining sputter-ion etching with ball cratering. The nitrocarburized surface treatment shows the advantage of the technique over the electron microprobe, since the latter instrument is relatively insensitive to the low

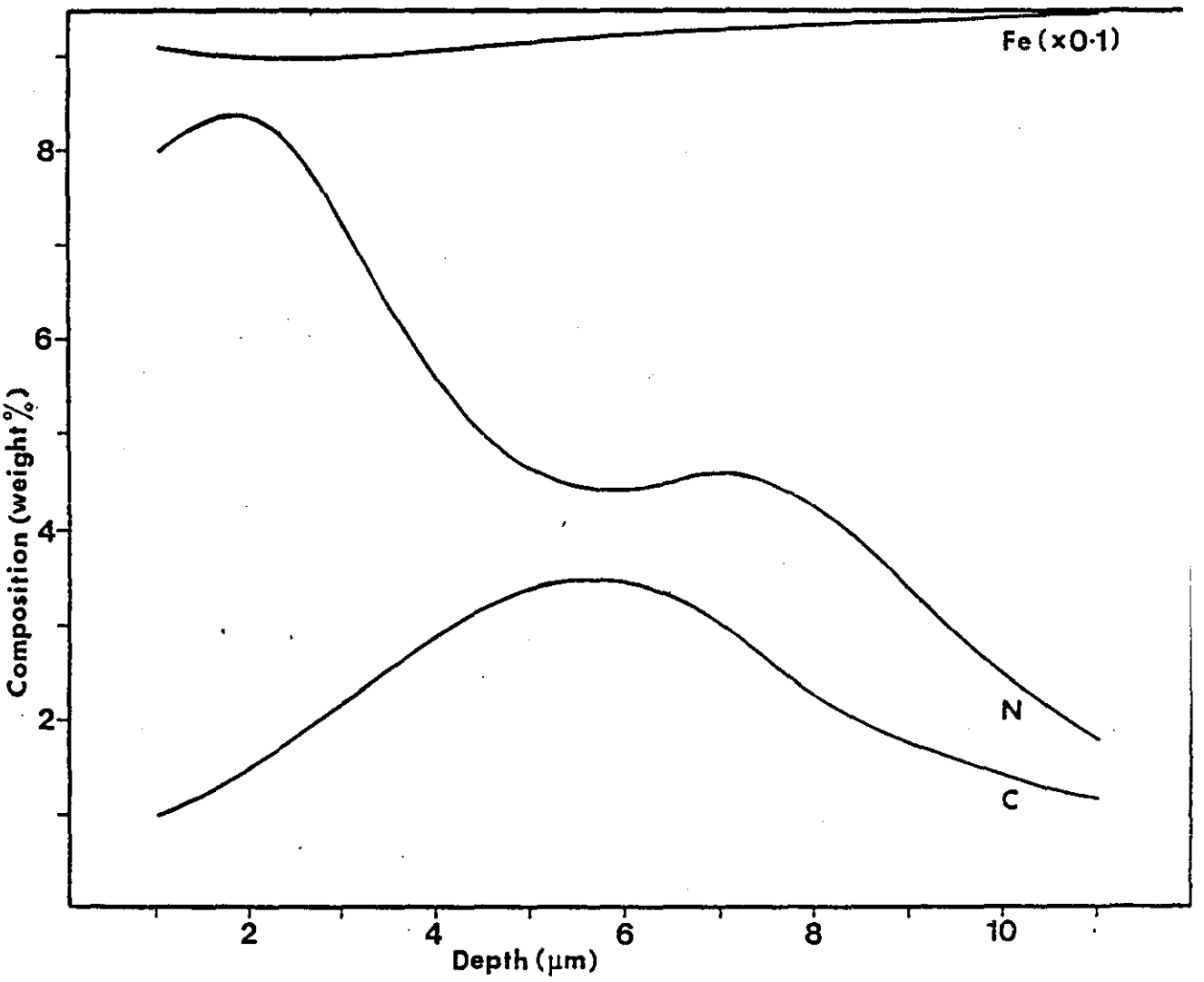

Figure 6.9 A composition-depth profile for a second nitroburised steel specimen with a less reliable service history

atomic number elements such as carbon and nitrogen.

Chapter 7 SUMMARY AND SUGGESTIONS FOR FUTURE WORK

1. Methods of surface analysis

A survey has been made of the principal surface analytical techniques and the major characteristics of each have been discussed. The high spatial resolution of Auger electron spectroscopy makes it the ideal technique for composition-depth profiling, particularly when used in combination with taper-sectioning techniques. In view of this a more detailed review of AES was presented in chapter 2, including a description of the experimental techniques and a consideration of the factors involved in obtaining quantitative analysis. Finally several artefacts arising from the electron beam were discussed, including electrostatic charging, specimen heating and electron beam induced composition changes.

2. Composition-depth profiling

The techniques available for obtaining composition-depth profiles using Auger electron spectroscopy were discussed in chapter 3. The most common method employs ion beam etching, but there are problems with this approach since surfaces are generally eroded in a non-uniform way. In addition ion etching is a relatively slow process, so that profiling to depths of more than about 1μm is inefficient and wasteful of instrument time. Taper-sectioning techniques provide a means for obtaining composition-depth profiles to much greater depths.

3. Ball-cratering

In contrast to profiles obtained by ion etching, the geometry of ball-cratering, described in chapter 3, provides a well-defined depth scale. Depth profiles can be obtained by point to point Auger analysis down the

walls of the crater, or by means of elemental linescans. The depth at any point is given simply in terms of the lateral distance from the crater edge.

It can be arranged for some region of specific interest, for example a coating-substrate interface, to be located near the base of the crater. The gradient of the crater wall becomes vanishingly small at this point, providin the maximum magnification. This gives ball-cratering an advantage over conventional angle-lapping, which is in general also limited to flat surfaces

The value of ball-cratering in composition-depth profiling has been demonstrated for a number of industrially important protective coatings and surface treatments. These were a commercially available electrodeposited coating, ion plated coatings produced under different conditions, and nitrocarburized surface treatments.

3.1 Depth-resolution

The factors which affect the depth resolution of profiles obtained by ball-cratering and Auger electron spectroscopy were discussed in chapter 4. These are principally the surface roughness produced by the wear process, and a geometrical contribution due to the finite diameter of the probing electron beam. An important advantage of ball-cratering over ion etching is that the depth resolution is independent of depth.

The depth resolution was examined for a model system consisting of an electrodeposited hard chrome coating on a mild steel substrate. In order to investigate the effects of surface topography, the contribution of the electron beam was kept constant by fixing the position of the interface relative to the base of the crater. The range of depth resolution obtained with each grade of diamond paste used was compared with values predicted from the quadratic sum of the individual contributions. There was found to be

good agreement between these values, showing that the depth resolution, in contrast to sputter depth profiling, can be controlled and predicted. In the case of 6μm diamond paste the major contribution to the depth resolution is the surface roughness of the crater, but when fine diamond paste (0.25μm) is used the depth resolution is limited mainly by the finite diameter of the electron beam.

3.2 Wear mechanisms

The surface finish obtained in ball-cratering is dependent on the precise nature of the wear processes involved. A detailed study of the wear mechanisms was presented in chapter 5 for a series of metals with a range of hardness. Evidence from scanning electron microscopy and the values of the wear coefficient indicate that the material is removed by abrasive wear for hard metals. In the intermediate range the mechanism is still predominantly abrasive, but in the case of the softest metals adhesive wear becomes the dominant process. This may lead to material transfer, or the impaction of diamond and wear debris, but these effects can be minimised by careful experimental procedures.

Although a better finish is generally obtained on hard surfaces, some caution is required on such surfaces since, if the hardness approaches that of the ball, significant wear and subsequent roughening of the ball can take place. This can lead to the unpredictable occurrence of scratches, possibly caused by the ball itself. It is advisable, therefore, when dealing with hard materials to discard the ball after each operation.

4. Suggestions for future work

The geometrical contribution to the depth resolution would be improved by the use of a ball having a greater diameter, since this would reduce the taper angle. However a larger ball would be correspondingly heavier,

increasing the load on the specimen, which may lead to problems with delicate materials. The depth resolution would also be improved by reducing the electron beam diameter.

Investigation could be made of the effects of using a ball of a different hardness. The use of a softer metal may lead to diamond becoming embedded in the ball, so approaching the condition for polishing. However there may also be a greater amount of wear on the ball itself, shortening its useful life.

Problems may occur with very soft metals due to material transfer, and a smearing of the interface in the case of surface coatings. This could be investigated using Auger electron spectroscopy for a suitable, well-characterised specimen.

As well as its use with AES, ball-cratering may also prove useful with other microfocus techniques such as the electron microprobe (EPMA) and the ion microprobe (dynamic SIMS).

REFERENCES

N. A. G. Ahmed and D. G. Teer — (Submitted to the 4th Int. Colloq. on Plasma and Sputtering, Nice, France, September 1982)

J. Ahn, C. R. Perleberg, D. L. Wilcox, J. W. Coburn and H. F. Winters — J. Appl. Phys. 46 (1975) 4581

G. C. Allen and R. K. Wild — J. Electron Spectroscopy 15 (1974) 409

H. H. Andersen — Appl. Phys. 18 (1979) 131

J. F. Archard — J. Appl. Phys. 24 (1953) 981

P. Auger — J. Phys. Radium 6 (1925) 205

E. Bauer — Vacuum 22 (1972) 539

Sir George Beilby — Aggression and Flow of Solids (Macmillan, London, 1921)

T. Bell — Heat Treat. Met. 2 (1975) 93

A. Benninghoven — Z. Phys. 230 (1970) 403

A. Benninghoven — Surface science 35 (1972) 427

A. Benninghoven — Thin Solid Films 39 (1976) 3

F. P. Bowden and T. P. Hughes — Proc. Roy. Soc. A160 (1937) 575

F. P. Bowden and D. Tabor — Friction, an Introduction to Tribology (Heinemann, London, 1973)

D. Briggs (editor) — Handbook of X ray and Ultraviolet Photoelectron Spectroscopy (Heyden, London, 1977)

I. K. Brown, D. D. Hall and J. M. Walls — Vacuum 31 (1981) 625

T. M. Buck — in Methods of Surface Analysis ed. A. W. Czanderna (Elsevier, Amsterdam 1975).

T. A. Carlson — Photoelectron and Auger spectroscopy (Plenum, New York, 1975)

B. Carriere and B. Lang — Surface Sci. 64 (1977) 209

G. Carter and J. S. Colligon — Ion Bombardment of Solids (Heinemann, London, 1968)

G. Carter, A. Gras-Marti and M. J. Nobes — Radiation Effects 62 (1982) 119

R. Castaing — Materials Science and Engineering 42 (1980) 13

C. C. Chang — in Characterisation of Solid Surfaces ed. P. K. Kane and G. B. Larrabee (Plenum, New York, 1974)

C. C. Chang	J. Vac. Sci. Technol. 18 (1981) 276
J. P. Chubb, J. Billingham, D.D. Hall and J. M. Walls	Metals Technology 7 (1980) 293
J. P. Coad, H. E. Bishop and J. C. Riviere	Surface. Sci. 21 (1970) 253
J. P. Coad and J.C. Riviere	Proc. Roy. Soc. A331 (1972) 403
J. W. Coburn	J. Vac. Sci. Technol. 13 (1976) 1037
A. W. Czanderna (editor)	Methods of Surface Analysis (Elsevier, Amsterdam, 1975)
L. E. Davis, N.C. McDonald, P.W. Palmberg, G.E. Riach and R.E. Weber	Handbook of Auger Electron Spectroscopy (Physical Electronics Industries Inc, 1976)
J. R. Dennis and E. B. Hale	Appl. Phys. Lett. 29 (1976) 523
S. Duncan, D.E. Sykes,, R. Smith and J. M. Walls	(1982) to be published
J. Erlewein and S. Hofmann	Thin Solid Films 69 (1980) L39
T. S. Eyre	Tribology International 11 (1978) 91
H. E. Farnsworth, R.E. Schlier, T. H. George and R.M. Burger	J. Appl. Phys. 29 (1958) 1150
D. R. Gabe	Principles of Metal Surface Treatment and Protection (Pergamon, Oxford, 1978).
J. T. Grant	Applications of Surface Science 13 (1982) 35
J. T. Grant, R.G. Wolfe, M. P. Hooker, R. W. Springer and T. W. Haas	J. Vac . Sci. Technol. 14 (1977) 232
T. W. Haas and J. T. Grant	Appl. Phys. Lett. 16 (1970) 172
P. M. Hall and J. M. Morabito	CRC Crit. Rev. Solid State Sciences 8 (1978) 53
P. M. Hall, J. M. Morabito and D. K. Cowley	Surface Sci. 62 (1977) 1
J. Halling	Introduction to Tribology (Wykeham, London, 1976).
W. W. Happ and W. Shockley	Bull. Am. Phys. Soc. Ser II 1 (1956) 382
L. A. Harris	J. Appl. Phys. 39 (1968) 1419
L. A. Harris	Surface Sci. 15 (1969) 77
S. M. Hercules and D.H. Hercules	in Characterisation of Solid Surfaces ed. P. K. Kane and G. B. Larrabee (Plenum, New York, 1974)

P. S. Ho and J. E. Lewis	Surface Sci. 55 (1976) 335
W. O. Hofer and H. Liebl	Appl. Phys. 8 (1975) 359
W. O. Hofer and P. J. Martin	Appl. Phys. 16 (1978) 271
D. W. Hoffman	Surface Sci. 50 (1975) 29
S. Hofmann	Appl. Phys. 9 (1976) 59
S. Hofmann	Appl. Phys. 13 (1977) 205
S. Hofmann	Talanta 26 (1979) 665
S. Hofmann	Surface and Interface Analysis 2 (1980) 148
S. Hofmann	Analusis 9 (1981) 181
S. Hofmann and A. Zalar	Thin Solid Films 39 (1976) 219
S. Hofmann and A.Zalar (1979a)	Thin Solid Films 56 (1979) 337
S. Hofmann and A. Zalar (1979b)	Thin Solid Films 60 (1979) 201
D. M. Holloway	J. Vac. Sci. Technol. 12 (1975) 392
P. H. Holloway	J. Vac. Sci. Technol. 12 (1975) 1418
P. H. Holloway	Advances in Electronics and Electron Physics 54 (1980) 241
P. H. Holloway and R. S. Bhattacharya	Surface and Interface Analysis 3 (1981) 118
P. H. Holloway and G. C. Nelson	J. Vac. Sci. Technol. 16 (1979) 793
M.P. Hooker and J. T. Grant	Surface Sci. 55 (1976) 741
G. A. Hutchins	in Characterization of Solid Surfaces ed. P. K. Kane and G. B. Larrabee (Plenum, New York, 1974)
D. R. Jennison	J. Vac. Sci. Technol. 17 (1980) 172
J. S. Johannessen, A.P. Grande and T. Notevarp	Materials Science and Engineering 42 (1980) 321
B. A. Joyce and J. H. Neave	Surface Sci. 34 (1973) 40
P. K. Kane and G. B. Larrabee editors	Characterization of Solid Surfaces (Plenum, New York, 1974).
N. Laegrid and G. K. Wehner	J. Appl. Phys. 32 (1961) 365
J. J. Lander	Phys. Rev. 91 (1953) 1382
P. Laty, D.Seethanen and F. Degreve	Surface Sci. 85 (1979) 353
C. Lea and M. P. Seah	Thin Solid Films 75 (1981) 67

H. Liebl	J. Vac. Sci. Technol. 12 (1975) 385
D. Lichtman	in Methods of Surface Analysis ed. A. W. Czanderna (Elsevier, Amsterdam, 1975).
N. C. MacDonald and J.R. Waldrop	Appl. Phys. Lett. 19 (1971) 315
H. H. Madden	J. Vac. Sci. Technol. 18 (1981) 677
T. E. Madey and J. T. Yates Jr.	J. Vac. Sci. Technol. 8 (1971) 525
S. S. Makh, R. Smith and J. M. Walls	J. Materials Sci. 17 (1982) 1689
J. B. Malherbe, J. M. Sanz and S. Hofmann	Surface And Interface Analysis 3 (1981) 235
H. J. Mathieu, D. E. McClure and D. Landolt	Thin Solid Films 38 (1976) 281
D. M. Mattox	J. Vac. Sci. Technol. 10 (1973) 47
R. G. Mazur and G. A. Gruber	Solid State Technology 24 (1981) 64
G. M. McCracken	Rep. Prog. Phys. 38 (1975) 241
B. McDonald and A. Goetzberger	J. Electrochemical Society 109 (1962) 141
G. E. McGuire	Auger Electron Spectroscopy Reference Manual (Plenum, New York, 1979).
J. A. McHugh	in Methods of Surface Analysis ed. A. W. Czanderna (Elsevier Amsterdam 1975)
F. Meyer and J. J. Vrakking	Surface Sci. 45 (1974) 409
J. F. Moulder, D. G. Jean and W. C. Johnson	Thin Solid Films 64 (1979) 427
V. Naundorf and M. P. Macht	Nuclear Instruments and Methods 168 (1980) 405
B. Navinsek	Progress in Surface Science 7 (1976) 49
C. Nordling, E. Sokolowski and K. Siegbahn	Ark. Fys. 13 (1958) 483
H. Oechsner	Appl. Phys. 8 (1975) 185
P. W. Palmberg	J. Vac. Sci Technol. 9 (1972) 160
P. W. Palmberg, G. K. Bohn and J.C. Tracy	Appl. Phys. Lett. 15 (1969) 254
C. G. Pantano and T. E. Madey	Applications of Surface Science 7 (1981) 115
R. L. Park	Physics Today 28 (1975) 52
L. G. Pittaway	Brit. J. Appl. Phys. 15 (1964) 967
E. Rabinowicz	Friction and Wear of Materials (Wiley, New York, 1965)

E. Rabinowicz — Science 6 (1970) 45

W. Reuter and J. E. E. Baglin — J. Vac. Sci. Technol. 18 (1981) 282

L. Rivaud A. H. Eltoukhy and J. E. Greene — Radiation Effects 61 (1982) 83

K. Roll — Applications of Surface Science 5 (1980) 388

K. Roll and C. Hammer — Thin Solid Films 57 (1979) 209.

K. Roll W. Losch and C. Achete — J. Appl. Phys. 50 (1979) 4422

D. Rosenberg and G.K. Wehner — J. Appl. Phys. 33 (1962) 1842

R. R. Rye T. E. Madey J. E. Houston and P.H. Holloway — J. Chem. Phys. 69 (1978) 1504

L. E. Samuels — J. Inst. Metals 85 (1956) 51

L. E. Samuels — Metallographic Polishing by Mechanical Methods (Pitman London 1967)

M. P. Seah and W. A. Dench — Surface and Interface Analysis 1 (1979) 2

M. P. Seah and C. Lea — Thin Solid Films 81 (1981) 257

M.P. Seah J.M. Sanz and S. Hofmann — Thin Solid Films 81 (1981) 239

P.J. Severin H. Bulle G. Poodt and J. Dwasscher — J. Electrochem. Soc. 122 (1975) 440

R. Shimizu — Appl. Phys. 18 (1979) 425

K. Siegbahn C. Nordling A. Fahlman R. Nordberg K. Hamrin, J. Hedman, G. Johansson T. Bergmark, S. E. Karlsson, I. Lindgren, and B. Lindberg — ESCA - Atomic, Molecular and Solid State Structure Studied by means of Electron Spectroscopy (Almqvist and Wiksells Uppsala, 1967).

P. Sigmund — J. Appl. Phys. 50 (1979) 7261

P. Sigmund — J. Vac. Sci. Technol. 17 (1980) 396

P. Sigmund and A. Gras-Marti — Nuclear Instruments and Methods 168 (1980) 389

R. Smith T. P. Valkering and J.M. Walls — Phil. Mag. A44 (1981) 879

R. Smith and J.M. Walls — Surface Sci. 80 (1979) 557

D. E. Sykes D.D. Hall R. E. Thurstans and J.M. Walls — Applications of Surface Science 5 (1980) 103

M .L. Tarng and D. G. Fisher	J. Vac. Sci. Technol. 15 (1978) 50
N.J. Taylor. J.S. Johannessen and W. E. Spicer	Appl. Phys. Lett. 29 (1976) 497
V. Thompson, H.E. Hintermann and L. Chollet	Surface Technology 8 (1979) 421
H.G. Tompkins	Surface Sci. 62 (1977) 293
H. G. Tompkins	J. Vac. Sci. Technol. 16 (1979) 778
A. H. Tong, E.F. Gorey and C. P. Schneider	Rev. Scientific Instrum. 43 (1972) 320
N. Treitz	J. Phys. E. Scientific Instrum. 10 (1977) 573
I.S.T. Tsong, G.L. Power, D. W. Hoffman and C.W. Magee	Nuclear Instruments and Methods 168 (1980) 399
N.H. Turner, J.S. Murday and D.E. Ramaker	Analytical Chemistry 52 (1980) 84
A. van Oostrom	Surface Sci. 89 (1979) 615
A. van Oostrom, L. Augustus, W. Nijman and W. Leswin	J. Vac. Sci. Technol. 17 (1980) 40
J.M. Walls	Thin Solid Films 80 (1981) 213
J.M. Walls, I.K. Brown and D.D. Hall	Applications of Surface Science (1982) (in press)
J.M. Walls, D.D. Hall, D.G. Teer and B.L. Delcea	Thin Solid Films 54 (1978) 303
J.M. Walls, D.D. Hall and D.E. Sykes	Surface and Interface Analysis 1 (1979) 204
R.D. Webber and J.M. Walls	Thin Solid Films 57 (1979) 201
R.E. Weber and W.T. Peria	J. Appl. Phys. 38 (1967) 4355
G.K. Wehner	in Methods of Surface Analysis ed. A.W.Czanderna (Elsevier, Amsterdam, 1975)
G.K. Wehner and D.J. Hajicek	J. Appl. Phys. 42 (1971) 1145
H.W. Werner	Materials Science and Engineering 42 (1980)
H.W. Werner	Surface and Interface Analysis 4 (1982) 1
L.F.G. Williams	Plating 59 (1972) 931
K. Wittmaack and F. Schulz	Thin Solid Films 52 (1978) 259
J. Yarwood	High Vacuum Technique (Chapman and Hall, London, 1967)
A. Zalar and S.Hofmann	Surface and Interface Analysis 2 (1980) 183

ACKNOWLEDGEMENTS

I would like to thank my supervisor Dr. J. M. Walls for his guidance and encouragement throughout the period when the work presented here was undertaken.

My thanks are due to the Science and Engineering Research Council and the National Physical Laboratory for the provision of a CASE award, and to the University for additional financial assistance. I wish to thank Dr. M. P. Seah of the National Physical Laboratory for the interest which he has shown in the work, and for many useful discussions.

I am grateful to Mr. D.D. Hall for his assistance with aspects of the work and for many useful discussions, and to Dr. A.B. Smith for useful discussions.

My thanks are also due to Mr. K.W. Topley for printing the photographs to such a high standard, and to Mrs Diane Evans for typing the thesis so proficiently.

Finally I wish to thank my parents for their constant support, understanding and encouragement, throughout the duration of the work.